Dissertation zur Erlangung des Doktorgrades
der Fakultät für
Chemie und Pharmazie
der Ludwig-Maximilians-Universität München

Photopharmacology: Restoration of Vision using Photochromic Ligands

von
Laura Anna Henriette Laprell
aus Kiel, Deutschland

2015

Erklärung

Diese Dissertation wurde im Sinne von §7 der Promotionsordnung vom 28. November 2011 von Herrn Prof. Dr. Dirk Trauner betreut.

Eidesstattliche Versicherung

Diese Dissertation wurde eigenständig und ohne unerlaubte Hifle erarbeitet.

München, den 21.5.2015

Laura Laprell

Dissertation eingereicht am 21.05.2015

Gutachter: 1. Prof. Dr. Dirk Trauner
2. Prof. Dr. Dr. Franz Grus

Tag der mündlichen Prüfung 22.06.2015

Um etwas Licht ins Dunkel zu bringen.

To light up the dark.

Research Summary

This dissertation describes the characterization of photochromic ligands and photopharmacological approaches for vision restoration approaches.

BACKGROUND

Photochromic ligands (PCLs) are small, freely diffusible molecules, which contain a photoswitchable moiety (azobenzene) and a pharmacophore. The pharmacophore is a functional group, such as a potassium channel blocker (triethyl ammonium) or glutamate. The azobenzene can exist in two different states, the thermodynamically stable *trans*-configuration or the less-stable *cis*-configuration. Illumination with specific wavelengths induces a change in the configuration of the PCL. Classic PCLs need shorter wavelengths for switching from *trans*- to *cis*- and longer wavelengths for switching from *cis*- to *trans*-configuration. In addition, azobenzenes can also relax back to *trans* thermally within milliseconds or days, depending on the substituents. By changing the configuration with light, the affinity of the PCL towards its target receptor is changed. Thereby, neural activity can be controlled by toggling between the two states (Figure 1). A great advantage of PCLs is that they can be actively switched off using light in contrast to the diffusion-limited off-kinetics of caged ligands.

The photopharmacological approach has been widely used not only for light-control of voltage-dependent ion channels, ionotropic glutamate receptors and GPCRs, but also for TRP-channels and even enzymes (Fehrentz et al. 2011, Broichhagen et al. 2014b, Schonberger and Trauner 2014, Stawski et al. 2012, Broichhagen et al. 2014a).

TOPICS

This work covers four main topics. Parts 1-3 describe the use of PCL for vision restoration approaches, whereas basic characteristics of PCLs are investigated in part 4.

In the first part the photochromic potassium channel blocker diethylamine-azobenzene-diethylamine (DAD) is described for the use in vision restoration approaches in blind mice. The second part covers the use of a photochromic AMPA receptor agonist, azo-tetrazol-AMPA (ATA), and in the third part a combination of both, DAD and ATA, is shown to elicit light-responses in blind retinae similar to those in wild type retinae. In the last part of this thesis the characterization of photochromic ligands, in particular azobenzene-triazole-glutamate (ATG) and its derivatives, are shown utilizing acute murine brain slices. All experiments and their outcome are summarized in tables at the end of this research summary.

RESULTS

Part 1

DAD: A photochromic potassium channel blocker for restoration of vision

DAD is non-permanently charged photochromic ligand. In acute coronal brain slices DAD blocks potassium channels in its thermodynamically stable *trans*-configuration. Switching from *trans*- and *cis*-configuration is achieved using 440-480 nm light and DAD relaxes back thermally within milliseconds.

When applied to blind retinae (TKO: cnga3$^{-/-}$, rho$^{-/-}$, opn4$^{-/-}$) on a multielectrode array (MEA) setup, DAD induces an increase in retinal ganglion cell (RGC) spiking upon illumination with blue light, whereas it is inactive in the dark (Figure 1E). Furthermore, pharmacological experiments revealed that DAD specifically activates retinal bipolar cells and that the remaining retinal network is utilized in the same fashion as in wild type retinae. In addition, experiments with five different blind and partially blind mouse models demonstrated that DAD photosensitizes bipolar cells in degenerating retinae, not affecting healthy tissue.

For application of DAD *in vivo*, concentrations between 5 mM and 7.5 mM DAD in PBS have been shown to reliably induce robust light responses after intravitreal injections. Between 2 and 6 hours post-injection the DAD-mediated light-responses were strongest. Based on these experiments, behavioral studies (light-dark box test) were performed in collaboration with Dr. Kuldeep Kaur (Prof. Russell Van Gelder, University of Washington, Seattle, USA). The experiments revealed that DAD is able to induce light-dependent behavior in blind mice. Further studies addressing learned-behavior could not be performed yet, because the persistence of DAD in the vitreal cavity is limited to approximately 12 hours. However, we are currently working on small-particle release approaches to have a constant level of DAD released over a longer time period post injection.

Part 2

ATA: A photochromic AMPA receptor agonist for restoration of vision

To date, only photochromic ion channel blockers have been used in vision restoration approaches (Tochitsky and Kramer 2015). In the present work the use of a freely diffusible photochromic receptor agonist for vision restoration is described for the first time. Here, ATA was used, which has been shown to be active in its dark-adapted *trans*-configuration and to selectively activate AMPA receptors in cortical neurons (Stawski et al. 2012). MEA experiments not only showed that ATA has the same selectivity for AMPA receptors in blind TKO retinae, but that it can be switched with both, blue and white light (Figure 1E). The light intensities required for switching from *trans*- to *cis*-configuration were in the same range as for activation of DAD.

Furthermore, detailed pharmacological experiments were performed to isolate input from different cell types, which revealed that ATA primarily activates amacrine and RGCs.

Part 3

Combination therapy: DAD and ATA induce wild type like responses when applied in combination

In contrast to DAD, which increases spiking activity in RGCs during illumination, ATA is active in the dark. When switching light on and off, wild type retinae respond only to the change in the stimulus with transient increases in RGC firing rate, so-called light-on and light-off responses. It is therefore conceivable that the combination of DAD and ATA would induce similar responses compared to wild type. Indeed, it could be shown that the combinatorial approach led to transient on/off responses and furthermore that not all cells responded in the same manner. Similar to wild type retinae, populations of cells increased spiking rate to either light-on or light-off or both stimuli.

CONCLUSION Parts 1-3

The results from these studies demonstrate that PCLs are powerful tools for vision restoration strategies. Although this approach is relatively new, it has many advantages over other, currently more developed, therapies (e.g. viral gene transfer or implantation of electronic light-sensing devices). The photopharmacological approach is not only minimally invasive, more flexible in terms of application and cheaper, but also treatment could be terminated in case of undesirable side-effects or other PCLs can be applied.

Part 4

Characterization of photochromic ligands in acute murine brain slices

The last part of this work mainly covers the characterization of the PCL azobenzene-triazole glutamate (ATG) in acute murine brain slices. ATG can be switched from *trans* to *cis* using near UV light (360-380 nm) and switching back to *trans* is maximally accelerated using blue light (420-440 nm)

ATG is the first PCL based on glutamate that is inactive in the dark-adapted *trans*-configuration and furthermore it is the first selective NMDA receptor PCL. This has been demonstrated in several experiments covering pharmacology, calcium imaging and coincidence detection. Due to an NMDA receptor specific magnesium block they are defined as coincidence detectors. Both, neurotransmitter binding and concomitant postsynaptic depolarization are required to activate the ion channel. Experiments with electrical stimulation and ATG-mediated light activation prior, during and after the electrical stimulation were able to demonstrate that ATG-activated NMDA receptors can also function as coincidence detectors. In collaboration with Dr. David DiGregorio (Institute Pasteur, Paris, Frankreich) we could further show that ATG can be switched to *cis* using two-photon activation (720 nm) and that it can be activated in very small areas, such as a single spine. Moreover, inactivation of ATG-activated NMDA receptors was achieved within milliseconds

using 420 nm light, which is significantly faster compared to caged agonists such as MNI glutamate.

Further studies of this work cover the application of ATG in Purkinje cells of the cerebellum and the investigation of ATG derivatives. In addition, I analyzed the activity of a photoswitchable α7-nicotinic acetylcholine receptor agonist, AzoCholine, in acute hippocampal brain slices using the MEA.

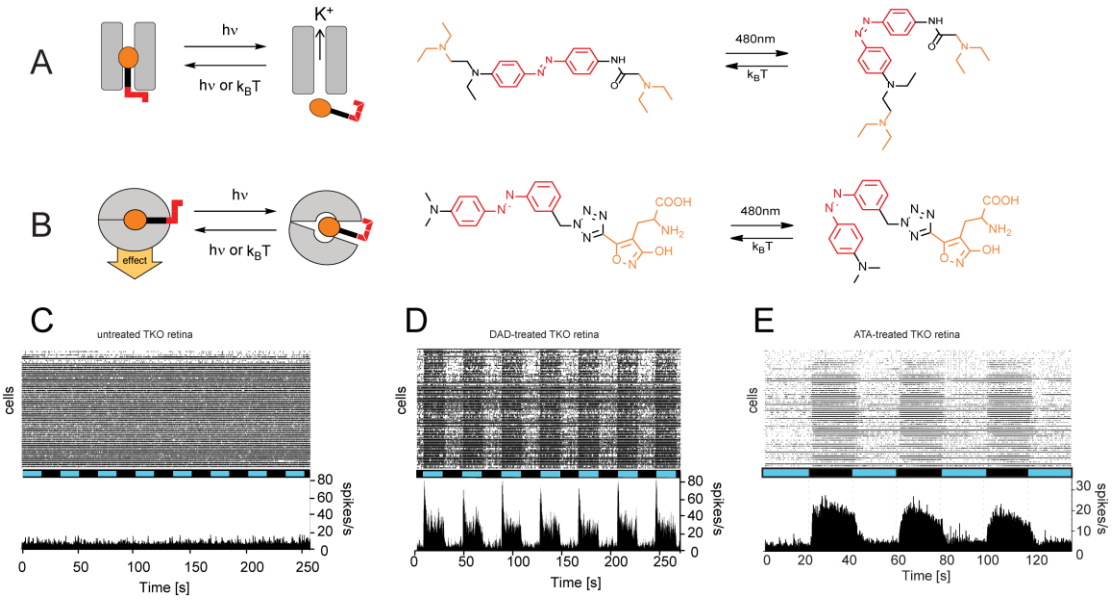

Figure 1 - Vision restoration approaches. (A) Schematic representation of the photoswitch mechanism. The azobenzene moiety (red) can be switched between *trans*- and *cis*-configuration using specific wavelengths. Depending on the ligand (orange ball) the photochromic ligand can either bind to a specific receptor or **(B)** function as a channel blocker. On the right: Molecular structures in *trans*- and *cis*-configuration of DAD (A) and ATA (B). **(C)** MEA recording of an untreated blind TKO retina. Raster plot is shown on the top, light stimulation protocol in the middle and histogram of all cells at the bottom. **(D)** MEA recording of an DAD-treated TKO retina. Same representation as in (C). **(E)** MEA recording of an ATA-treated TKO retina with the same representation as in (C) and (D).

Table of Contents

Abbreviations

°C	degree Celsius
µM	micromolar
A	ampere
AAQ	acrylamide azobenzene quaternary
AC	amacrine cell
Ach	Acetylcholine
AchR	Acetylcholine receptor
ACSF	Artificial cerebrospinal fluid
AMD	age-related macular degeneration
AMPA	α-amino-3-hydroxy-5-methyl-4-isoxazolepropionic acid
ATD	Amino-terminal domain
D-AP5	(2*R*)-amino-5-phosphonovaleric acid
ATA	azo-tetrazol AMPA
ATG	azobenzene triazole glutamate
ATP	adenosine triphosphate
Ba^{2+}	barium
Ca^{2+}	calcium
CaM	calmodulin
cAMP	cyclic adenosine monophosphate
Cav	voltage gated calcium
CBP	cone bipolar cell
cd	candela
Cd^{2+}	cadmium
CDI	calcium-dependent inactivation
CDF	calcium-dependent facilitation
cGMP	cyclic guanosine monophosphate
ChAT	choline acetyltransferase
ChR	channelrhodopsin
Cl^{-}	chloride
cm^2	squarecentimeter
CNG	cyclic nucleotide gated channel
cnga3	cyclic nucleotide gated channel alpha 3
CNQX	6-cyano-7-nitroquinoxaline-2,3-dione
CNS	central nervous system
CO_2	carbon dioxide
CPPG	(*RS*)-α-Cyclopropyl-4-phosphonophenylglycine
CREB	cAMP response element-binding protein
Cs^{+}	cesium
DAD	diethyl-azobenzene-diethyl
DCG-IV	(2*S*,2'*R*,3'*R*)-2-(2',3'-Dicarboxycyclopropyl)glycine
DENAQ	diethyl-amine-azobenzene quaternary ammonium
DMSO	dimethyl sulfoxide
DNQX	6,7-dinitroquinoxaline-2,3-dione
EC50	effective concentration
EPSP	excitatory postsynaptic potential
Fel	felodipine
G	gauge
GABA	γ-Aminobutyric acid
GCL	ganglion cell layer
GluAzo	glutamate -azobenzene
GluR	glutamate receptor
GMP	guanosine monophosphate
gnat	transducin
GPCR	G-protein coupled receptor
HCl	hydrochloric acid
HEK	human embryonic kidney cell
HEPES	4-(2-hydroxyethyl)-1-piperazineethanesulfonic acid
HR	hepes Ringer
HVA	high-voltage activated
Hz	Hertz
i.a.	inter alia
i.e.	id est
iGluR	iontotropic glutamate receptor
IH	hyperpolarizing currents

INL	inner nuclear layer
IPL	inner plexiform layer
ipRGC	intrinsically photosensitive retinal ganglion cell
IPSP	inhibitory postsynaptic potential
IV	Current-voltage relationship
K^+	potassium
KATP	ATP-sensitive potassium channel
K_{ca}	calcium-sensitive potassium channel
kHz	kilohertz
K_{ir}	irward-rectifier potassium channel
K_v	voltage gated potassium
L-AP4	L-2-amino-4-phosphonobutyric acid
LBD	Ligand-binding domain
Lc	lurcher
LCA	Leber's congenital amaurosis
LGIC	ligand-gated ion channel
LiGluR	light-gated glutamate receptor
L-SOP	L-serine-O-phosphate
LVA	low-voltage activated
m	meter
m^2	square-meter
MEA	multi-electrode array
mel	melanopsin
Mg^{2+}	magnesium
mGluR	metabotropic glutamate receptor
min	minute
MK-801	Dizocilpine
mm	millimeter
mM	millimolar
ms	millisecond
mV	millivolt
n	number
Na^+	sodium
NASP	1-naphthyl acetyl spermine
Na_v	voltage gated sodium
NBQX	2,3-Dihydroxy-6-nitro-7-sulfamoyl-benzo[*f*]chinoxalin-2,3-dion
NGS	normal goat serum
nm	nanometer
NMDA	N-methyl-D-aspartate
NpHR	Halorhodopsin from Natronomonas
NPY	neuropeptide Y
ns	nanosecond
o/n	over night
O_2	oxygen
ONL	outer nuclear layer
OPL	outer plexiform layer
opn4	melanopsin
p	pico
P	Postnatal day
P_2X	purinoreceptor
PBS	phosphate buffered saline
PCL	photochromic ligand
PDE	phosphodiesterase
PFA	para formaldehyd
PhENAQ	phenyl-ethyl aniline azobenzene quaternary ammonium
PI	photoswitch index
PTL	photochromic tethered ligand
q.v.	*quod vide*
RBP	rod bipolar cell
rd	retinal degeneration
RGC	retinal ganglion cell
rho	rhodopsin
RIS	rod inner segment
ROS	rod outer segment
RP	retinitis pigmentosa
RPE	retinal pigment epithelium
rs	red-shifted
rt	room temperature
s	second
SD	standard deviation

SEM	standard error of the mean
SR	sucrose Ringer
SRIF	somatostatin
STG	Stilbene Triazole Glutamate
TASK	tandem-pore domain potassium channel
TEA	tetraethylammonium
THIP	4,5,6,7-tetrahydroisoxazolo-5,4-cpyridin-3-ol
TKO	triple knock out
TMD	transmembrane domain
TMH	transmembrane helix
TPMPA	(1,2,5,6-tetrahydropyridin-4-yl)methylphosphinic acid
tra	transducin
TRP	transient-receptor potential
TTX	tetrodotoxin
UV	ultraviolet
V	volt
VDI	voltage-dependent inactivation
VGEF	vascular endothelial growth factor
VIP	vasoactive intestinale peptide
vis	visible
W	watt
w/	with
w/o	without
WHO	world health organization
wt	wild type

1 Introduction

1.1 The eye/retina

Human eyes are remarkable organs making it possible to sense the world around us in great detail. Vision is probably the most fundamental sense in humans and its loss is devastating.

In the late 19th century Ramón y Cajal was the first person describing neural cell types in the retina in comprehensive detail, providing essential information about their structures and building the basis for the future understanding of the retina's function (Masland 2001, Cajal 1893). Now, more than 100 years later, the retina is probably the best understood neural network in sensory neuroscience, however, many mechanisms remain unclear.

Visual perception underlies an astonishing system, which is capable of remarkable tasks, such as detecting single photons in the dark and, on the other hand, coping with more than 10^{16} photons cm^{-2} s^{-1} in bright sunlight.

1.1.1 Basic anatomy of the eye

The functional properties of the eye for transferring the image onto photoreceptor cells are the iris, pupil size, cornea and lens. Using these four features an inverted image is projected onto the retina.

The amount of light hitting the retina is controlled by the pupil size; the iris serves as an aperture, which is a contractile structure consisting mainly of smooth muscle. The iris is situated between the cornea and the lens in the anterior chamber of the eye. At bright light intensities the iris constricts, thereby decreasing the number of photons entering the eye and vice versa at low light intensities.

The refractive properties of the eye are determined by the cornea and the lens. While the cornea's curvature is fixed, the lens can be adjusted by smooth muscles. In relaxed mode the lens is flattened thereby bringing objects in the distance into focus. Together, cornea and lens are producing a sharp image on the level of photoreceptor cells, which are the integral part of the retina (Figure 1.1 A) (Squire et al. 2008).

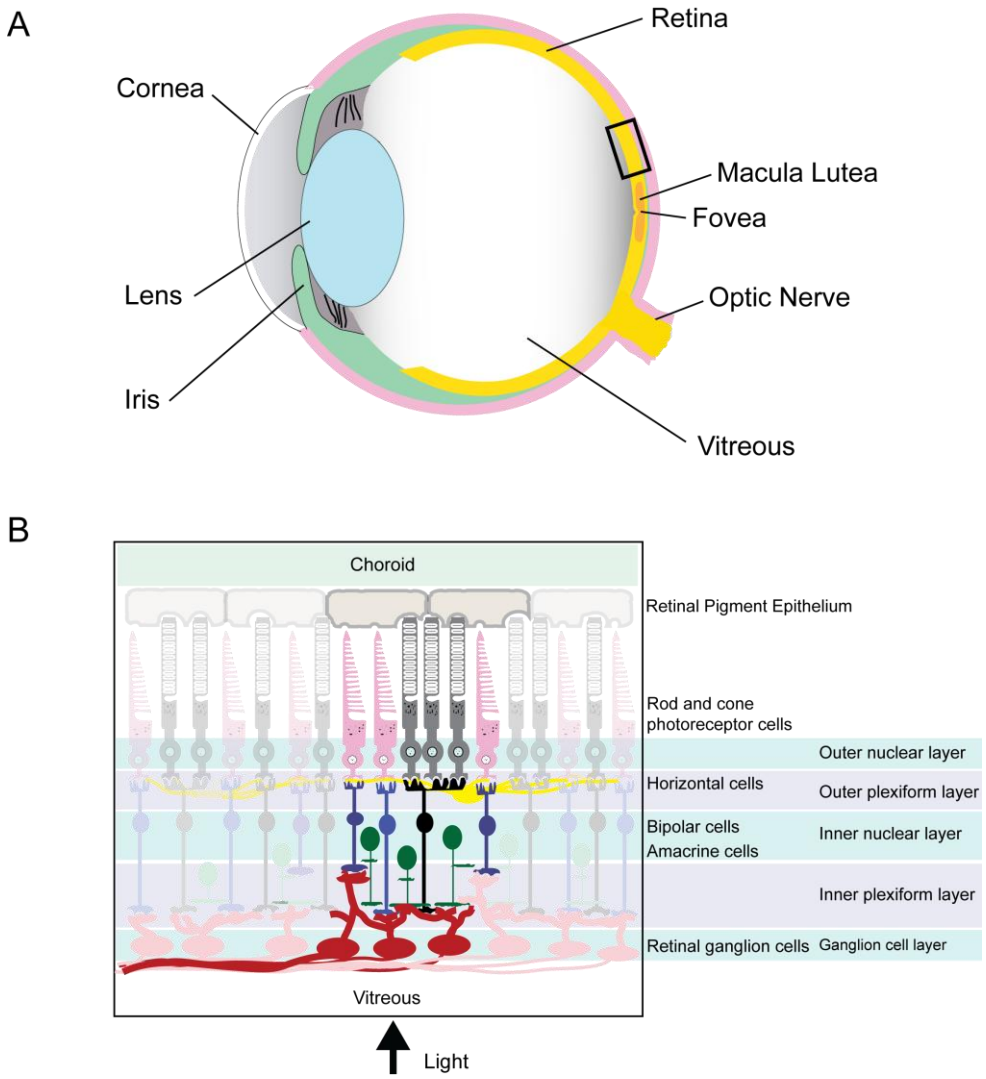

Figure 1.1 - Structure of the eye and the retina. (A) Schematic section of the human eye. Light enters the eye via the pupil, an aperture surrounded by the iris. The iris and pupil therefore control how much light enters the eye. The cornea and the lens focus the light onto the retina. The accommodation reflex controls the shape of the lens, thereby focusing on objects nearby or at greater distance. **(B)** Enlargement of the box in (A) with a schematic representation of the retina. Light is perceived by photoreceptor cells and transmitted to the brain via bipolar cells and retinal ganglion cells. Horizontal and amacrine cells provide lateral inhibitory input in the outer plexiform and inner plexiform layer, respectively.

1.1.2 Structure of the retina

The retina is the fundamental element responsible for light perception and image processing. Essentially, the retina is a biological extension of the brain, receiving its information directly from the outside and transmitting it to the brain. The retina has evolved to already process much of the information, thereby providing a first phase of computation and relaying the rest to higher brain regions (Hoon et al. 2014).

The retina is composed of five different cell types, divided in a vertical (photoreceptor, bipolar and retinal ganglion cells) and a lateral signaling pathway (horizontal and amacrine cells) (Figure 1.1 B). These cells are arranged in five distinguishable retinal layers: Three

layers of cell bodies (outer nuclear layer, ONL; inner nuclear layer, INL; ganglion cell layer, GCL) separated by two layers of neural processes, in which the cells interact via synaptic contacts (outer plexiform layer, OPL; inner plexiform layer, IPL). The only cell type bridging the two plexiform layers are bipolar cells by having processes in both, the IPL and OPL. Light hitting the retina needs to travel through all these layers until reaching the photoreceptor cells, which are in tight contact to the retinal pigment epithelium (RPE) (Figure 1.1 B). The ONL contains the cell bodies of rod and cone photoreceptor cells, while the INL contains cell bodies of interneurons, i.e. bipolar cells, horizontal cells and amacrine cells. Retinal ganglion cells (RGC) located in the innermost layer, the ganglion cell layer (GCL), provide the sole output of the retina. The axons of RGCs form the optic nerve, the pathway from the retina to the rest of the central nervous system (Figure 1.1 B).

1.1.3 Pathways/cell types in the retina

*Photoreceptor cells

Photoreceptor cells are neurons that transform light, an electromagnetic signal, into a chemical signal. Two different classes of photoreceptor cells evolved, rods and cones. In humans, rods and cones exhibit a distinct distribution pattern in the retina. While cones are almost exclusively located in the foveal region (Figure 1.1 B), rods are evenly distributed over the peripheral parts of the retina. The functional relevance is reflected by the physical properties of the respective photoreceptors and the synaptic connectivity of the photoreceptor cells. Rods are optimized for scotopic vision, i.e. under low light conditions, primarily contributing to peripheral vision and the detection of movements. Whereas they are able to detect single photons, they are not able to discriminate between colors. In contrast, cones are optimized for photopic vision, i.e. under bright light conditions, allow color perception and exhibit high spatial resolution. In an adult human retina approximately only 5 % of photoreceptor cells are cones and the remainder are rods (Curcio et al. 1990).
In humans only one type of rod photoreceptor and three different kinds of cone photoreceptors exist (trichromats). The absorption spectra of cones cover the electromagnetic spectrum from 380 nm (near UV light) to 760 nm (red light), i.e. the visible range: short wavelength cone (S-cone: absorption peaks at 420–440 nm), green (M-cone: 534–545 nm) and red (L-cone: 564–580 nm) cone photoreceptor. The spectral variation depends on the expression of different cone opsins (Nathans et al. 1986) (Figure 1.2). Usually less than 10 % to 15 % of all cones are S-cones and the remaining 80 % are M- and L-cones (Wikler and Rakic 1990, Wikler et al. 1990). For color perception at least two wavelengths need to be compared. Missing either the red or the green cone leads to the commonly known red-green blindness (dichromacy). This term, however, is misleading, since these people are not completely color-blind. They just cannot discriminate between red and green, but all other colors. With the exception of primates, all other mammals are

in principle dichromats, possessing one type of rod and two types of cone photoreceptor cells, one for shorter and one for longer wavelengths (Bowmaker 1998).

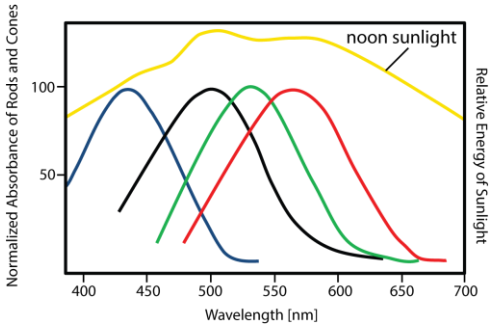

Figure 1.2 - Spectral sensitivity of rods and cones in primates. Blue: Short wavelength (S-) cones. Black: Rod photoreceptor. Green: M-cones. Red: L-cone. In yellow wavelength spectrum of daylight.

In addition to the previously described rod and cone photoreceptor cells, melanopsin has been described as a third class of photoreceptor cell. Melanopsin is expressed in intrinsically photosensitive retinal ganglion cells (ipRGCs), exhibits slow kinetics and do not contribute to normal visual perception, but are responsible to set the circadian rhythm (Foster et al. 1991).

*Phototransduction cascade

Photoreceptor cells in the outer retina consist of two major components, the inner segments and the outer segments. The inner segments comprise the nucleus, mitochondria and other important organelles and form the synaptic connections to bipolar and horizontal cells. In the outer segments of photoreceptor cells the molecular machinery for the phototransduction cascade is located (Figure 1.3) (Fu 2011, Pulagam and Palczewski 2011).

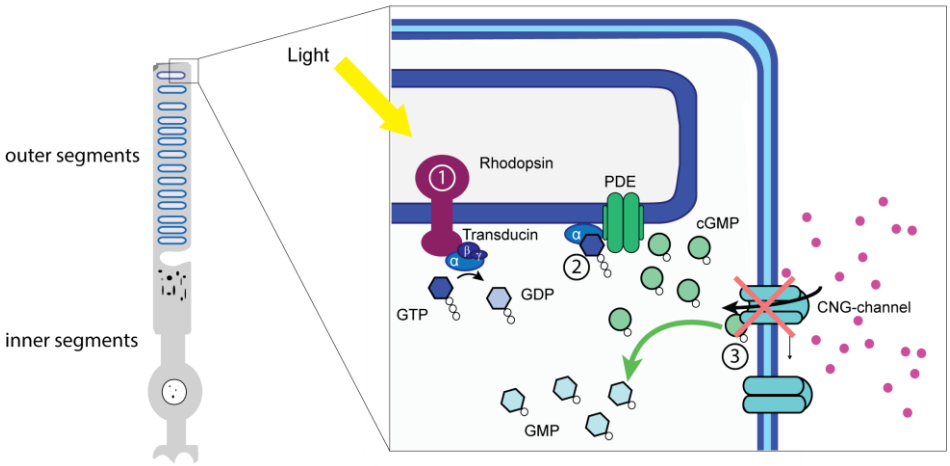

Figure 1.3 - Phototransduction cascade in rod photoreceptors. (1) Light activation of rhodopsin leads to the activation of the G-protein transducin. (2) The $G_{\alpha o}$ subunit of transducin activates the phosphodiesterase (PDE), resulting in a decreased level of cGMP. (3) Lower cGMP levels allow CNG-channels to close, thereby stopping the influx of cations (red circles) and hyperpolarizing the cell in light.

The different cone opsins are the essential parts for light perception. The detected wavelength depends on the cone opsin expressed, whereas rod photoreceptors only express one type of opsin, rhodopsin. Rhodopsin and cone opsins are holoproteins consisting of the apoprotein and a covalently bound 11-*cis* retinal via a protonated Schiff base (Wald 1968, Palczewski 2006). Upon illumination 11-*cis* retinal isomerizes to all-*trans* retinal, thereby inducing molecular changes in the opsin, which lead to the activation of an intracellular G-protein signaling cascade (Figure 1.3 - 1). Exchange of a G-protein (Transducin)-bound GDP for GTP leads to the dissociation of G_{α} and $G_{\beta\gamma}$ subunits. G_{α}(GTP) activates the phosphodiesterase (PDE), which in turn result in the hydrolyzation of cGMP to GMP (Figure 1.3 - 2). The reduction of intracellular cGMP levels leads to closure of cyclic nucleotide-gated cation channels (CNG-channels) in the outer segment membrane (*see* section 1.1.5 CNG-channels) (Figure 1.3 - 3). Thereby the photoreceptor cell hyperpolarizes and reduces the glutamate release; the neurotransmitter of photoreceptor cells. Taken together, incoming light leads to photoreceptor cell hyperpolarization and reduction in neurotransmitter release, while decrements of light lead to depolarization and increase neurotransmitter release (Squire et al. 2008).

*Principles of cone vision

The vertical pathway

Color perception is mediated by different types of cone photoreceptors, which are sensitive to specific wavelengths (*see* section 1.1.3 Photoreceptor cells). These cone photoreceptors are associated with different types of cone-driven bipolar cells, each of them possessing a specific function in visual processing. Bipolar cells are divided into two main classes, on- and off-bipolar cells. On-bipolar cells respond to light increments, while off-bipolar cells are activated by light decrements. Importantly, photoreceptor cells as well as bipolar cells respond to light with graded potentials rather than action potentials, due to constant stimulation of either the on- or off-pathway.

In darkness photoreceptor cells constantly release glutamate from their synapses to bipolar cells, the so-called 'dark current' (Trifonov 1968). Light stimulation, in contrast, leads to a hyperpolarization in photoreceptor cells and less glutamate release due to a decrease in cGMP levels. Depending on bipolar cell type the change in glutamate release is detected either as an on- or an off-response (Figure 1.4). The polarity of the light response is determined by the subtype of glutamate receptor expressed in the bipolar cell dendrites (Kolb et al. 2001). On-bipolar cells become depolarized upon less glutamate release from photoreceptor cells. This signal is processed via the metabotropic glutamate receptor mGluR6. In darkness, mGluR6 is activated in on-bipolar cells leading to the closure of TRPM1 channels via $G_{\alpha o}$ and therefore to hyperpolarization (Figure 1.4 A). Therefore less glutamate release from photoreceptor cells during light stimulation reduces the stimulation of mGluR6, thereby activating TRPM1 channels, which depolarizes the on-bipolar cell. In

contrast, glutamate release from photoreceptor cells onto off-bipolar cells leads to the activation of non-NMDA receptors (AMPA and kainate receptors). This leads to a depolarization of off-bipolar cells in darkness and no stimulation during light (Figure 1.4 B).

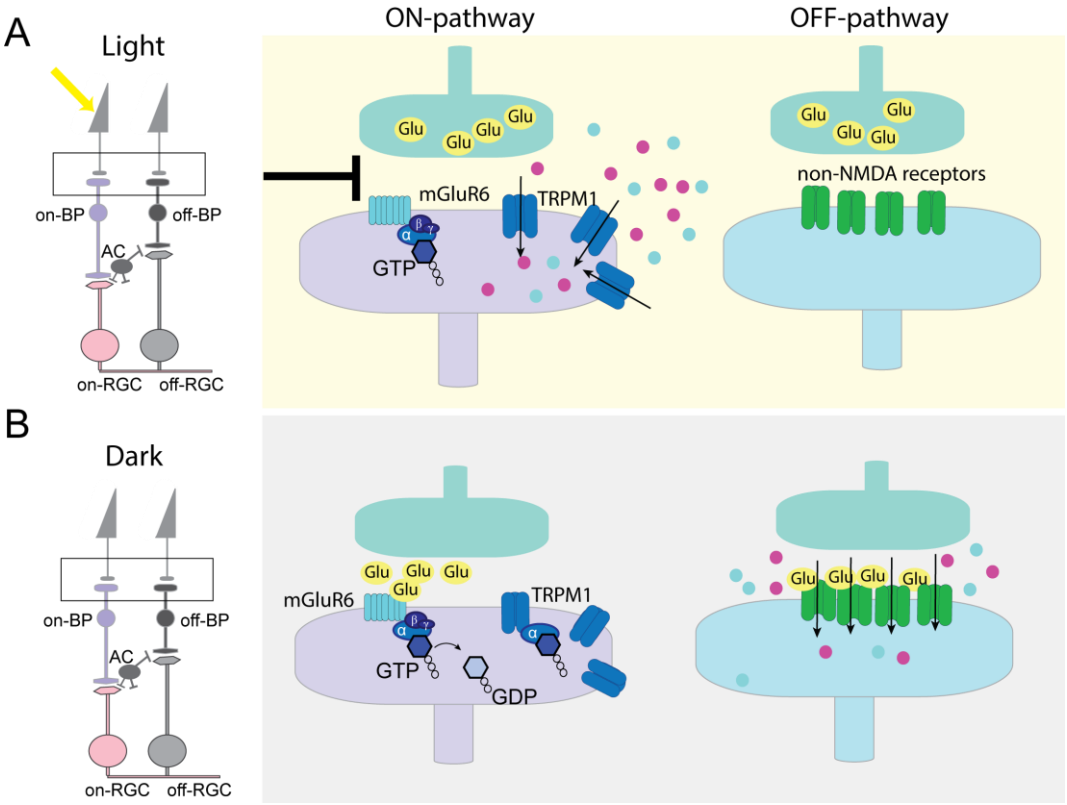

Figure 1.4 - Bipolar cell light responses. (A) On- and off-bipolar cell responses during a light flash. Left: Schematic drawing of the retina. Right: Enlargement of photoreceptor to bipolar cell synapse. In on-bipolar cells expression of mGluR6 leads to an inversion of the photoreceptor cell stimulus. Hyperpolarization of photoreceptor cells during light prevents the activation of mGluR6, thereby allowing TRPM1 to open and to depolarize the on-bipolar cell (i.e. influx of cations). The off-pathway is determined by the expression of non-NMDA receptors, thereby less glutamate during light stimulation induces less activation of the off-bipolar cell (i.e. no current through non-NMDA receptors). **(B)** Same structure as in (A). In darkness, glutamate is released from photoreceptor cells, thereby activating mGluR6 (on-bipolar cell) and non-NMDA receptors (off-bipolar cells).

Cone bipolar to RGCs signal transmission is directly mediated via ionotropic glutamate receptors (iGluRs). RGCs can be divided into three different classes: On, off and on/off RGCs depending on the bipolar cells they are connected with. On-RGCs receive glutamatergic input during illumination of their receptive fields and therefore depolarize, while off-RGCs are depolarized in darkness (Figure 1.5 top). When light is applied surrounding the receptive fields, on-RGCs are inactivated during the stimulation and depolarize after switching light off. Off-RGCs, however, become depolarized with peripheral applied light stimulation (Figure 1.5 bottom). RGCs responding to light on as well as light off within their receptive fields are connected to both types of bipolar cells, therefore receive both stimuli. Importantly, RGCs are not only the sole output of the retina, but are

also the only cell type of the vertical pathway, which transmits its signals with action potential firing (Chaudhuri 2011).

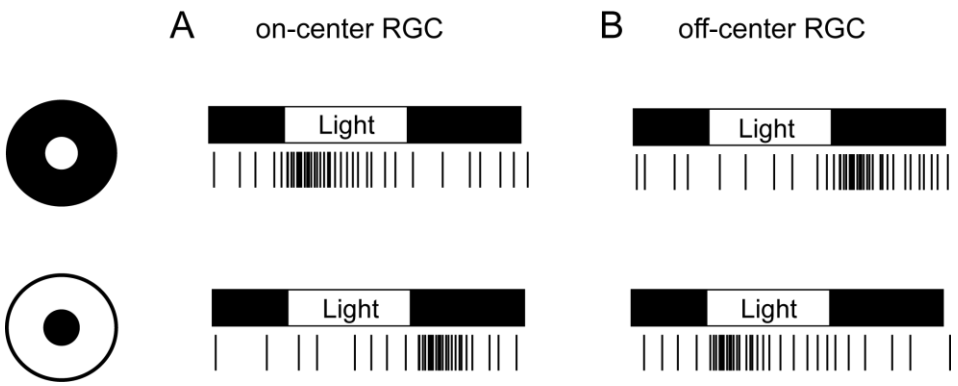

Figure 1.5 - Receptive field properties of RGCs. Left: Schematic representation of light stimulation shape. (A) On-center/off-surround RGC response. When flashing a spot of light in the receptive field, the spontaneous firing rate increases. A light flash to the surrounding area of the receptive field does not change spontaneous firing rate of the RGC, however, when light is switched off, the spiking frequency transiently increases. **(B)** Off-center/on-surround RGC response. The RGC responds to the same stimulation as in (A) with the exact opposite in firing pattern. Bars indicate light protocol and raster plots show the spiking activity of the RGCs.

In the human fovea the retinal cells underwent an additional specialization. The fovea is located in the macula lutea of the retina (Figure 1.1), and is composed of cone photoreceptor cells only, which are densely packed. Each cone photoreceptor in the fovea is in general connected to a single bipolar cell (midget bipolar cell), which are again connected almost solely to a single midget RGCs (Kolb and Dekorver 1991, Kolb and Marshak 2003, Adams et al. 2013). Midget RGCs represent around 70% of all RGCs and are therefore the most numerous of all RGCs. This specialized structure in the focal point of the retina allows a point-to-point resolution of the image only limited by the packing density of the cone photoreceptor cells .

The lateral pathway: Horizontal and amacrine cells

Horizontal cells are the interneurons of the outer retina, which modulate the synaptic activity between photoreceptor and bipolar cells (Figure 1.1 B). As their name already indicates, horizontal cells span laterally over a large area. They provide diverse feedback signals, such as gain adjustment of photoreceptor synaptic output or lateral surround inhibition to improve spatial resolution (Thoreson and Mangel 2012, Baylor et al. 1971). In most mammals, horizontal cells are divided into two morphologically distinct cell types, which are both GABAergic and feed back onto cone axon terminals in the center of the bipolar cell's receptive field.

In addition to center-surround modulation between cone photoreceptor and bipolar cells, it has also been demonstrated, that receptive field surround responses are dramatically shaped by amacrine cell inputs in the inner retinal circuits (Lukasiewicz 2005, Zhang and Wu 2009) (Figure 1.1 B). To date, more than 30 different morphological subtypes of

amacrine cells have been classified (Cherry et al. 2009). These can be structurally divided into four distinct groups by both, their dendritic field diameter (narrow-field, small-field, medium-field and wide-field) and by their stratification (Kolb et al. 1981, Masland 2001). Most amacrine cells use either GABA or glycine as their neurotransmitter. However, it has been shown, that some amacrine cell types co-release, acetylcholine and GABA, and are therefore not exclusively inhibitory interneurons (O'Malley et al. 1992). Besides the major amacrine cell neurotransmitters GABA, glycine and acetylcholine, eight other neurotransmitters are released, including several neuropeptides (*see* section 1.1.4 Neuropeptides) (Squire et al. 2008). In contrast to horizontal cells, amacrine cells exhibit much more specialized functions, with each amacrine cell type connecting to a particular type of bipolar cell. Although great progress has been made in the understanding of amacrine cell function, most of the amacrine cell mediated interactions are still poorly understood (Chaudhuri 2011).

Taken together, horizontal and amacrine cells mediate lateral inhibition in the OPL between photoreceptor and bipolar cells, and in the IPL between bipolar and retinal ganglion cells, respectively.

*Principles of rod vision

The retina is able to cover changes in light level by a factor of 100,000,000, from starlight (10^{-3} cd/m^2) to bright sunlight 10^5 cd/m^2 (Heeger 2015). Whereas cone photoreceptors are responsible for vision under bright daylight conditions (>3 cd/m^2), rod photoreceptors are able to detect single photons and transmit light below approximately 0.01 cd/m^2. In most mammalian retina, rod photoreceptor cells outnumber cone photoreceptor cells by approximately 20-fold, but cone bipolar cells outnumber rod bipolar cells (Martin and Grunert 1992, Strettoi and Masland 1995, Curcio et al. 1990). The reason for this phenomenon is, that many rod photoreceptor cells converge onto a single rod bipolar cell. Therefore, the rod system trades acuity for sensitivity. In addition, rods evolved after cones and piggyback on the cone visual system. Rod photoreceptor cells do not directly transmit their signal via rod bipolar cells to RGCs, but instead use an indirect route via AII amacrine cells to the axon terminals of cone bipolar cells (Figure 1.1 B) (Famiglietti and Kolb 1975). Therefore, a single set of RGCs can be used under daylight and starlight conditions and the network did not have to be reinvented for the additional rod pathway. Furthermore, the rod system is much simpler compared to the cone pathways. Only one type of rod photoreceptor cell exists, which exclusively synapse onto a single type of rod bipolar cell (Cajal 1893, Bloomfield and Dacheux 2001).

Interestingly, not only the vertical rod pathway is build on the preexisting cone pathway, but also rod photoreceptors take advantage of preexisting horizontal cells. In the OPL, rod photoreceptors have contact to a specialized horizontal cell (b/H2 type), which synapse to both, cone and rod photoreceptors. Synaptic connections between cone photoreceptors

and horizontal cells are made over large dendritic areas and induce lateral inhibition over a wide range of neighboring cones. Rod photoreceptors, on the other hand, make synaptic connection far away from the horizontal cell's soma and are isolated within the dendritic tree. Therefore, lateral inhibition between rod photoreceptors is not influencing the lateral inhibition between cones, although both use the same horizontal cell (Nelson et al. 1975).

1.1.4 Neurotransmitter receptors in the retina

This section covers some of the important neurotransmitter receptors in the retina and is not meant to be a comprehensive review of all neurotransmitter receptors in the retina.

***Glutamate receptors**

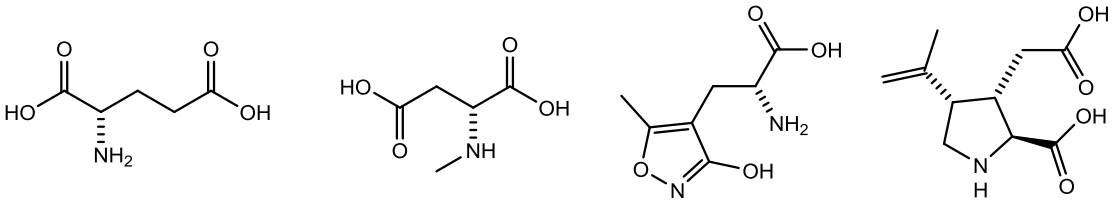

Glutamate NMDA AMPA Kainate

The synaptic connections in the retina, which shape the vertical pathway from photoreceptors via bipolar cells to RGCs are entirely mediated by glutamate (Thoreson and Witkovsky 1999). Two distinct classes of glutamate receptors contribute to this pathway, (i) ionotropic and (ii) metabotropic glutamate receptors.

Ionotropic glutamate receptors (iGluRs)

Ionotropic glutamate receptors (iGluRs) are classified according to their specific agonists into NMDA, AMPA and kainate receptors. They are composed of an extracellular amino-terminal domain (ATD), a transmembrane domain (TMD) and a ligand binding domain (LBD). The ATD is responsible for receptor assembly, trafficking and localization, whereas the TMD builds a four-fold symmetrical pore structure of 16 helices. The LBD has a two-fold symmetry, the so-called clamshell domain. Binding of glutamate leads to a conformational change that closes the clamshell, resulting in a tightly bound glutamate and opening of the non-selective cation channel.

Non-NMDA (AMPA and kainate) receptors act as non-selective cation channels upon activation and are more permeable to sodium (Na^+) and potassium ions (K^+) compared to calcium ions (Ca^{2+}). Competitive antagonists are CNQX (6-cyano-7-nitroquinoxaline-2,3-dione), NBQX (1,2,3,4-tetrahydro-6-nitro-2,3-dione-benzoquino-xaline-7-sulfonamide), and DNQX (6,7-dinitroquinoxaline-2,3-dione) (Alford and Grillner 1990, Goldstein and Litwin 1993). GYKI52466 has been shown to be a potent non-competitive antagonist for non-

NMDA receptors (Donevan and Rogawski 1993, Solyom and Tarnawa 2002).

NMDA receptors, like non-NMDA receptors, form non-selective cation channels. However, they comprise three special features compared to non-NMDA receptors: (i) they have a higher permeability to Ca^{2+}, (ii) for full activation they require in addition to glutamate binding to GluN2 subunits, a co-agonist (either glycine or D-serine) binding to the GluN1 subunits of the heterotetramer (Stevens et al. 2003, Johnson and Ascher 1987); (iii) they exhibit a voltage-dependent block by magnesium ions (Mg^{2+}) at membrane resting potential. Therefore these channels can act as a coincidence detector of presynaptic glutamate release and postsynaptic depolarization (Nowak et al. 1984, Mayer et al. 1984). In addition, this mechanism is thought to prevent NMDA receptor-mediated excitotoxicity (Nowak et al. 1984). Several antagonists are available, which act on different sites of the receptor: (i) D-AP5 (competitive glutamate site antagonist), (ii) 7-Cl-kynurenate (competitive glycine site antagonist), (iii) MK-801 (channel blocker).

In the retina non-NMDA receptors play a significant role not only for signaling between photoreceptor cells and off-bipolar cells (Figure 4B), but have also been identified in horizontal, amacrine and RGCs (Gilbertson et al. 1991, Zhou et al. 1993, Boos et al. 1993, Cohen and Miller 1994, Yu and Miller 1995). NMDA receptors are expressed to a lesser extend compared to non-NMDA receptors and were primarily detected in RGCs as well as subsets of amacrine cells. In very few species, NMDA receptors were also found in horizontal and bipolar cell subtypes, but their specific functions in these cell types remain to be elucidated (Shen et al. 2006).

The distribution of NMDA and non-NMDA receptors in the retina is thought to strongly influence signal transmission. NMDA receptors mediate rather slow sustained light-responses, while non-NMDA receptors are in principle responsible for a more transient light-response transmission (Shen et al. 2006, Ozawa et al. 1998).

Metabotropic glutamate receptors

Metabotropic glutamate receptors (mGluRs) belong to the group C family of G-protein coupled receptors (GPCRs) and are structurally and physiologically very different from iGluRs. Each mGluR consists of a single protein chain and does not form an integral ion channel pore, but activates second messenger cascades. These cascades mediate various intracellular responses, such as release of Ca^{2+} from intracellular stores or inhibition of adenylyl cyclase (AC) (Squire et al. 2008). Overall eight mGluRs have been cloned so far, which can be divided into three distinct groups, depending on their agonist or activated second messenger system: Group I (mGluR1 and mGluR5), group II (mGluR2 and mGluR3) and group III (mGluR4, mGluR6, mGluR7 and mGluR8) (Conn and Pin 1997, Niswender and Conn 2010). Receptors of group I respond most strongly to L-quisqualate, those of group II react to DCG-IV (dicarboxycyclopropyl), while L-SOP and L-AP4 selectively activates receptors of group III.

In the retina all mGluR subtypes have been detected, except for mGluR3 (Koulen et al. 1996, Koulen et al. 1997). Most mGluRs are expressed in the IPL or in both the IPL and OPL. The only exception is the mGluR6 receptor, which has been shown to be exclusively expressed in the OPL or more precisely, in on-bipolar cell dendrites. This specific expression pattern was further explored in studies of mGluR6 knock-out mice, which revealed that this receptor is mandatory for synaptic transmission from photoreceptors to on-bipolar cells (Masu et al. 1995, Nomura et al. 1994). More recent studies on the sign-inverting intracellular pathway of on-bipolar cells discovered, that mGluR6 activation leads to the inhibition of the transient receptor potential cation channel TRPM1 (Figure 1.4 A) (Xu et al. 2012, Shen et al. 2012). The majority of mGluRs, however, are less specific than mGluR6 and are mostly found postsynaptically to off- and on-cone bipolar cells (Brandstatter et al. 1996, Koulen et al. 1996, Koulen et al. 1997).

*Neurotransmitters of inhibitory pathways

GABA receptors

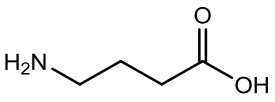

GABA

Gamma-aminobutyric acid (GABA) is the major inhibitory neurotransmitter in the vertebrate retina. Most lateral interactions by amacrine cells and horizontal cells are mediated by GABA in the inner and outer retina, respectively. GABA receptors are divided into three functional families, the ionotropic $GABA_A$ and $GABA_C$ receptors and the metabotropic $GABA_B$ receptors (Chebib and Johnston 1999).

$GABA_A$ receptors are ligand-gated chloride (Cl^-) channels mediating fast inhibition in a wide distribution of neurons throughout the central nervous system (CNS). In the retina $GABA_A$ receptors have been found to be ubiquitously expressed throughout all retinal cell types (Wassle et al. 1998, Feigenspan and Weiler 2004, Yang 2004). Specific $GABA_A$ activation is achieved using either muscimol or THIP (4,5,6,7-Tetrahydroisoxazolo5,4-*c*pyridin-3-ol) and can be blocked by bicuculline or the unselective chloride channel blocker picrotoxin. In addition, modulation of $GABA_A$ activation is possible by benzodiazepines, barbiturates, ethanol or steroids (Johnston 1996, Moehler et al. 2010).

Like $GABA_A$ receptors ionotropic $GABA_C$ receptors are permeable for chloride (Cl^-) ions, but mediate rather slow and sustained responses compared to $GABA_A$ receptors (Lukasiewicz et al. 2004). Until today no selective agonist have been identified for $GABA_C$ receptors. Effective antagonists of $GABA_C$ activation are 1,2,5,6-Tetrahydropyridin-4-

yl)methyl-phosphinic acid (TPMPA), THIP and picrotoxin, with only one exception: In the mammalian retina $GABA_C$ receptors are only slightly blocked by picrotoxine (Ragozzino et al. 1996, Zhang et al. 1995, Johnston et al. 2003, Feigenspan et al. 1993). In addition, $GABA_C$ receptor mediated currents can be modulated by divalent cations, in particular by low concentrations of zinc ions (Wang et al. 1995).

Metabotropic $GABA_B$ receptors, in contrast to ionotropic GABA receptors, mediate responses indirectly via G-proteins, which activate potassium or calcium channels. G-protein mediated signaling not only provides the possibility of signal amplification, but can also induce intracellular changes, such as the reduction of AC activity. To date, the only specific agonist and antagonist for $GABA_B$ receptors identified, are baclofen and phaclofen, respectively (Bettler et al. 2004).

In contrast to $GABA_A$ receptors, $GABA_B$ and $GABA_C$ receptors are found only in subsets of retinal neurons and are not ubiquitously distributed. In addition, $GABA_C$ receptors have also predominantly been found in the vertebrate retina compared to the remaining CNS, reinforcing a more important role of $GABA_C$ receptors for signal processing in the visual system (Lukasiewicz 1996, Lukasiewicz et al. 2004).

Glycine receptors

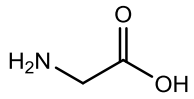

Glycine

Glycine is the second most important inhibitory neurotransmitter in the mammalian retina. Glycine receptors are ligand-gated chloride channels, hyperpolarizing the postsynaptic membrane in mature neurons upon ligand binding. Complete block of the glycine receptor ion channel can be achieved with the competitive antagonist strychnine, while no agonist or potentiating compounds are known to be selective for glycine receptors (Betz and Laube 2006, Webb and Lynch 2007). About half of the amacrine cells in the mammalian retina, which synapse onto bipolar cells, other amacrine cells and RGCs, are glycinergic. The most prominent glycinergic amacrine cells are small-field amacrine cells, which network within the different sublayers of the IPL, as well as AII amacrine cells, which transmit the signal from rod bipolar cells to RGCs via cone bipolar cell axon terminals (Menger et al. 1998). Overall glycine receptors are widespread throughout the retina and have been identified in all retinal cell types (Lam 1997, Balse et al. 2006).

Dopamine receptors

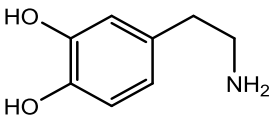

Dopamine

Dopamine is a slow modulator of the fast neurotransmission mediated by glutamate and GABA. Five different dopamine receptors have been identified (D1-D5), which all belong to the group of GPCRs (Beaulieu and Gainetdinov 2011). They can be further divided into two major groups, namely D1 and D2 (Andersen et al. 1990). D1 receptor subtypes (D1 and D5) generally stimulate the AC via $G_{\alpha s}$ or $G_{\alpha o}$ proteins, thereby indirectly activating cAMP-dependent kinases (Spano et al. 1978, Tiberi et al. 1991). D2 dopamine receptor subtypes (D2, D3, D4) on the other hand inhibit the AC generally via $G_{\alpha i}$ proteins (Kebabian and Calne 1979, Niznik and Van Tol 1992). In addition to G-protein mediated signaling, it has been shown that dopamine receptors also connect to a G-protein independent signaling pathway, namely the late D2-arrestin mediated signaling. This pathway is involved in important cellular functions such as actin cytoskeletal rearrangement and cell migration (Luttrell et al. 1999, Luttrell and Lefkowitz 2002, Luttrell and Gesty-Palmer 2010).

In the mammalian retina the presence of dopamine has been identified by Tyrosine hydroxylase (TH) immunostaining in a specific set of amacrine cells, with the most prominent staining in A18 amacrine cells (Kolb et al. 1991, Witkovsky 2004, Kolb et al. 1981, Tauchi et al. 1990). Dopamine receptors of the D1- and D2-families are expressed widely throughout the retina and have been recognized in rod and cone photoreceptor cells (D2 family), as well as in bipolar, horizontal, amacrine and RGCs (D1 family) using autoradiography and immunocytochemistry (Muresan and Besharse 1993, Veruki and Wassle 1996, Nguyen-Legros et al. 1997, Witkovsky and Schutte 1991). In amacrine cells, which release dopamine, only D1 dopamine receptors are expressed. Their function is auto-inhibitory (autoreceptors), i.e. dopamine bound to the receptor leads to less dopamine release (Dubocovich and Weiner 1985). In the rod pathway dopaminergic neurons synapse onto AII and A17 amacrine cells, but also bipolar cells have been shown to be negatively affected by dopamine (Hampson et al. 1992).

Acetylcholine receptors (AChRs)

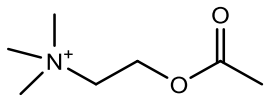

Acetylcholine

Acetylcholine (ACh) is a classic neurotransmitter for fast excitatory neurotransmission in the nervous system, where it can bind to two very different types of receptors, muscarinic and nicotinic AChRs (mAChR and nAChR, respectively). Muscarinic AChR are named as such, because they are more sensitive towards muscarine than nicotine and all mAChRs belong to the class of GPCRs. They are not only expressed in various types of neurons, but also in other cells, such as smooth muscle cells. Nicotinic AChRs (nAChRs), on the other hand, are more sensitive to nicotine and form non-selective cation channels. Although nAChRs are permeable to most cations, such as Na^+, K^+ and Ca^{2+}, monovalent cations are preferred (Squire et al. 2008). To date, 12 different genes have been cloned forming a heterogeneous family of pentameric receptors (Le Novere et al. 2002). In general, two main classes of nAChR subunits are distinguished: (i) α-subunits, which are responsible for ACh-binding, and (ii) other subunits (β,γ,δ) which are not able to bind the agonist, but contribute to the binding affinity (Lindstrom et al. 1996, Corringer et al. 2000).

In the vertebrate retina two types of ACh-releasing amacrine cells ("starburst") have been described, of which one has its cell body in the amacrine cell layer (ACh-b type), and the other is located more in the RGC layer (ACh-b type) (Masland and Tauchi, 1986). Both ACh-type amacrine cells exhibit a two mirror symmetry and importantly, co-release GABA, implying two different functionalities (Vaney and Young 1988, Brecha et al. 1988). ACh-type amacrine cells receive input from various sites, including cone bipolar cells and other amacrine cells. The only site of synaptic output, however, is through distal dendrites onto RGCs. Both, ACh-a and ACh-b type amacrine cells connect to ON-OFF directional selective RGCs, while ACh-b type amacrine cells additionally synapse to ON-directionally selective RGCs (Amthor et al. 1984, Amthor et al. 1989, Famiglietti 1987, Tauchi and Masland 1984, Vaney 1994, Famiglietti 1991, Briggman et al. 2011).

In addition, it has been demonstrated that the earliest stages of development, before phototransduction and during neural outgrowth and synaptogenesis, critically rely on spontaneous bursting activity (retinal waves) induced by ACh-neurotransmission (Bansal et al. 2000). These retinal waves have been shown to be necessary for correct size and complexity of RGC dendrites as well as for the refinement of connections between retinal axons and higher brain regions (Wong 1999, Feller 2002, Moretti et al. 2004).

*P2X receptors

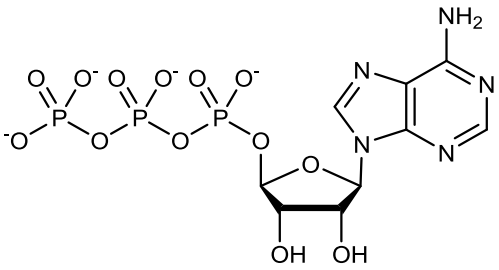

Adenosine-5'-triphosphate

Purinergic P2X receptors are ligand-gated ion channels, which are activated by extracellular adenosine-5'-triphosphate (ATP). Although it was believed for a long time that P2X receptors play only a minor role in direct signal transmission, their indispensability for neural activity becomes more and more evident. In the CNS P2X receptors were shown to mediate fast synaptic transmission in addition to their several regulatory functions (Buell et al. 1996, Brake and Julius 1996). Therefore, ATP is now a well established extracellular neurotransmitter for fast synaptic transmission (Evans et al. 1992).

To date, eight P2X receptor subunits have been cloned, $P2X_{1\text{-}7}$,P2XM, of which four are expressed in retinal neurons ($P2X_{2\text{-}5}$) (Brandle et al. 1998). P2X mRNA was detected in various cell types of the retina, including photoreceptors, neurons of the outer nuclear layer and RGCs (Greenwood et al. 1997). ATP as well as adenosine were reported to not only influence ACh-release from amacrine cells, but P2X receptor activation is also correlated with GABAergic, glutamatergic, glycinergic, dopaminergic and serotonergic neurotransmission (Blazynski and Perez 1991, Feigenspan and Bormann 1994, Brandle et al. 1998). Although substantial progress has been made in the past decade, many effects of extracellular ATP on visual processing still remain unclear.

*Neuropeptides

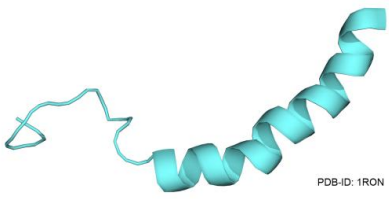

Neuropeptide Y

Neuropeptides are small polypeptides, varying in length between 3 and 36 amino acids. They can act either endocrine as neurosecretory peptide hormons or paracrine as co-transmitters, which are almost always co-released with classical neurotransmitters (Lundberg 1996). In the mammalian brain about 100 different neuropeptides have been

characterized influencing all sets of different brain functions including metabolism, reward and learning and memory (neuropeptides). In addition, neuropeptides and their receptors have been shown to play an important role during the maturation of the nervous system (Hoyer and Bartfai 2012).

In the retina most neuropeptides appear early in development, when synaptic connections are still immature; and exhibit transient features, which mature with eye opening (Bagnoli et al. 2003). During this period neuropeptides are believed to induce several direct and indirect effects, including cell division, neuronal survival and neurite sprouting (Emerit et al. 1992, Muller et al. 1995, Bagnoli et al. 2003, Akiyama et al. 2008). In the mature retina, neuropeptides have been shown to be expressed in amacrine cells and RGCs in the inner retina. Neuropeptide receptors, however, have been found in a wide distribution among several retinal cell populations. This finding suggests, that neuropeptides act in a more paracrine manner, thereby influencing retinal circuits in a more general mode. In this context, recent studies demonstrated that neuropeptides in the retina not only influence neurotransmitter release directly, but also have an impact on cellular activity of bipolar, amacrine and RGCs (Bruun and Ehinger 1993, Zalutsky and Miller 1990b, Zalutsky and Miller 1990a). In the mammalian retina several peptidergic systems have been identified, including tachykinin peptides, vasoactive intestinal peptide (VIP), PACA, somatostatin (SRIF), neuropeptide Y (NPY), opioid peptides and others, all of which are summarized in great detail elsewhere (Bagnoli et al. 2003, Akiyama et al. 2008, Casini 2005).

1.1.5 Ion channels in the retina

This section, as the one before, is only a short summary of some important ion channels in the retina and is not meant to be a comprehensive review.

*Voltage-gated sodium (Na_v) channels

Voltage-gated sodium (Na_v) channels are integral membrane proteins essential for action potential initiation and propagation in excitable cells. They are composed of a large pore-forming α-domain and smaller auxiliary β-subunits. Overall nine sodium channel α-isoforms have been identified in mammals ($Na_v1.1$-1.9), with each consisting of a long polypeptide chain organized into four domains. Each of the four domains has six transmembrane helices (TMH) and are connected via intra- and extracellular loops (Figure 1.6) (Dib-Hajj and Priestley 2010). The voltage sensor is located in TMH S4, which contains a positively charged amino acid in every third position.

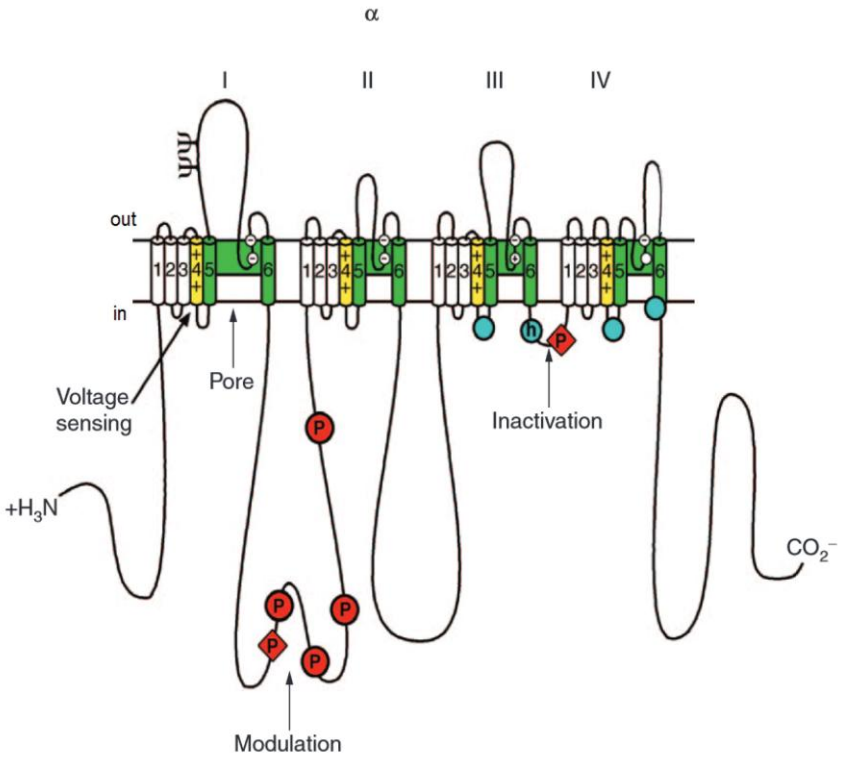

Figure 1.6 - Schematic representation of the sodium-channel subunits. Roman numerals indicate the domains of the α subunit (I-IV); segments 5 and 6 (shown in green) are the pore-lining segments and the S4 helices (yellow) make up the voltage sensors. The blue circles in the intracellular loops of domains III and IV indicate the inactivation gate motif h, its inactivation gate; P, phosphorylation sites for either PKA (red circles) or PKC (red diamonds); The circles in the re-entrant loops in each domain represent the amino acids that form the ion selectivity filter (the outer rings have the sequence EEDD and inner rings DEKA). (Adapted from(Yu and Catterall 2003))

The central pore is generally opened by an increase in membrane potential up to –30 mV to –20 mV and pore block can be achieved by various types of neurotoxins. All together six different neurotoxin receptor sites have been identified and the most prominent Na_v blockers are tetrodotoxin (TTX) and saxitoxin (STX), which both block via neurotoxin receptor site 1 (Catterall et al. 2005). Na_v-channels can exist in three different states, (i) closed, (ii) open and (iii) inactivated. The open state of the channel usually lasts less than 1 ms after which the channel becomes quickly inactivated. This inactivation is due to the movement of a globular portion containing the hydrophobic cluster of amino acids in the III-IV linker region, the IFMT motif ('ball-and-chain' mechanism), which occludes the channel pore. Only when the membrane potential repolarizes, the block is relieved and the channel is back in its closed-state, ready for a new activation (Goldin 2003). In addition, the intracellular C-terminal domain has been shown to play a role in fast-inactivation as well as modulation by accessory β subunits was reported (Zimmer and Benndorf 2002, Chen and Cannon 1995, McCormick et al. 1998, McCormick et al. 1999).

In the retina Na_v channels are primarily expressed in RGCs, the sole output of the retina, and are responsible for inducing and propagating action potentials. However, some amacrine cell types, such as AII and dopaminergic A18 amacrine cells, are able to induce TTX-sensitive spike-like potentials as well (Miller et al. 2002, Boos et al. 1993, Feigenspan

et al. 1998). Interestingly, Na_v channels have also been found in retinal cells, which are not able to fire action potentials, such as A17, starburst amacrine cells (Hartveit 1999, Cohen 2001), cone bipolar cells (Pan and Hu 2000, Zenisek et al. 2001, Ichinose et al. 2005) and cone photoreceptor cells (Ohkuma et al. 2007). The specific role of Na_v currents in these cell types remain to be elucidated. Recent work, however, could demonstrate that Na_v channels in these cell types are important for adjusting the sensitivity over a wide range of illuminations and that they are directly involved in amplifying the light response of cone bipolar cells (Smith et al. 2013).

*Voltage-gated potassium channels

Voltage-gated potassium channels belong to a large family of potassium channels comprising the classic voltage-gated (K_v), Ca^{2+}-activated (K_{Ca}), inward-rectifier (K_{ir}), tandem-pore domain (K_2P) and ATP-sensitive (K_{ATP}) channels (Coetzee et al. 1999, Szabo et al. 2010).

Based on their membrane topology with two, four and six membrane spanning domains, potassium-channels can be subdivided into three groups,. wherein K_v-channels belong to the last group with six transmembrane domains (S1-S6). A single K_v-channel is formed by four of these subunits. Transmembrane segments S5 and S6 of each subunit are connected to the pore loop, being responsible for ion selectivity and gating, while S4 confers membrane voltage sensitivity (Figure 1.7 A) (MacKinnon and Yellen 1990, Yool and Schwarz 1991). In vertebrates at least 8 different subfamilies have been described, which show this typical structure, containing the voltage sensor domain (S4), toxin binding sites and a single ion-conducting pore (Lehmann-Horn and Jurkat-Rott 1999). Interestingly, K_v-channels are found in both excitable and non-excitable cells and are responsible for a variety of different functions. Not only do they control membrane resting potential and influence the frequency of action potential firing, but they are also important for neural development and have shown to be regulators of programmed cell death (Jan and Jan 1997, Augustine 1990, McFarlane and Pollock 2000, Szabo et al. 2010, Pollock et al. 2002, Zhong et al. 2013).

Under normal conditions K_v-channels open upon depolarization and inactivate relatively fast even with prolonged stimulation. To date, two inactivation mechanism have been characterized: (i) N-type inactivation and (ii) P/C-type inactivation. The N-type inactivation is achieved through the cytoplasmic N-terminal domain that acts as a blocking peptide entering the channel pore. This model is also called 'ball-and-chain' mechanism and is relatively fast (Aldrich 2001, Hoshi et al. 1990). The P/C-type mechanism has not been fully understood, but the basic principle of this deactivation is a time-dependent conformational change that reduces the pore opening (Hoshi et al. 1991).

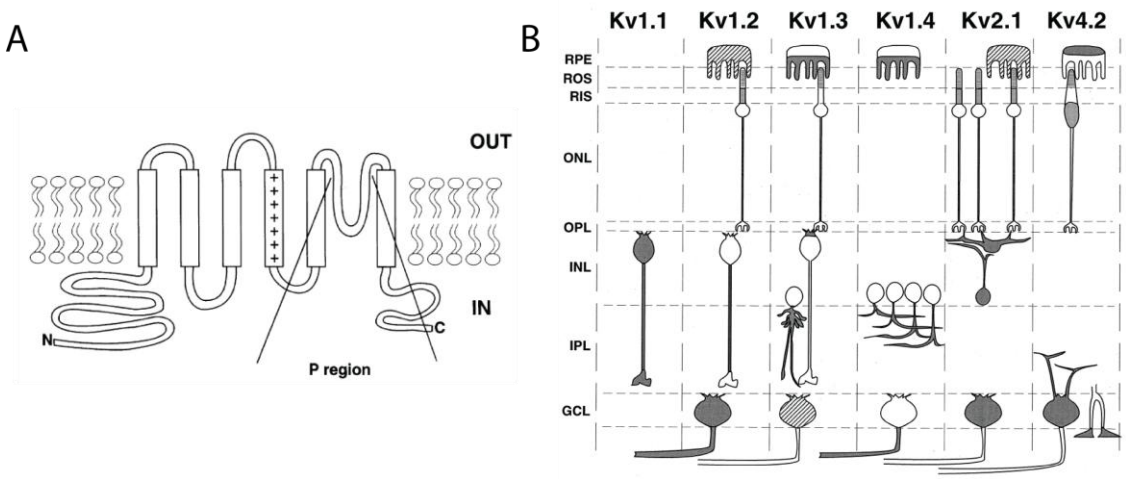

Figure 1.7 - Voltage-gated potassium channels. (A) Model of the structure of *Shaker*. A single *Shaker* subunit consists of six transmembrane alpha helices. The positive charges on the fourth transmembrane helix represent basic amino acids which function as the voltage sensor. The segment between the fifth and sixth helices is the pore region (P). In a tetramer of *Shaker* subunits four P regions form the channel pore. **(B)** Summary of K_v channel expression patterns in the retina. The summary is based upon immunohistochemical localization, *in situ* hybridization and RT-PCR results from identified neurons Stippled regions indicate known sub-cellular location; striped regions indicated presence of mRNA in that cell type with unknown protein subcellular distribution. RPE: Retinal pigment epithelium; ROS: Rod outer segments; RIS: Rod inner segements; ONL: Outer nuclear layer; OPL: Outer plexiform layer; INL: Inner nuclear layer; IPL: Inner plexiform layer; GCL: Ganglion cell layer. Adapted from (Pinto and Klumpp 1998).

In the mouse retina at least six different K_v-channels have been identified, each expressed in specific cell types (Figure 1.7 B). In RGCs K_v-channels exhibit a specific expression pattern in the axon, thereby controlling action potential shape. In photoreceptor cells K_v-channels are important for the neuronal excitability and are thought to shape postsynaptic responsiveness, signal integration and neurotransmitter release (Misonou et al. 2005, Klumpp et al. 1995, Beech and Barnes 1989). In addition, K_v-channels have been identified in cholinergic and dopaminergic amacrine cells (Tian et al. 2003). For instance, studies demonstrated that K_v3-channels play an important role in electrical isolation of starburst amacrine cells, which is thought to be essential for the specific input on direction-selective RGCs (Ozaita et al. 2004). In the mouse rod bipolar cell different K_v-channels ($K_v1.1$.-$K_v1.3$.) with very specific subcellular distribution have been identified by immunohistochemistry and RT-PCR. $K_v1.1$. immunoreactivity was primarily detected in the dendrites and axon terminals, whereas $K_v1.2$. subunits were localized to the axon and $K_v1.3$. to the postsynaptic membrane of the rod ribbon synapse. Their delayed outward rectifying currents are thought to allow complex modulation of retinal synaptic signals and therefore play a role in modulation of physiologic responses (Klumpp et al. 1995).

Hyperpolarization-activated and cyclic nucleotide-gated (HCN) channels are widely distributed throughout the CNS. The family of HCN-channels comprises four members (HCN1-4), with each possessing different gating properties and expression levels. As their name indicates HCN-channels belong to the super family of voltage-gated ion channels,

being activated by hyperpolarizing membrane potentials and display a reversal potential between −20 mV and −30 mV under physiological conditions (Seifert et al. 1999, Gauss et al. 1998, Ludwig et al. 1998, Kuisle and Luethi 2010). The channel pore is selective for both, K^+ and Na^+, and can be fully blocked by extracellular cesium (Cs^+), depending on membrane potential (Pape 1996). In addition, HCN-channels can also be effectively modulated by cAMP and cGMP from the intracellular site (Ludwig et al. 1998)
In the retina, HCN-currents were first characterized in rod photoreceptor cells in 1978, in which they counteract the strong hyperpolarization at high light intensities and shape the light response (Fain et al. 1978). In depolarizing cells, such as on-bipolar cells, it is hypothesized that HCN-channels set a suitable membrane potential under constant darkness for a fast light-response onset. Throughout the retina HCN-channels have been identified in various cell types, including rod and cone photoreceptor cells, bipolar cells and RGCs (Fyk-Kolodziej and Pourcho 2007, Muller et al. 2003, Stradleigh et al. 2011).
Studies in isolated rod bipolar cells from rats revealed slow inward-rectifying currents during hyperpolarizing steps, which are similar to H-type rectifier I_h currents, first described in cardiac cells and rod inner segments in salamander (Karschin and Wassle 1990).

K_{ir} channels induce a different potassium current in retinal bipolar cells besides K_v- and hyperpolarization-activated channels. These time-independent K_{ir} currents are primarily present in a subset of cone bipolar cells and show typical biophysical and pharmacological properties, i.e. inward-rectification, sensitivity towards Barium (Ba^{2+}) and a reversal potential of around −87 mV (Ma et al. 2003). However, K_{ir} channels are also highly expressed in retinal glial cells, thereby controlling extracellular K^+ concentration by K^+–buffering currents, due to their high open-probability around resting potential (Ishii et al. 1997).

It is supposed, that the combination of outward- and inward-rectifying potassium channels may be responsible for setting the membrane resting potentials in bipolar cells. However, the differential expression of K_v, I_h and K_{ir} currents in specific subsets of retinal bipolar cells suggest a more complex role in respect of physiological relevance.

*Voltage-dependent calcium channels

In contrast to sodium and potassium ions, calcium not only play an electrogenic role for altering the membrane potential, but it is also a major intracellular signal controlling numerous cellular events (Berridge et al. 2000). Opening of voltage-dependent calcium channels (Ca_vs) lead to the influx of calcium into the cytosol. Under normal resting potential the intracellular calcium concentration only reaches about 100 nM due to calcium buffering molecules and intracellular stores (Clapham 2007). Upon activation of Ca_vs, the intracellular concentration can rise into the high micromolar range (Wadel et al. 2007),

ultimately leading to diverse processes, such as neurotransmitter release, activation of calcium-dependent enzymes or gene transcription. Therefore Ca_vs are transmitting information between electrical, i.e. depolarization of the cell membrane, and chemical signals, i.e. activation of a signaling cascade.

Ca_vs are large, multi-subunit transmembrane proteins and are divided into two major groups, low voltage-activated (LVA) and high voltage-activated (HVA) channels(Armstrong and Matteson 1985, Bean 1985). LVA calcium channels require only modest depolarization to activate, around the resting membrane potential of −70 mV, and show rapid inactivation, whereas HVA channels require larger depolarization. The threshold for HVA Ca_v-activation usually lie between −40 mV and −20 mV (Baumgart and Perez-Reyes 2010). HVA Ca_vs are heteromultimeric receptors comprising the channel domain $Ca_v\alpha1$ and two ancillary proteins $Ca_v\beta$- and $Ca_v\alpha_2\delta$, whereas LVA Ca_vs do not require additional subunits (Catterall et al. 2005).

All α1-subunits are composed of four domains (I-IV) and each domain consist of six transmembrane helices (S1-6). The voltage-sensor (S1-4) and the pore-forming amino acid residues (S5-6) both belong to domain I (Catterall 2000, Arikkath and Campbell 2003). The sides for intracellular communication reside at the cytoplasmic N- and C-termini, as well as in three inter-domain loops (I-II, II-III and III-IV) (Van Petegem and Minor 2006) (Figure 1.8).

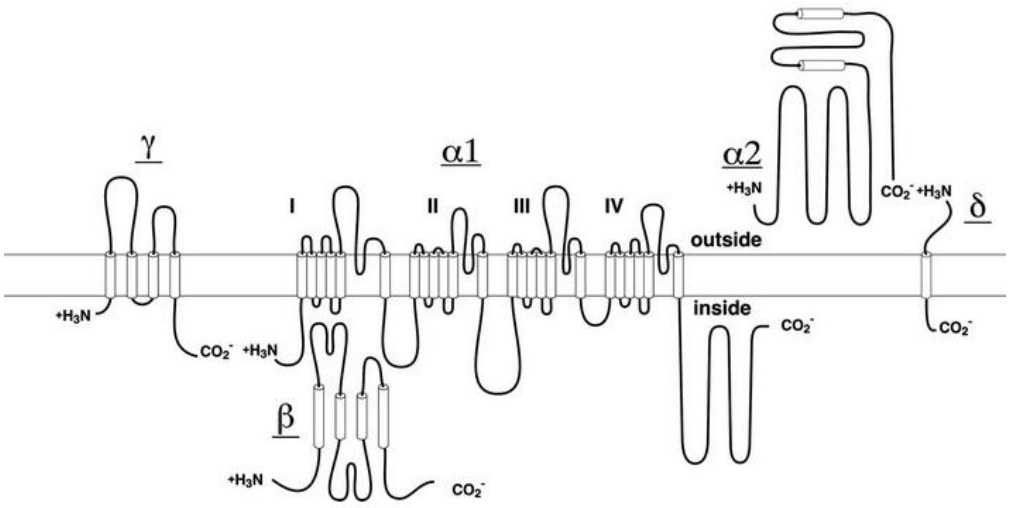

Figure 1.8 - Subunit structure of Ca_V1 channels. The subunit composition and structure of calcium channels purified from skeletal muscle are illustrated. The model is updated from the original description of the subunit structure of skeletal muscle calcium channels. This model fits available biochemical and molecular biological results for other Ca_V1 channels and for Ca_V2 channels. Predicted α-helices are depicted as cylinders. The lengths of lines correspond approximately to the lengths of the polypeptide segments represented. Click image for full size. Figure adapted from (Catterall et al. 2005).

The $Ca_v\alpha1$-subunits are divided into three major groups, Ca_v1, Ca_v2 and Ca_v3 (Figure 1.9). The Ca_v1-family encodes four different channels ($Ca_v1.1$-$Ca_v1.4$), which are sensitive to various dihydropyridines (DHP) agonists and antagonists (Randall and Tsien 1995). Except for $Ca_v1.1$, which is a skeletal muscle L-type calcium channel, the remaining three Ca_v1 are

all neuronal L-type calcium channels. These channels exhibit a long-lasting activation with slow deactivation kinetics and play a major role in heart tissue, neuroendocrine cells and in the retina. $Ca_v1.2$ channels interact with Calmodulin (CaM) and have been linked to play an essential role in CREB signaling in the hippocampus during LTP and spatial learning, as well as cardiac contraction. $Ca_v1.3$ channels have been identified in the dendritic arbors of postsynaptic cells regulating its excitability, whereas $Ca_v1.4$ channels are mainly expressed in the retina. Dysfunction of $Ca_v1.4$ channels has been linked to myopia and night blindness (Morgans et al. 2005), as it is mainly localized at the ribbon synapse of rod photoreceptor cells. Here, they regulate sustained neurotransmitter release by tonic calcium influx at low depolarization.

The Ca_v2-family is divided into three subtypes ($Ca_v2.1$, $Ca_v2.2$, $Ca_v2.3$), of which the $Ca_v2.1$ subtype give rise to P- and Q-type channels, $Ca_v2.2$ to N-type channels and $Ca_v2.3$ to R-type channels (Figure 1.9). P-/Q-type, and N-type calcium channels have been linked to neurotransmitter release at the presynaptic terminal and exhibit fast activation kinetics (<3 ms). R-type channels are mainly expressed in the brain, but have been also found in the pancreas, kidney and the heart (Grabsch et al. 1999, Vajna et al. 1998). They exhibit fast activation and inactivation kinetics (1 ms and >100 ms, respectively) providing a transient surge of calcium influx.

For the family of Ca_v3-channels three members have been identified ($Ca_v3.1$, $Ca_v3.2$ and $Ca_v3.3$), which all belong to the group of T-type calcium channels. T-type calcium channels are activated in the same range as voltage-dependent sodium channels near resting potential (−55 mV) and are important for repetitive firing of action potentials (i.e. burst firing) for instance in cardiac myocytes.

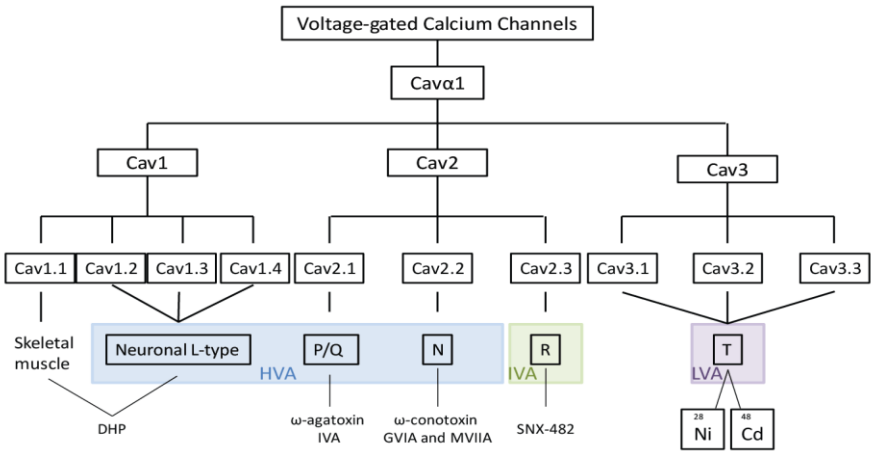

Figure 1.9 - Graphical overview of voltage-gated calcium channel α1-subunits. Ca_v-subunits are structurally divided into three main groups 1-3, comprising three to four subtypes. Blue: High-voltage activated (HVA), green: Intermediate-voltage activated (IVA) and purple: Low-voltage activated (LVA) calcium channels. At the bottom of the diagram the specific blockers for the channel families are shown.

Due to the importance of calcium as a cellular signal and the fact that prolonged calcium entry is associated with cell death, calcium-influx is tightly regulated.

All Ca_vs are regulated by voltage- and/or calcium-dependent inactivation (VDI and CDI, respectively). In HVA calcium channels the VDI is partially modulated by the ancillary $Ca_v\beta$-subunit and amino acid residues in the I-II linker region or in S6 of the major transmembrane domains. The $Ca_v\beta$-subunits are cytoplasmic proteins which are furthermore important for the trafficking of the $Ca_v\alpha1$-subunit, as they prevent ubiquitination and mask intrinsic ER-retention signals leading to higher cell surface expression levels. For LVA calcium channels, on the other hand, VDI has been proposed to be mediated by an inactivation particle in the linker III-IV domain similar to sodium channel inactivation (Simms and Zamponi 2014). Yet, exact mechanism is still unclear and need further investigation.

CDI has been described in greater detail and has been shown to be highly dependent on CaM, which is anchored to the C-terminus of the $Ca_v\alpha1$-subunit. Upon binding of Ca^{2+}, CaM undergoes conformational changes inducing CDI. For $Ca_v1.2$ and $Ca_v1.3$ only local Ca^{2+} rises are required, whereas global Ca^{2+} increase is necessary for CDI in Ca_v2 channels. $Ca_v2.1$ channels exhibit an additional Ca^{2+}-dependent regulation, calcium-dependent facilitation (CDF), which is also mediated through CaM-binding and requires only local calcium concentration increase, in contrast to CDI (Chaudhuri et al. 2007).

Current density is furthermore affected by Ca_v-expression, which is highly influenced by expression of $Ca_v\alpha_2\delta$ subunits. $Ca_v\alpha_2\delta$ subunits are only associated with HVA channels and are mainly responsible for channel trafficking to the plasma membrane. They are composed of two peptides ($Ca_v\alpha_2$ and $Ca_v\delta$) that are linked through disulfide bonds. The $Ca_v\delta$ subunit contains a transmembrane helix anchoring the $Ca_v\alpha_2$-subunit which extends to the extracellular space (Wolf et al. 2003).

An additional ancillary protein, $Ca_v\gamma$, has been identified for skeletal muscle $Ca_v1.1$ channels. $Ca_v\gamma$ subunits are not only responsible for regulating channel functions of $Ca_v1.1$, but have also been shown to influence AMPA receptor trafficking ('stargazin'). Therefore, their function may be more general and it is a matter of debate whether they are true Ca_v subunits (Simms and Zamponi 2014).

*Transient receptor potential (TRP) channels

Transient receptor potential (TRP) channels, are non-selective cation channels (Owsianik et al. 2006). Altogether 28 TRP channels have been identified in mammals, divided into six subfamilies, TRPA, TRPC, TRPM, TRPML, TRPP and TRPV channels, which are combined to either homo- or heterotetramers (Gilliam and Wensel 2011).

TRP channels are expressed in neural as well as non-neural tissue and their physiological roles are diversified. Activation and modulation of TRP channels can be achieved by many different stimuli, *inter alia*: ligand binding, membrane stretch, temperature change, endocannabinoids or phospholipids (Song and Yuan 2010, Damann et al. 2008).

Although most TRP channels have not been characterized in detail in the retina, diseases affecting TRP channels provide deep insight into their physiological roles. For instance, TRP

channels have been reported to contribute to pressure-induced apoptosis in RGCs in glaucoma (TRPV1 and TRPV4) (Sappington et al. 2009, Ryskamp et al. 2011). Due to the essential role of TRPM1 and TRPML1 in the excitability of on-bipolar cells (see section 1.1.3), mutations in these genes are a major cause for night blindness and retinal degeneration (Audo et al. 2009, Sun et al. 2000). A more comprehensive overview of TRP channel expression and function in the mammalian retina has been provided by Gilliam and Wensel, 2011.

*Cyclic nucleotide-gated (CNG) channels

Cyclic-nucleotide gated (CNG) channels are opened by intracellular binding of cGMP and cAMP, and are only weakly voltage-dependent; nonetheless, the CNG-channels belong to the class of voltage-gated ion channels. Six different subtypes divided into two groups (A1-A4 and B1-B2) combine to three distinct heterotetrameric channels with either two or three different subunits (Kaupp and Seifert 2002). Each subunit possesses six transmembrane segments and the pore loop between S5 and S6 is the best conserved region among channel subtypes.

CNG-channels are non-selective cation channels and are therefore permeable to Na^+, K^+, as well as divalent cations, in particular Ca^{2+}. Interestingly, for Ca^{2+} permeation the divalent cation needs to bind to a specific site inside the pore, thereby prohibiting the permeating of monovalent cations, allowing only Ca^{2+} to pass through the pore. This Ca^{2+} block is strongly voltage-dependent with inward currents being much more effected than outward currents (Colamartino et al. 1991, Frings et al. 1995).

CNG channels have first been described in by Fesenko et al. in 1985. They revealed that cGMP can directly open light-dependent channels in rod photoreceptor cells. Shortly thereafter, CNG channels have also been identified in cone photoreceptors and in cilia of olfactory sensory neurons (Fesenko et al. 1985, Haynes and Yau 1985, Nakamura and Gold 1987). In the retina CNG-channels are strongly discriminating between cGMP and cAMP, while in chemosensitive cilia of the olfactory system most receptors respond to both cyclic nucleotides equivalently (Tanaka et al. 1989, Frings et al. 1992). Besides the retina and the olfactory system, CNG-channels have also been found in several other types of neurons and even in non-excitable cells, such as human aveolar cells or endothelial cells of pulmonary artery (Xu et al. 1999, Wu et al. 2000). Their specific role in non-excitable cells, however, is rarely understood and requires further investigation (Biel and Michalakis 2007).

1.2 Retinal diseases/Retinal degeneration

Degenerative diseases that affect the retina, such as retinitis pigmentosa (RP) or age-related macular degeneration (AMD), result in visual impairment and blindness, with no cure currently available. To date, it is estimated that more than 270 million people are

suffering from blindness or impaired vision worldwide (WHO 2014). In the progression of most retinal degeneration diseases at first rod and secondly cone photoreceptor cells slowly degenerate, which eventually is followed by a remodeling of the remaining retinal circuitry (Marc et al. 2014, Marc et al. 2008).

1.2.1 Inherited retinal diseases (RP and AMD)

In industrialized countries, retinitis pigmentosa (RP) and age-related macular degeneration (AMD) are the two most occurring inherited retinal diseases causing blindness by photoreceptor cell degeneration. RP has a prevalence of about 1:4,000, thus affecting more than 1 million people worldwide (Hartong et al. 2006). The age of disease onset strongly depends on the type of RP and varies from early childhood to late adulthood. Generally three types of RP are distinguished based on their mode of inheritance: (i) autosomal recessive, (ii) autosomal dominant, or (iii) X-linked recessive mode. However, some cases have also been linked to other systemic diseases, such as Usher syndrome and Bardet-Biedl syndrome (Samardzija et al. 2010). Often the onset of RP is accompanied with some degree of night blindness, caused by rod photoreceptor cell death in the periphery. In many cases also the cone-mediated peripheral vision is lost in early stages of the disease, leading to an effect called tunnel vision (Figure 1.10 B).

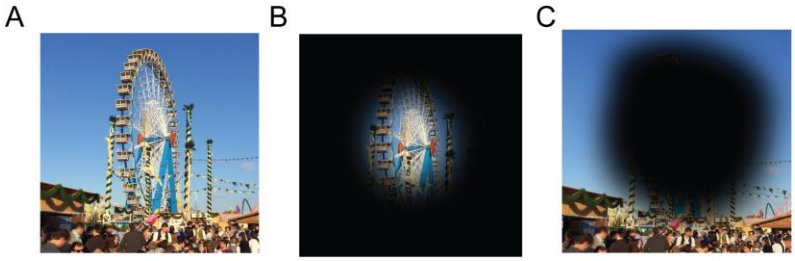

Figure 1.10 - Examples for visual experiences of RP and AMD patients. (A) Example of a normal visual perception. **(B)** Visual perception in RP patients. Peripheral vision is lost first due to death of rod photoreceptor cells eventually leading to complete blindness. **(C)** Visual perception in AMD patients. Due to drusen accumulation and neovascularisation central vision in the macula lutea is lost first followed by death of photoreceptor cells in the periphery of the retina.

In the final stage of the disease, people eventually undergo complete photoreceptor degeneration, although in most types of RP only rod photoreceptor genes are affected. This effect is also described as rod-cone dystrophy (FoundationFightingBlindness 2015).

AMD is a very heterogeneous disease affecting mainly adults older than 65 years (Klein et al. 2002). The disease is not only caused by genetic factors, but also environmental aspects play a role in its emergence. As the name indicates, the disease first manifests in the macula lutea (Figure 1.1 A), therefore central vision is lost first (Figure 1.10 C and Figure 1.11). AMD can occur in two different forms, "dry" and "wet" AMD. "Dry" AMD is a non-neovascular form and is the most common type of macular degeneration. It is characterized by the presence of yellow deposits (drusen), accumulation of extracellular material between the RPE and Bruch's membrane (Figure 1.11 A). Small and rigid deposits

appear normally during the aging process, while in AMD patients an increased number and much softer drusen appear (Figure 1.11 C and D). This different appearance of drusen is leading to an atrophy in the RPE. With the RPE being the main source of nutrients of the photoreceptor cells, drusen eventually cause photoreceptor cell death.

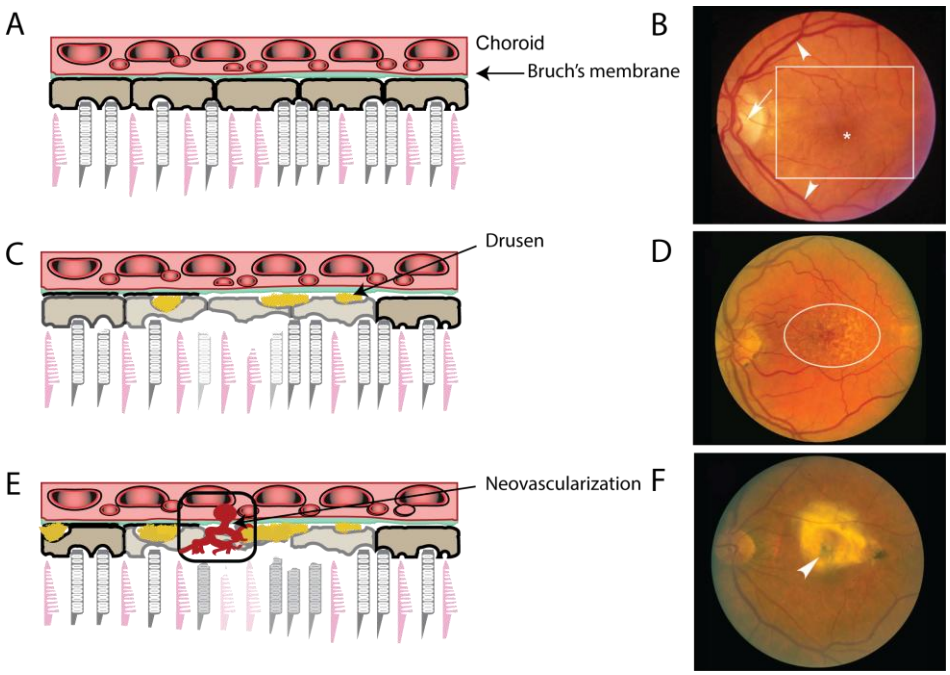

Figure 1.11 - Age-related macular degeneration. (A) Schematic drawing of a healthy retina. **(B)** Normal macula of an elderly patient. The asterisk represents the location of the fovea, which lies directly in the visual axis. The macula (boxed area), which is adapted for high acuity vision, is located temporal to the optic nerve (arrow). It is approximately 6 mm in diameter and centered on the fovea. The vascular arcades are indicated by arrowheads. **(C)** Schematic drawing of a retina with "dry" AMD. **(D)** Color fundus photograph from an individual with dry AMD. Numerous small and intermediate-sized drusen are visible in the macular region (oval). **(E)** Schematic drawing of a retina with "wet" AMD. (F) Color fundus photograph from an individual with end stage "wet" AMD. A large disciform scar (arrowhead) covering the macular region is distinctly visible. Figure B, D and F adapted from (Hagemann).

While this degenerative process is rather slow, in "wet" AMD retinal degeneration progresses more rapidly. Deposits and other factors, such as genetic predisposition, eye color or sex are associated with "wet" AMD and may induce inflammatory processes and oxygen deficiency in the eye (Green 1999, Zarbin et al. 2014, Age-Related Eye Disease Study Research 2000, Klaver et al. 1998). This in turn leads to increased release of the growth factor VGEF-A (vascular endothelial growth factor A), which induces the outgrowth of new blood vessels (neovascularization) (Kvanta et al. 1996, Lopez et al. 1996). These blood vessels even break through Bruch's membrane, invading the retina, thereby causing even stronger inflammation (Figure 1.11 E and F). This turns into a vicious cycle, since stronger inflammatory processes cause stronger neovascularization, which leads to fast degeneration of the photoreceptor cells, not only effecting central vision, but eventually leading to complete blindness (Zarbin 2004, Zarbin et al. 2014).

1.3 Mouse models of retinal degeneration

Animal models of retinal degeneration are indispensible for understanding the underlying mechanisms of retinal diseases and testing possible treatments. Numerous mouse lines exist, which exhibit specific mutations linked to retinal diseases. The most prominent RP model is the naturally occurring rd1 mouse model. In this mouse line rod phosphodiesterase 6B (PDE6B) is affected, inducing an early onset and very aggressive form of RP, similar to the progression in PDE6B-associated autosomal recessive RP in human patients (Bowes et al. 1990, Chang et al. 2002, Danciger et al. 1995, McLaughlin et al. 1995). Like rd1 other naturally occurring mouse lines have been identified for retinal degeneration, such as the rd10 mouse model. In this mouse line, PDE6B is also affected, however the mutation has less impact on protein function, thereby leading to a much later onset and slower progression of disease. In contrast to early onset of retinal degeneration in rd1 mice, in rd10 mice the retina is terminally matured before signs of disease occur (Chang et al. 2007, Gargini et al. 2007, Han et al. 2013). In addition to naturally occurring mouse lines with retinal degeneration, also transgenic animals have been developed. By mutating specific proteins important for vision, progression and impact on diseases can be closely monitored.

In addition to the specific retinal degeneration models mimicking human diseases, mouse models have been developed that have no light perception from birth. These mouse lines lack all essential proteins for light perception in rod and cone photoreceptor cells as well as melanopsin (opn4), the light perceiving protein in ipRGCs. Two of these mouse lines are the opn4$^{-/-}$,rd1/rd1 mice (Polosukhina et al. 2012) and a not yet published mouse line cnga3$^{-/-}$,rho$^{-/-}$,opn4$^{-/-}$, which is based on the double knock-out mouse line cnga3$^{-/-}$,rho$^{-/-}$ by Claes et al. 2004.

Many diseases, such as AMD, RP, diabetic retinopathy, however, have multiple origins, *inter alia* mutations in different gene loci, and may also be influenced by environmental factors (Fletcher et al. 2011). Therefore, mouse models of retinal degeneration can provide only limited information about the causes of disease and progression in human patients. For instance several mouse models for AMD have been established, but none of the lines are able to mimic both, early and late features of the disease (Zeiss 2010). Furthermore, the major drawback of using mouse models is the lack of an anatomical macula, the area of AMD onset and the area for central high-acuity vision in humans (Pennesi et al. 2012). Therefore, mouse models can only provide first insights into possible treatments and experiments must be followed up in higher animals.

1.4 Current approaches for restoration of vision

Restoration of vision is a complex challenge and several research approaches are currently under investigation. The furthest in terms of clinical application is retinal prosthesis implantation. However, other approaches including gene therapy and photopharmacology have made substantial progress within the past decade, representing promising alternative approaches.

1.4.1 Retinal prostheses

Prostheses are divided into extraocular prostheses, i.e. cortical and optic nerve prostheses. and intraocular, i.e. epi- and subretinal implants (Figure 1.12 A, red and blue, respectively). Epiretinal prostheses are sitting closely on top of the RGC layer stimulating the remaining RGCs with an image captured and transformed by a digital camera (Kien et al. 2012, Chuang et al. 2014). The most prominent epiretinal prostheses is the Intraocular Retinal Prosthesis by Mark Humanyun (Second Sight Medical products, Inc.) (Javaheri et al. 2006). This device was the basis for further development resulting in Argus I, which has firstly been used in humans, and the second version currently available, Argus II (Stronks and Dagnelie 2014, da Cruz et al. 2013).

Subretinal prostheses are micro-photodiode arrays based on a semiconductor chip technology. In this approach the electric current is generated within the device by transforming light into electric current. This current is transmitted directly from micro-photodiodes to the output of the device, the micro-electrodes (Zrenner et al. 1997, Zrenner et al. 1999). The principle has first been designed by Chow et al. (Chow 1993) and to date different approaches that utilize this technology, such as alpha-IMS, are under investigation in animal studies (Chow and Chow 1997, Colthurst et al. 2000, Chow et al. 2002, Gekeler and Zrenner 2005, Stingl et al. 2013).

Prosthetic approaches are promising for restoration of low resolution images, nevertheless, they entail certain drawbacks. Not only is implantation of a retinal device highly invasive and expensive, but also the durability of the materials is limited and further research for better components needs to be done (Colthurst et al. 2000, Chow et al. 2002, Weiland et al. 2011, Chuang et al. 2014).

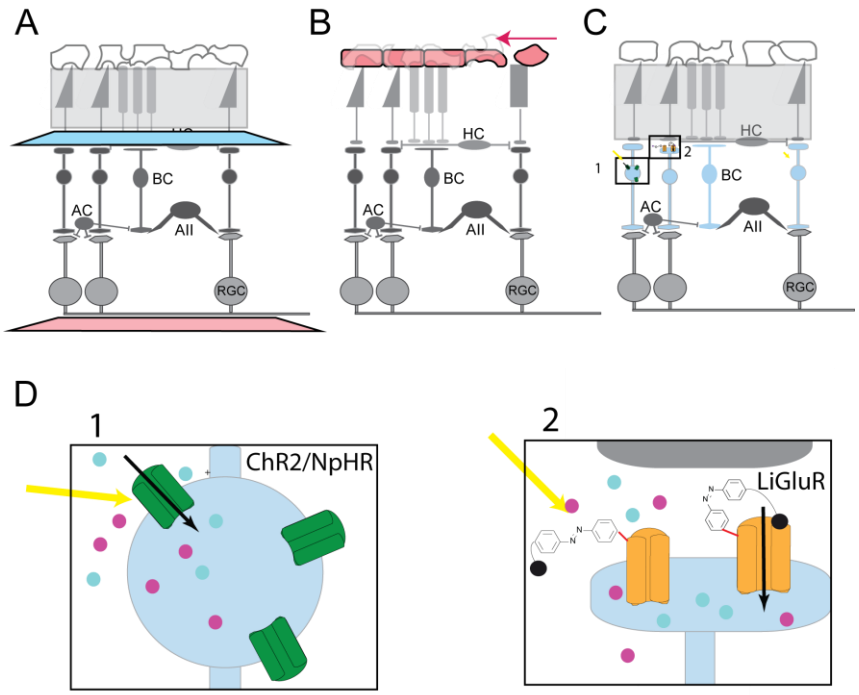

Figure 1.12 - Vision restoration approaches. (A) Retinal implants, such as Argus II (red) or the alpha-IMS subretinal microchip (blue) are the most advanced approach for vision restoration in terms of clinical application. **(B)** Stem cell transplantation is used in the context of replacing the RPE for diseases such as LCA and recessive dystrophies. **(C)** Channelrhodopsin-2 and other light-sensitive proteins can be virally delivered to retinal cells, thereby rendering them sensitive to light. **(D)** Enlargement of boxes in figure (C). D1: In this approach, ChR-2 is expressed in on-bipolar cells. D2: The light-sensitive kainate receptor LiGluR is specifically expressed in on-bipolar cells. The photoswitch needs to be injected into the intravitreal cavity to bind to the genetically engineered receptors.

1.4.2 Gene therapy

*Stem cell therapy

Stem cell therapy approaches for retinal diseases are currently in phase I clinical. Many different cell types are under investigation, such as human embryonic, fetal or umbilical cord-tissue derived stem cells as well as bone-marrow derived stem cells (Ramsden et al. 2013). To date, stem cell transplantation is primarily used in the context of replacing the RPE (Figure 1.12 B). Not only in diseases like Leber's Congenital Amaurosis (LCA) and recessive retinal dystrophies, but also in AMD the RPE is a major component involved in retinal degeneration (Jazwa et al. 2013, den Hollander et al. 2010, Schwartz et al. 2012).

Many clinical trials are currently recruiting patients, nevertheless, this approach still has challenges to overcome. Firstly, this approach is only limited to early onset of disease, when the retina is still intact. Secondly, the surgical approach is highly invasive and surgeons need to be trained accordingly, which is associated with high costs, as it is the case for retinal prosthetics. Thirdly, the approach is irreversible, which will be problematic for future innovation and improvement of the therapy in single patients. And finally, possible

immune responses (immunogenicity) cannot be eliminated, neither short term nor long term.

*Channelrhodopsin *et al.*

A different genetic approach is based on the introduction of optogenetic tools (Figure 1.12 C and D). Microbial opsins, such as Channelrhodopsin (ChR) and Halorhodopsin (NpHR) (Figure 1.12 D1) have been demonstrated to successfully restore visual responses in animal models of RP (Lagali et al. 2008, Busskamp et al. 2010, Doroudchi et al. 2011, Bi et al. 2006, Thyagarajan et al. 2010). A more recent approach has shown that a chimera of mGluR6 and melanopsin, the intrinsic photoreceptor of ipRGCs, (opto-mGluR6) is able to elicit light responses in rd1/rd1 mice, activating the native signaling pathway at ambient light intensities (van Wyk et al. 2015). In a similar approach, an intrinsic receptor iGluR is modified in such a way that an introduced artificial azobenzene-based photochromic ligand can light-activate the receptor (photochromic tethered ligand (PTL) approach) (Figure 1.12 D2) (Caporale et al. 2011, Gaub et al. 2014). The receptors can be expressed in retinal cells using either viral or non-viral gene transfer, and have successfully been implemented in remaining cone photoreceptors, on-bipolar cells and RGCs (Busskamp et al. 2010, Lagali et al. 2008, Doroudchi et al. 2011, Thyagarajan et al. 2010, Bi et al. 2006).
Both approaches, however, have their caveats and tradeoffs. Gene transfer, and especially *xenotransplantation*, can be critical for immune responses and furthermore, the implementation is irreversible. Although the introduction of the gene is irreversible, the PTL approach has the advantage of an interchangeable photoswitch ligand. This not only rises the opportunity for further optimization by developing novel molecules, but also leaves the possibility of silencing the system, if required. Yet, once expressed, the target receptor cannot be optimized any further.

1.4.3 Photopharmacology

*Principles of photopharmacology

The photopharmacological approach is a simple, yet effective way using a photochromic ligand (PCL) for the activation of a native channel with light. PCLs are small molecules that combine a pharmacophore with a photoswitchable moiety, such as an azobenzene (Fehrentz et al. 2011, Fortin et al. 2008). These PCLs can exist in two different configurations, i.e. (i) in their dark-adapted, thermodynamically stable *trans*-configuration, and (ii) in their less stable *cis*-configuration when illuminated with certain wavelengths (Figure 1.13 A). By changing the configuration of the PCL with light, its efficacy is changed, thereby controlling the open probability or activity of a channel or receptor, respectively. This approach has been used successfully to photosensitize various membrane proteins, such as voltage-gated potassium channels, K_{ATP} channels, GPCRs and AMPA receptors

(Fehrentz et al. 2011, Broichhagen et al. 2014b, Schonberger and Trauner 2014, Stawski et al. 2012). Furthermore, it has been demonstrated that also enzymes like the acetylcholine esterase can be activated and inactivated by light using photochromic ligands (Broichhagen et al. 2014a).

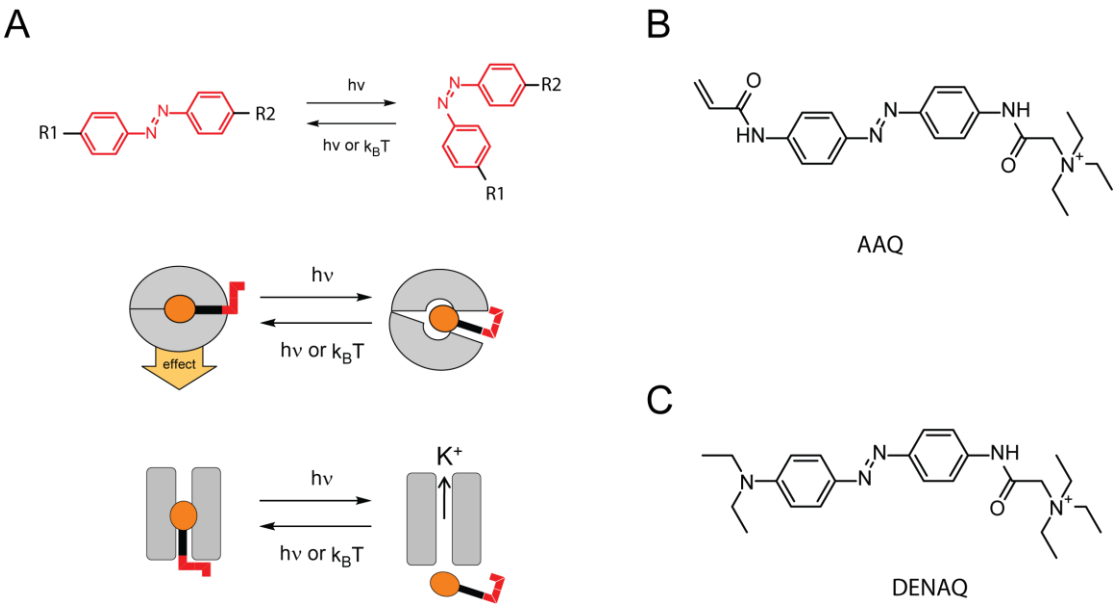

Figure 1.13 - Principle of Photopharmacology. (A) Schematic representation of the photoswitch mechanism. The azobenzene moiety (red) can be switched between *trans*- and *cis*-configuration using specific wavelengths. Depending on the ligand (orange ball) the photochromic ligand can either bind to a specific receptor or function as a channel blocker. **(B)** Molecular structure of AAQ, a first generation photoswitchable potassium channel blocker sensitive to UV light. **(C)** DENAQ, a second generation photoswitchable potassium channel blocker sensitive to blue and white light.

This approach has great advantages by being a mere pharmacological treatment. Most importantly no genetic manipulation is required, and therefore the approach is less invasive and comparatively cheap. In addition, the photochromic ligand can be added or removed from the system as needed. This allows for further development and application of new photochromic ligands and in case of undesirable side effects treatment can be stopped at any time.

*Photopharmacology for restoration of vision

The application of photochromic open-channel blockers to blind retinae has been shown to be a promising approach towards restoration of vision. For sake of simplicity the blockers will divided into generations based on their basic properties. The first PCL applied to blind retina was AAQ (Figure 1.13 B), which has the basic characteristics of an azobenzene-based photochromic ligand, i.e. the switching wavelengths are near UV light (360–380 nm) for *trans*- to *cis*-isomerization and blue light (440–480 nm) for reverting the molecule back to its thermodynamically more stable *trans*-configuration. Thermodynamic relaxation back to *trans*-configuration is too slow, therefore AAQ needs to be switched back actively for

application in fast biological systems (Polosukhina et al. 2012). In the retina, AAQ activates multiple retinal cell types, but primarily inhibitory neurons. With intravitreal injections of high AAQ concentration (80 mM AAQ containing 40 % DMSO) light-dependent behavior could be restored in rd1/rd1 mice, however, UV light and the very low solubility are two severe limitations for possible applications in human patients.

The second generation PCL, DENAQ, was already superior to the first generation, by being switched to its active *cis*-configuration with blue light (440–480 nm). Furthermore the thermodynamic relaxation back to *trans*-configuration is fast enough with no need for switching it back actively (Figure 1.13 C). In the retina, DENAQ primarily targets RGCs and interestingly, it does only photosensitize retina undergoing degeneration. This effect is caused by an up-regulation of HCN-channel expression, the target channel of DENAQ, in RGCs during retinal degeneration (Tochitsky et al. 2014, Tochitsky and Kramer 2015). In addition, DENAQ was able to restore light-dependent behavior after intravitreal injections with lower concentrations compared to AAQ. Nevertheless, the solubility of DENAQ is too low to apply the molecule without the need of additional solvents, such as DMSO (Tochitsky et al. 2014).

Both, first and second generation photochromic blockers, have made great progress in the field of vision restoration using PCLs. However, PCLs with different selectivity and mode of action, as well as with higher solubility need to be developed to further improve the treatment of vision loss using this approach.

1.5 Objectives

1.5.1 Restoration of light sensitivity in blind retina

The overall goal of this work is the restoration of light-sensitivity in blind retinae *ex-vivo* using novel (next-generation) PCLs. *Ex-vivo* studies represent the very first step towards vision restoration in human patients. To achieve this goal, different PCLs need to be analyzed for their mode of action and efficacy in explanted blind murine retinae. Investigation of possible candidates can be done by a combinatorial approach using multi-electrode arrays (MEAs) and the whole-cell patch clamp technique.

In this work I will not only provide information about a new, third generation photochromic open-channel blocker with a different mode of action than to AAQ and DENAQ. I will also demonstrate that a freely diffusible photochromic agonist for LGICs is able to induce light-dependent spiking patterns in blind retinae, which has not been investigated before.

1.5.2 Basic characterization of PCLs in murine brain slices

In the second part of my thesis I will investigate the specificity and properties of PCLs in murine brain slices. PCLs can be widely used in neuroscience to indentify underlying mechanisms of receptor activation. However, novel PCLs first need to be thoroughly tested to ensure high specificity for certain receptors. This can be done by heterologously expressing target receptors in HEK cells and performing patch clamp experiments. To gain even deeper insight into the working mode of newly-synthesized PCLs, investigation of their actions in intact neural tissue, such as hippocampal brain slice from mice, is very useful. Using the patch-clamp technique and MEA recordings with different pharmacological profiles, one can thus identify target receptors in their native environment.

2 Materials and Methods

2.1 Materials

2.1.1 List of compounds

Table 1 - **List of compounds investigated in this work**

COMPOUND	SYNTHESIZED BY ...
ATG	Dr. Vilius Franckevicius
rsATG	Dr. Vilius Franckevicius
cis-Stilbene	Felix Hartrampf
ATA	Dr. Philipp Stawski
ATA-Na^+	Katharina Hüll
DAD	Dr. Marco Stein
DAD-HCl	Dr. David Barber
GluAzo	Dr. Matthew Volgraf, Dr. Alwin Reiter
rsGluAzo	Dr. Alwin Reiter
AzoCholine	Dr. Tatsuya Urushima
BisQ	Dr. Tatsuya Urushima, Dr. Johannes Broichhagen

2.1.2 Solutions for patch-clamp and MEA recordings.

Extracellular solutions

Solutions were freshly prepared on the day of experiment to prevent bacterial outgrowth. For brain slice preparation a cutting solution was used for maximal integrity of neurons (Bischofberger et al. 2006). This solution was sucrose based and contained high Mg^{2+} concentrations (table 2). Patch-clamp as well as MEA experiments were performed in ACSF (table 2). Both cutting solution and ACSF were oxygenated with carbogen

(5 % CO_2/95 % O_2) to set pH at 7.2. In 0$MgCl_2$-ACSF Mg^{2+} was not replaced by a different ion.

For retinal slice preparation the pH needed to be set at 7.2-7.4 without oxygenation, therefore $NaHCO_3$ was replaced by HEPES and the pH was set to 7.4 using 1M NaOH or 1M HCl (HEPES ringer) (table 2). Slices were prepared in a 3 % low-melting agarose block in HEPES ringer (see section 2.2.3).

Table 2 - **Buffers and extracellular solutions**

BUFFER	COMPOSITION
ACSF [mM]	125 NaCl, 2.5 KCl, 1.25 NaH_2PO_4, 26 $NaHCO_3$, 2 $CaCl_2$, 1 $MgCl_2$, 20 glucose saturated with carbogen (95% O_2 and 5% CO_2)
Cutting Solution [mM]	87 NaCl, 2.5 KCl, 1.25 NaH_2PO_4, 25 $NaHCO_3$, 0.5 $CaCl_2$, 7 $MgCl_2$, 25 glucose, 75 sucrose saturated with carbogen (95 % O_2/5% CO_2)
HEPES Ringer (HR) [mM]	125 NaCl, 2.5 KCl, 1.25 NaH_2PO_4, 20 HEPES, 2 $CaCl_2$, 1 $MgCl_2$, 20 glucose (pH 7.4)
PBS [mM]:	137 NaCl, 2.7 KCl, 10 Na_2HPO_4, 1.8 KH_2PO_4
low-melting agarose (3%)	25 mL HEPES Ringer w/ 0.75 g low melting agarose
Eylea	40 mg/ml Eylea in 10 mM sodium phosphate, 40 mM sodium chloride, 0.03% polysorbate 20, and 5% sucrose, pH 6.2

Intracellular solutions

Intracellular solutions for patch-clamp recordings are listed in table 3. All components except for ATG and GTP were added to 8 ml water. The solution was stirred for 30 min at room temperature and ATP and GTP were added. The pH was adjusted to 7.3 using KOH and the volume was filled to reach 10 ml. Finally the osmolarity was checked to be approximately 300 mOsm (table 3). For storage aliquants of approximately 200 µL were prepared and stored at −20 °C until further use. For patch-clamp recordings using LL2 the intracellular solution needed to be diluted with ddH_2O (80:20 LL2'/ddH_2O). For Ca^{2+} imaging experiments Fura-2 was added to the intracellular solution to a final concentration of 50 µM. For immunohistological analysis a final concentration of 0.1 % neurobiotin (v/v) and for intracellular block of NMDA receptors a final concentration of 1 mM MK-801 was added to the LL2 solution. Before use the LL2 solution was filtered through a 0.2 µM filter device.

All other intracellular solutions were filtered prior preparation of aliquants and stored at −20 °C until further use.

Table 3 - **Intracellular solutions**

NAME	COMPOSITION
LL1 [mM]	110 Cs-gluconate, 15 NaCl, 10 HEPES, 5 TEA, 0.16 EGTA, 4 Mg-ATP, 0.4 Na-GTP pH 7.3 with CsOH (300 mOsm)
LL2' [mM]	140 K-gluconate, 10 HEPES, 12 KCl, 4 NaCl, 4 Mg-ATP, 0.4 Na-GTP, pH 7.3 with KOH (360 mOsm)
LL3 [mM]	120 Cs-methansulfonate, 5 TEA-Cl, 10 HEPES, 3 NaCl, 10 EGTA, 2 QX-314·Cl, 2 ATG-Mg, 0.3 GTP-Na, pH 7.3 with CsOH, 0.1 % Neurobiotin (300 mOsm)

Antagonists and Blockers

Antagonists and blockers were all added to the extracellular solution except for TEA, QX-314 and MK-801, which were added to the intracellular solution, if required (table 3).

Table 4 - **List of antagonists and blockers**

BLOCKER	WORKING CONCENTRATION [µM]	INTRA/EXTRA-CELLULAR	DISTRIBUTER
NBQX	25	E	Abcam
D-AP5	50	E	Abcam
TTX	1	E	Abcam
Felodipine	40	E	BioTrend
MK-801	1000	I	Abcam
TEA	5000	I	Sigma Aldrich
QX-314	2000	I	Tocris
$CdCl_2$	500	E	Roth
Strychnine	1	E	Sigma Aldrich
Picrotoxin	5	E	Sigma Aldrich
TPMPA	10	E	Sigma Aldrich
L-AP4	10	E	Tocris
Ivabradine	50	E	Sigma Aldrich
Cilobradine	50	E	Sigma Aldrich

2.1.3 Solutions for immunofluorescence staining

Paraformaldehyde (PFA) solution was prepared under the hood to avoid inhalation of evaporating gases during the preparation process. 200 ml ddH_2O with 10 g PFA and two drops 1 M NaOH were stirred at 60 °C for at least 30 minutes. Then 25 ml of 10x phosphate buffered saline (PBS) was added to the cleared solution and ddH_2O was added

to a total volume of 250 ml (Table 5). The solution was filtered and aliquants of approximately 2 ml were stored at –20 °C.

For immunohistological stainings wash and blocking solutions were prepared according to table 5. The blocking solution was also used for antibody incubation (see section 2.2.8).

Table 5 - **Solutions for immunofluorscence stainings**

SOLUTION	COMPOSITION
PFA (4 %)	200 ml of 1 X PBS with 10 g of paraformaldehyde powder, adjust volume to 250 l
wash solution	PBS + 0.3 % Triton X-100
blocking solution	PBS + 5 % normal goat serum (NGS) + 0.3 % Triton X-100

2.2 Methods

2.2.1 Acute brain slice preparation

Brain slices were prepared from wild-type (wt) mice (P10-P15) if not stated otherwise. Mice were decapitated at the level of the cervical medulla using curved scissors. Skin and skull were cut sagitally from the caudal to the frontal until reaching the olfactory bulb. The left and right parts of the skull were carefully removed using curved forceps. The brain was cut caudal of the olfactory bulb and in rostral of the cerebellum. The brain was quickly removed using a spatula and transferred to ice-cold cutting solution. For coronal slices the brain was glued to the specimen disc with the rostral side downwards (UHU Sekundenkleber, Buehl, Germany). Slices (250 µm) were cut from the caudal side using a Campden vibratome 7000 smz-2 (NPI Electronic). The hemispheres were divided and transferred to an incubation chamber (Figure 2.1 A). The slices were incubated at 34°C for at least 30 min and no longer than 1 hour in ACSF (O_2/CO_2). After incubation, slices were stored at room temperature for no longer than 5 hours prior recording and experiments were performed at room temperature unless stated otherwise.

For preparation of horizontal slices the brain was placed rostral side down on a filter paper. Approximately 1 – 3 mm of the dorsal part of the brain was removed using a razor blade. The brain was then glued to the specimen disc with the dorsal side downwards. And the chamber was filled with ice-cold cutting solution. Slices were cut starting from the rostral side (Figure 2.1 B).

For preparations of cerebellar slices the skull was opened and the brain was vertically cut in the center using a razor blade. The brain was carefully removed with the cerebellum still attached to the cortex. The sides were sagitally cut by 0.5 – 1 mm and the brain was glued to the specimen disc sagitally (Figure 2.1 C).

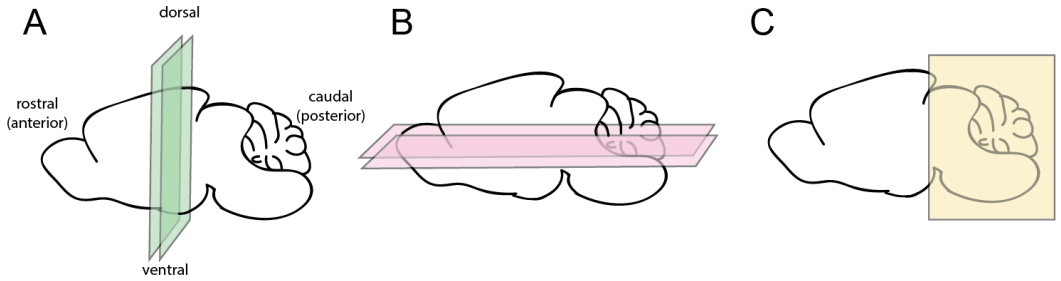

Figure 2.1 - Graphical representation of the three planes of section in the mouse brain. (A) The coronal plane cuts the brain into anterior and posterior parts. **(B)** The horizontal plane cuts the brain into dorsal and ventral parts. **(C)** The mid-sagittal plane would cut the left and right sides of the brain into two equal parts.

2.2.2 Whole-mount retina preparation

Retinae were dissected from wt mice (3 – 6 months) or from cnga3$^{-/-}$, rho$^{-/-}$, opn4$^{-/-}$ (TKO) mice (3 – 6 months) if not stated otherwise.

After cervical dislocation eyes were rapidly removed using curved scissors and transferred to a petri dish containing ACSF (room temperature, aerated with 95%O_2/5%CO_2). Eyes were punctured using a cannula (25G) behind the conjunctiva (between the cornea and the choroid) to allow diffusion of buffer solution into the intravitreal cavity. The eye which was not readily dissected was moved to a falcon filled with ACSF and aerated.

Dissection: Spring scissors were used to remove the cornea (Figure 2.2 A-B). The lens and remaining vitreous were gently removed using forceps and discarded (Figure 2.2 C). The eyecup was inverted and retina was detached (Figure 2.2 D and E). The connection to the optic nerve was cut using forceps. Retinae were immediately used for the experiments after dissection. For MEA experiments retinae were cut in two halves (Figure 2.2 F). For use in patch-clamp experiments retinae were incised at four to six sides to allow flattening and used as whole mount.

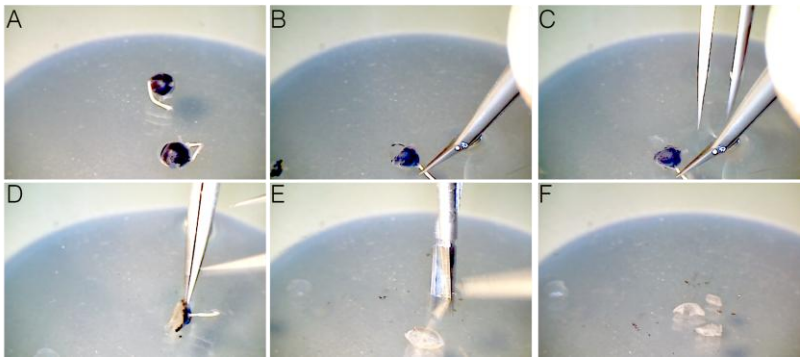

Figure 2.2- Pictures of a retina preparation. (A) Removed eyes after cervical dislocation in ACSF. **(B)** Cornea was removed by cutting behind the conjunctiva. **(C)** After removing the lens with forceps. Remaining vitreous is carefully removed. **(D)** Retina is detached from the eye cup. **(E)** Dissected retina. **(F)** Retina was cut in two halves for MEA experiments.

2.2.3 Retinal slice preparation

Retinae were dissected as described in section 2.2.2. A small Pasteur pipette was used to fill a 35 mm Petri dish with low melting-agarose (3 % in HEPES Ringer (HR), pH=7.4). Forceps were used to test consistency and after begin of solidification the flattened retina was transferred to the top of the agar. Excess solution was removed with a filter paper and a few drops of melted agar were placed directly on top of the retina. A circular plastic cylinder was placed over the retina to form a wall around it. Then the cylinder was filled with melted agar and the petri dish was placed on an ice water bath to cool. After complete solidification of the agar (approximately 1 min) the cylinder was removed and the agar containing the retina was extruded. A razor blade was used to cut out a small block of agar containing the retina. The agar block was glued to the specimen disc and filled with ice-cold HR (Figure 2.3). Slices with a thickness of 250 – 350 µm were cut using a Campden vibratome 7000 smz-2 (NPI Electronic) and directly transferred to the recording chamber. The slice anchor was mounted to hold down the surrounding agar, while the retina is unobstructed for recordings.

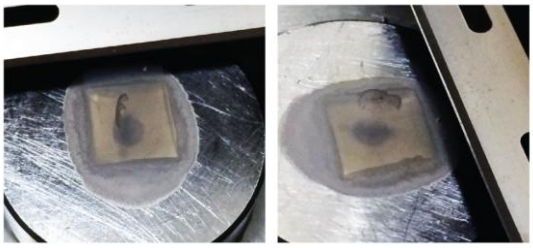

Figure 2.3 - Retinal slice preparation. Photos of a whole retina in a low-melting agarose block glued to the specimen disc of the vibratome.

2.2.4 Multielectrode Array (MEA) recordings

For extracellular spike recordings, one half of a flat-mounted retina was placed RGC layer down onto an MEA (200/30 ITO, Multichannel Systems, Reutlingen). The electrodes were 30 µm in diameter, spaced 200 µm apart, and arranged in an 8 × 8 rectangular grid. The MEA with the mounted retina was placed in an MEA 1060-inv-BC system (Multi-Channel Systems) for read out (Figure 2.4 A). Prior each experiment it was checked whether the electrodes were clean. If many channels show a noise larger than 20 µV, the MEA was cleaned using 100 % Ethanol, as were the readout electrodes of the 1060-inv-BC.

Retinae were pretreated with 200 µM DAD for 3 min or 25 µM ATA (or both simultaneously for combination approach), followed by a brief wash in ACSF. During the incubation as well as the wash period light stimulation of alternating 10 s with 460 nm light (High Power LED, Prizmatix) and darkness were applied. Afterwards the retinae were mounted on the MEA and constantly perfused with ACSF (at 34 °C with a flow rate of approximately 2-3 ml/min) for at least 15-30 min prior recording, while illuminating with the previously described protocol (Figure 2.4 B). Light stimulation was achieved through the EPC 10 USB amplifier,

controlled through the Patchmaster software (HEKA), externally triggered by the MCS system. Control experiments were performed with untreated retinae under the same conditions. In addition, wash-in experiments have been performed under illumination to demonstrate that baseline firing rate is not altered by photoswitch application.

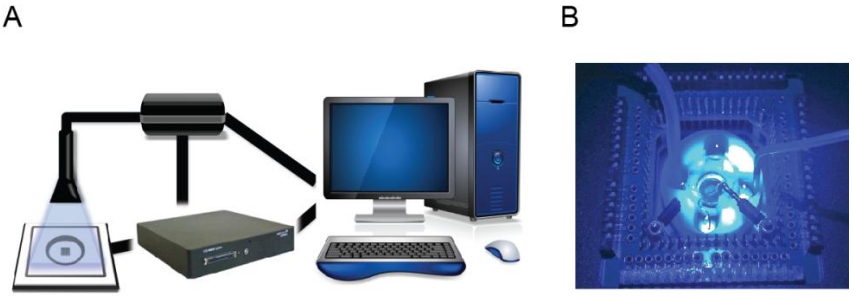

Figure 2.4 - Multielectrode array setup. (A) Graphical overview of the MEA setup. The computer controls the light stimulation protocol while recording via the MC_Rack software (Multichannel Systems). **(B)** Photo of a flat mounted retina on the 1060-inv-BC system MEA system. Illumination from the top with 460 nm light.

For MEA experiments of acute hippocampal brain slices the slices were placed with the hippocampus centered onto the electrodes. Perfusion of ACSF (34 °C, flow rate 2-3 ml/min) was performed for at least 15 min prior each recording. After reaching baseline firing, 7.5 mM K^+-ACSF was perfused until reaching constant bursting activity. AzoCholine was prepared in 7.5 mM K^+-ACSF and perfused while constantly switching between 370 nm and 440 nm using the Polychrome V monochromator (FEI systems). Control experiments were performed, (i) without increased K^+ concentration to demonstrate that AzoCholine has no effect on baseline activity and (ii) with 7.5 mM K^+-ACSF alone under illumination and (iii) with AzoCholine in 7.5 mM K^+-ACSF without illumination.

For all MEA experiments extracellular spikes were high-pass filtered at 300 Hz and digitized at 20 kHz. Generally a spike threshold of 4 SD (standard deviation) was set for each channel. Since each electrode recorded spikes from one to three cells a waveform analysis was performed with the MC_Rack software (Multi-Channel Systems). Spike times as well as light stimulation protocols were saved as .dat-files and further analysis was done using routines written in Matlab (Matlab R2013a) (see appendix 7.1).

2.2.5 Light application

High power LEDs (365 nm and 460 nm, Prizmatix) or a Polychrome-V monochromator (FEI systems) were used to switch between wavelengths. The light stimulation was controlled by the Patchmaster software (HEKA) and was brought to the slice/retina either coupled to microscope for patch-clamp recordings or directly via a glass fiber for MEA recordings.

2.2.6 Patch-clamp recordings in acute murine brain slices

Hippocampal, coronal and cerebellar brain slice preparations

Hippocampal and layer 2/3 coronal cells were patched using fire-polished glass electrodes with a resistance between 6-9 MΩ and for Purkinje cells between 2-6 MΩ.
Current-clamp recordings with ATG and voltage-clamp recordings with DAD in acute brain slice preparations were performed using the LL2 intracellular solution (table 3), whereas the LL1 intracellular solution was prepared for voltage-clamp recordings with ATG. The photoswitches were prepared as stock solutions in DMSO and diluted in ACSF 1:1000. To improve solubility the ACSF was heated to 40 °C. Due to the hydrophobicity of the azobenzene moiety, the solution was not filtered. Photoswitches were constantly perfused during the experiments, if not stated otherwise.

Antagonist and blocker application

Antagonists and channel blockers were bath applied, except for MK-801, TEA and QX-314, which was loaded into the patch pipette (table 4). For voltage-clamp recordings in brain slices and RGCs 1 µM TTX was generally added to the ACSF.

Hardware and software for patch clamp recordings

Recordings were made using an EPC 10 USB amplifier controlled by the patchmaster software (HEKA) to record and to control light stimulation. Data was filtered at 2.9 - 10 kHz and digitized at 50 kHz.

Puff application

Puff application of NMDA (Sigma-Aldrich) was performed through a glass pipette and a pressure ejection system (PDES, NPI Electronic). The pipette was placed close to the dendritic field of the patched cell and the pressure was adjusted, so that no pressure-induced artifacts were seen. Control experiments were performed with ACSF in the puff pipette. The temporal pattern of the puff application was controlled and recorded by the Patchmaster software (HEKA).

Data analysis

For analysis cells were rejected if leak currents were larger than −200 pA in cortical and hippocampal neurons, and if larger than −700 pA in RGCs or Purkinje cells. In addition, cells with a series resistance larger than 25 MΩ were also rejected. The Igor Pro (Wavematrics) liquid-junction potential (LJP) calculator was used to calculate the correction of the holding potential for the LJP. Data analysis was done using the Patcher's Power Tools (MPI Goettingen) and by routines written in IgorPro (Wavemetrics) and Matlab.

Calcium imaging experiments

For calcium imaging experiments the photoswitch, azobenzene-triazole-glutamate (ATG), was switched between *trans*- and *cis*-configuration using the Polychrome V monochromator controlled by the Live Analysis software (FEI). Slices were incubated with the calcium indicator Quest-Fluo-8-AM (50 µM, MobiTec) added to ACSF for at least 20 minutes at 37 °C inside a cell culture incubator. ATG activation was achieved using 380 nm and calcium transients were recorded at 480 nm. The images were digitized at 10 Hz and background was corrected. Further analysis was performed using IgorPro (Wavematrics) routines and ImageJ (NIH) to calculate $\Delta F/F_0$.

Coincidence detection

Coincidence detection experiments were performed in presence of 200 µM ATG. Glass electrodes with resistances between 4-6 MΩ were filled with ACSF and placed in close proximity of the axon hillock (20 µm). The electrical antidromic stimulation was controlled by an isolated stimulation unit (A-M Systems) and intensity was set subthreshold, i.e. no action potential firing was induced. The stimulus pulse duration was 100 ms and the inter-pulse interval of the paired-pulse stimulation was set 20 ms with an output range of 70 V. The temporal patterns of the antidromic stimulation and the ATG-mediated light-stimulation were controlled through the Patchmaster software (HEKA).

2.2.7 Patch-clamp recordings in retinal whole mount preparations

For patch-clamp recordings in RGCs pipettes with resistances between 3-5 MΩ were pulled and the intracellular solution LL3 (table 3) was used. This intracellular solution was specifically chosen to prevent any internal activity thereby isolating the excitatory and inhibitory inputs from bipolar and amacrine cells, respectively. Retinae were incubated for 3 minutes at 200 µM diethyl-azobenzene-diethyl (DAD) in ACSF prior the experiments. During recording the retinae were constantly perfused with ACSF at 34 °C.

2.2.8 Immunohistology

Immunohistological stainings were performed immediately after patch-clamp experiments. The retinae were incubated in 4 % PFA for 30 minutes and then washed 3x10 min with wash solution (table 5). Afterwards the retinae were incubated in 30 % sucrose solution in PBS overnight (o/n) at 4 °C and three freeze-and-thaw cycles at −80 °C and room temperature were performed the next day. Afterwards the retinae were incubated in blocking solution (table 5) and incubated for at least 1 hour at room temperature or o/n at 4 °C. Antibody solution containing streptavidine antibodies was prepared in blocking solution (table 6). A petri-dish was covered with parafilm and approximately 200 µl were drops were made for each retina. To transfer the retinae from the blocking solution into the

drop of antibody solution a brush was used. During incubation time evaporation was prevented using a water-soaked tissue paper, which was placed along the edge of the petri-dish. The dish was closed using parafilm and the slices were incubated at room temperature for 1 hour.

Table 6 - **Antibody preparations**

ANTIBODY TYPE	TARGET	DILUTION	DISTRIBUTER
MFP 485 nm	Streptavidine	1:1000	mobitec

After incubation with the antibody the retinae were washed 3x10 min with PBS and embedded in Vectashield Mounting Medium for confocal imaging.

2.2.9 Confocal imaging

Confocal analysis was performed on a Leica TCS SPE confocal System. Scanning was performed using a 20x objective or a 40x oil immersion objective. The fluorescent label was excited using 485 nm and readout was performed at 560 nm (table 7).

Table 7 - **Excitation and emission of secondary antibodies**

DYE	EXCITATION WAVELENGTH [nm]	EMISSION PEAK [nm]
MFP485	485	560

Laser intensity, photomultiplier voltage, detector gain, offset and pinhole size were adjusted for each scan and both channels were scanned separately. To reduce background noise 2 to 4 images of the same stack were acquired and averaged.

2.2.10 Intravitreal injections

Before injection, animals were anesthetized with isofluorane (2 %) and their pupils were dilated with tropicamide (1 %). Mice were mounted in a stereotactic frame and eyes were covered with GenTeal Severe Dry Eye Gel Drops (Novartis Pharmaceuticals). A Hamilton syringe (Hamilton Neuros #7002, 30G) was filled with 2 µL of 5 mM DAD-HCl (in PBS) and fixed on the stereotactic frame to reduce movement during injection. An incision was made using a 30G needle through the sclera below the ora serrate. The Hamilton syringe was lowered and 1 µL DAD solution or vehicle only (sham) was injected. The mouse was removed from stereotax and put in a separate cage for wake-up. The experiments were all performed according to the ARVO Statement for Use of Animals in Ophthalmic and Vision Research.

2.2.11 UV/vis measurements and extinction coefficients

50 µM of compound were dissolved in either DMSO or ACSF. UV/vis spectra were taken in a quartz cuvette (1 cm diameter) with the switching light (either monochromator or LED light sources (Prizmatix)) introduced through a glass fiber from the top of the cuvette perpendicular to the light path of the spectrometer (Varian, Cary 50). The kinetics of the *trans*- to *cis*-conversion were recorded at the maximal absorption wavelength of analyzed compound in *trans*-configuration.

For determination of the extinction coefficient of DAD, the molecule was dissolved in DMSO as well as ACSF in concentrations ranging from 1.25 µM – 25 µM. Pre-illumination for at least 5 minutes with 460 nm was performed to achieve maximal *cis*-DAD. Absorption was measured for each concentration at maximal absorption of the *cis*-compound (i.e. 450 nm – 460 nm) (Figure 2.5 A). Line fitting shows the acuity of the measurements (Figure 2.5 B). Extinction coefficient is determined by the Lambert-Beer equation (#1) for each concentration and the average taken from all.

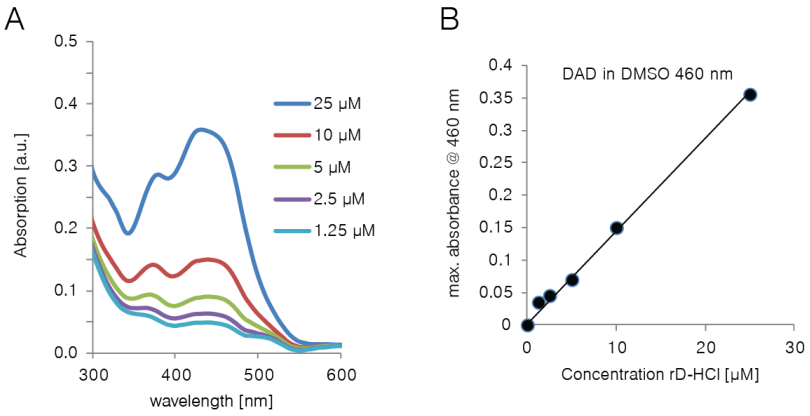

Figure 2.5 - Determining the extinction coefficient of DAD. (A) UV/vis spectra of different DAD concentrations in DMSO during illumination with 460 nm light. **(B)** Linear fit of maximal absorption at 460 nm light to determine the acuity of UV/vis measurements.

(#1) $$E = \varepsilon \cdot c \cdot d \longrightarrow \varepsilon = {}^{E}/_{(c \cdot d)}$$

3 Results: Vision restoration

Most PCLs are designed after common receptor agonists, antagonists or pore blockers and their structural design already suggests their mode of action. However, subtle changes in molecular structure have been shown to induce dramatic changes in biological function (e.g. Picenadol (Zimmerman et al. 1985)). Therefore, the exact functional and biological properties of newly synthesized PCLs need to be investigated in several experimental steps. The basic characterization comprises properties such as solubility and switching behavior analyzed by UV/Vis spectroscopy. In the next step biological activity of the molecules need to be investigated in physiological experiments, e.g. with electrophysiology or Ca^{2+} imaging experiments.

3.1 DAD: A red-shifted photoswitchable open channel blocker for vision restoration

3.1.1 DAD characterization in acute murine hippocampal brain slices

DAD is a non-permanently charged PCL for blocking and unblocking potassium channels (Figure 3.1 A and B). Its basic properties and biological activity have been investigated in acute murine hippocampal brain slices. For this, slices were incubated with 200 µM DAD in ACSF (0.1% DMSO) for 3 minutes and then transferred to the patch-clamp chamber. During the experiments ACSF without DAD was constantly perfused. In whole-cell patch-clamp experiments wavelength screenings revealed that optimal switching occurs with visible light between 400 nm and 480 nm, which is in accordance with previously measured UV/Vis spectra of DAD in physiological buffer (Stein 2014). In the dark-adapted thermodynamically more stable *trans*-configuration, DAD has been shown to block the channel pore, while illumination with blue light, i.e. the *cis*-configuration (480 nm) leads to unblocking of the channel pore (Figure 3.1 C-E) with a τ-value of approximately 25 ms ($\tau_{unblock}$ = 26.5±0.001 ms) (Figure 3.1 F). Thermal relaxation from *cis*- to *trans*-configuration occurred within 200 ms in the dark (τ_{off} = 201±0.01ms), however, τ_{off} could be significantly decreased using green light (520 nm) (τ_{off} = 72.1±0.01ms, $p < 0.001$) (Figure 3.1 G). On the other hand, switching from darkness to 520 nm also led to DAD-mediated currents (Figure 3.1 C, D), demonstrating that after switching off using 520 nm a small amount of *cis*-DAD remains.

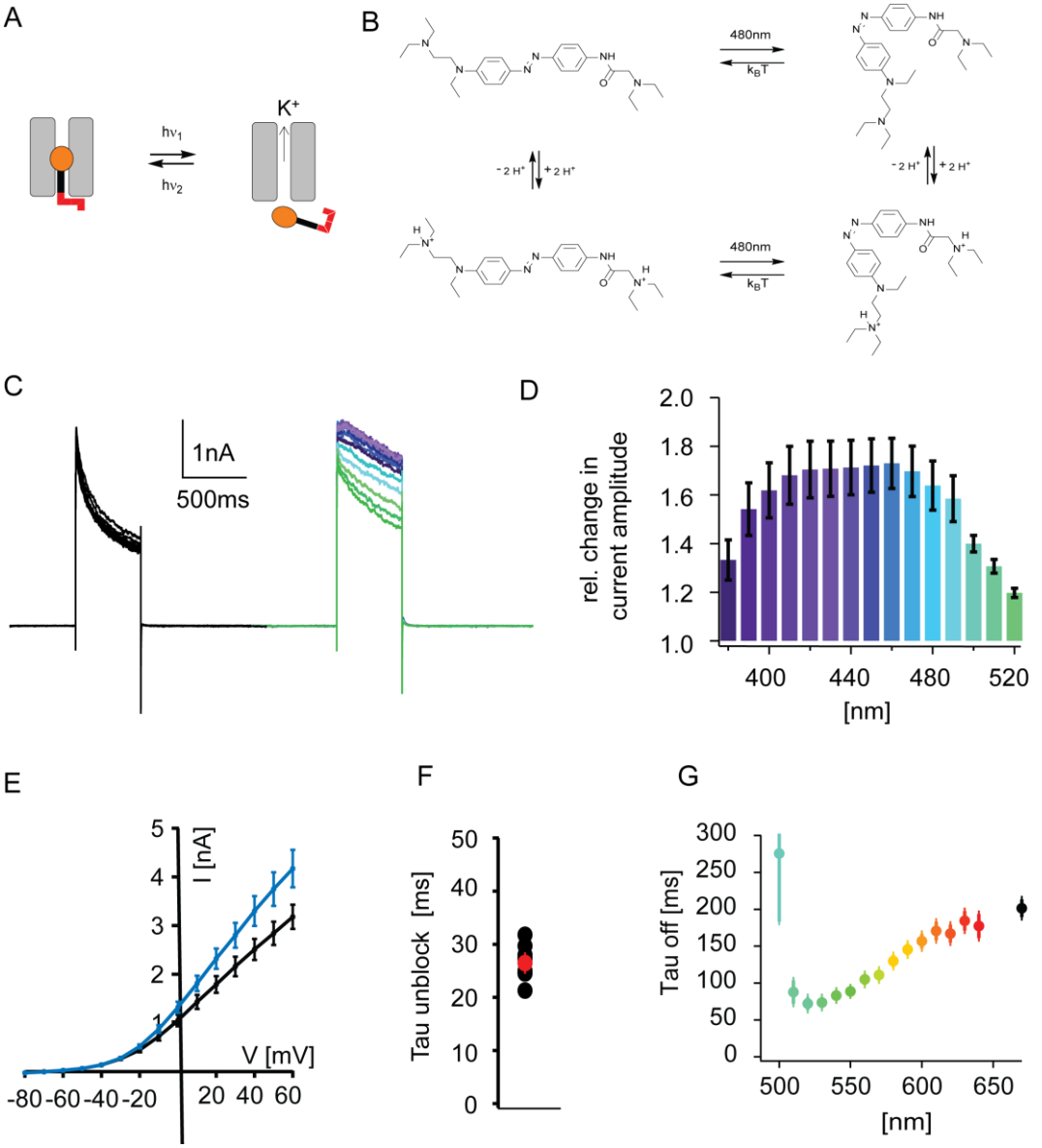

Figure 3.1 - DAD, a red-shifted potassium channel blocker. **(A)** Schematic drawing of DAD-mediated actions on K^+-channels. **(B)** Molecular structure of DAD. The molecule is non-permanently charged. It can exist either deprotonated (top) or protonated ($+2H^+$) (bottom) form. Irradiation with blue or white light converts DAD to its less stable *cis*-form, which converts back to its *trans*-form quickly in darkness. **(C)** Whole-cell voltage-clamp recording of a layer 2 neuron in an acute murine brain slice preparation after incubation with 200 µM red-DAD and 1 µM TTX. Voltage jump from –70 mV to +50 mV induce large potassium outward currents. Currents in darkness are compared to currents in presence of light (380 nm – 520 nm). **(D)** Quantification of experiments as performed in (C). Currents induced by voltage jump to +50 mV in darkness were normalized to 1. All wavelengths without exception induce larger currents compared to darkness. **(E)** Current-voltage relationships compared in darkness (black) and under 480 nm light (blue). **(F)** Kinetic of unblocking the pore of potassium channels. Recording were performed at +50 mV holding potential. $\tau_{unblock}$ = 27±0.86 ms (n = 11 cells). **(G)** Quantification of off-kinetics in respect to wavelength. Fastest off-kinetics were achieved at 520 nm light (τ_{off} = 72±8.7ms, n = 9 cells). DAD thermodynamically switches off within 201±12.1 ms (n = 8 cells). Figure adapted from (Laprell et al. 2015c).

3.1.2 DAD restores light responses in blind degenerating retinae

Photoswitchable potassium channel blockers have been shown to be a promising pharmacological approach for restoration of vision (Polosukhina et al. 2012, Tochitsky et al. 2014, Tochitsky and Kramer 2015). In addition to previously published first and second

generation photochromic blockers, DAD exhibits different chemical properties. Not only is the molecule not permanently charged (Figure 3.1 B) and thereby crosses biological barriers more easily, but also the molecule has enhanced solubility in physiological buffers and more importantly in vitreous fluid (Figure 3.2).

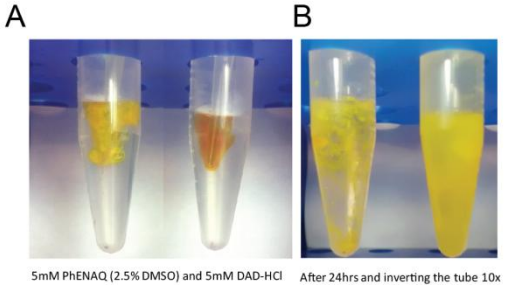

Figure 3.2 - Comparison of solubility of the second generation photochromic blocker PhENAQ with DAD in macaque vitreous. (A) Injection of 5 mM PhENAQ (a second generation VGIC blocker, 2.5% DMSO, left) and 5mM DAD-HCl in PBS (right) in macaque vitreous. DAD instantly dissolves well in vitreous whereas PhENAQ does not. **(B)** Vitreous with PhENAQ and DAD-HCl after 24 hours incubation, DAD-HCl diffused through the whole vitreous solution ,while PhENAQ agglutinated. Figure has been adapted from (Laprell et al. 2015c).

To test the ability of DAD to restore light sensitivity in blind, degenerating retinae, 3- to 6-month old blind triple knock-out (TKO) mice (cnga3$^{-/-}$,rho$^{-/-}$,opn4$^{-/-}$) were utilized. These mice natively lack all light-responses and undergo complete photoreceptor degeneration within the first few months after birth (Claes et al. 2004). Retinae were dissected and placed RGC-layer down on a multi-electrode array (MEA) to record the spiking activity of RGCs. Before application of DAD, the retinae did not exhibit any changes in spiking frequency when switching between blue light and darkness (Figure 3.3 A). A short 3-minute incubation of the retina with 100–200 µM DAD, however, was sufficient to endow the retina with light sensitivity. Illumination with 460 nm light results in a short transient light-dependent increase in spiking frequency followed by a smaller plateau phase (Figure 3.3 B).

The difference in spiking frequency from dark to light is quantified in the photoswitch index (PI), which has been previously described by Polosukhina et al. (2012). The PI is the normalized change in spiking frequency and consequently, a PI around zero indicates no light-dependent changes in spiking frequency (equation #2). A positive or negative PI, on the other hand, represents an increase or decrease upon illumination, respectively.

$$\text{(\#2)} \qquad \text{Photoswitch Index} = \frac{\text{spiking frequency (light) - spiking frequency (dark)}}{\text{spiking frequency (light) + spiking frequency (dark)}}$$

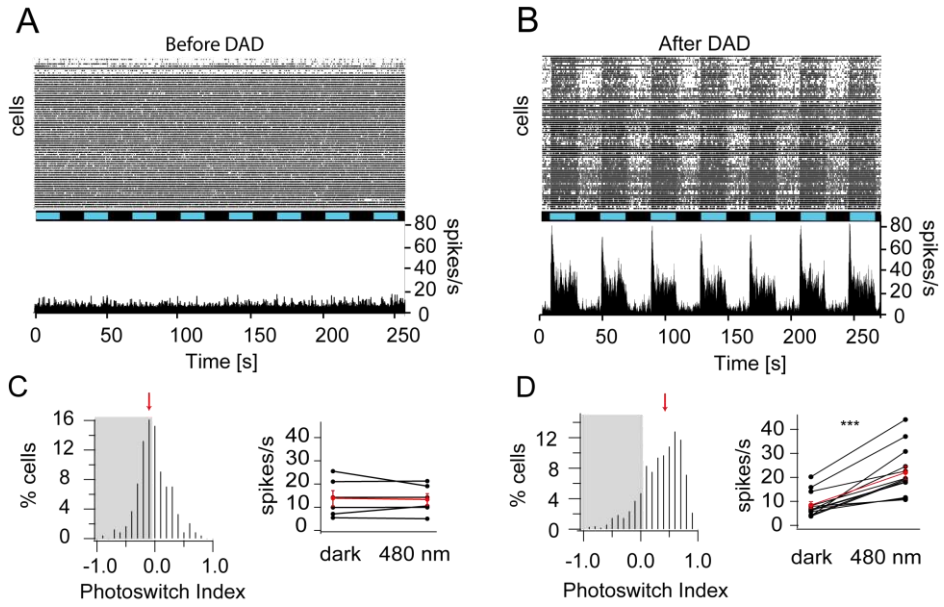

Figure 3.3 - DAD restores light-sensitivity in blind retinae. (A) Raster plot and histogram of a MEA recording in TKO retinae and **(B)** after treatment with 200 µM DAD. The bar underneath the raster plot indicates light/dark stimulation (blue: 460 nm, black: dark). **(C)** Statistics of light responses in untreated TKO retinae and **(D)** DAD treated TKO retinae. (Left) Distribution of PI for RGC populations (before n = 300 cells and after n = 1024 cells). The red arrow indicates the mean PI of all experiments. (Right) Average spiking rate in darkness and with 460 nm light (before and after DAD application: n = 6 retinae and n = 13 retinae, respectively). Statistical significance was calculated using the Wilcoxon rank sum test, * p<0.05, ** p<0.01, *** p<0.001. Figure adapted from (Laprell et al. 2015c).

In untreated TKO retinae no correlation between the light stimulus and the spiking frequency (13.9 and 13.4 spikes/s, respectively, p = 0.43) could be determined, which resulted in an average PI of around zero (0.016±0.025, n = 6 retinae) (Figure 3.3 C). In contrast, after DAD-treatment a light-dependent 2.6-fold increase in RGC spiking frequency could be detected (p<0.001, n = 13 retinae) (Figure 3.3 D). This spiking increase resulted in a positive PI of 0.42±0.05 (n = 13 retinae). Interestingly, in some retinae a small transient light-off response was present (Figure 3.4 A).

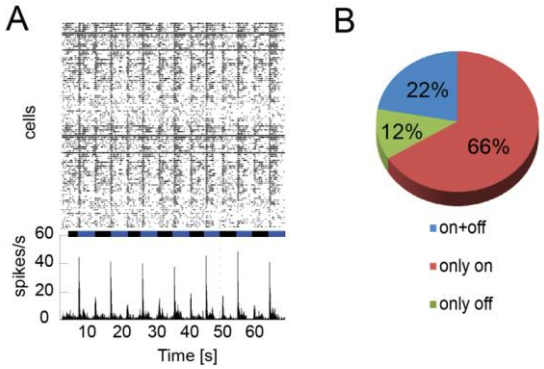

Figure 3.4 - DAD induces both, on and off responses in blind retinae. (A) Raster plot and histogram of DAD-treated retina with strong transient on- and off-light responses. The bar underneath the raster plot indicates light/dark stimulation (blue: 460 nm, black: dark). **(B)** Quantification of light responses from MEA recordings in DAD-treated TKO retinae. In 66 % of all recorded RGCs spiking rates increased only with onset of light stimulation, whereas 22 % of all RGCs responded with an increase in firing rate upon onset, but also offset of light. 12 % off the recorded cells solely responded to switching off light (n = 687 RGCs in 11 retinae). Figure modified from (Laprell et al. 2015c).

Quantification of all experiments on single cell level revealed that 66 % of all RGCs (n = 687) responded to the onset of light with a transient increase of spiking frequency. However, in 12 % of RGCs an increase in spiking frequency could only be detected shortly after switching off light and 22 % of all RGCs respond to both, light onset and offset (Figure 3.4 B). The correlated firing of RGCs in response to a light stimulus is depicted in figure 3.5, before, during and after illumination of DAD-treated TKO retina. Before illumination no correlation between the single RGCs could be detected (blue-green) (Figure 3.5 A), whereas upon illumination almost all RGCs correlated positively with each other, i.e. they increased in spiking rate at the same time (yellow-red) (Figure 3.5 B). Furthermore, as indicated by the analysis of single cell responses (Figure 3.4 B), some RGCs exhibit a positive correlation within the first second after switching off the light (yellow-red) (Figure 3.5 C).

These complex and distinct RGC responses can only be explained with DAD acting upstream of RGCs, utilizing the remaining retinal circuitry to induce on- and partially off-responses in RGCs.

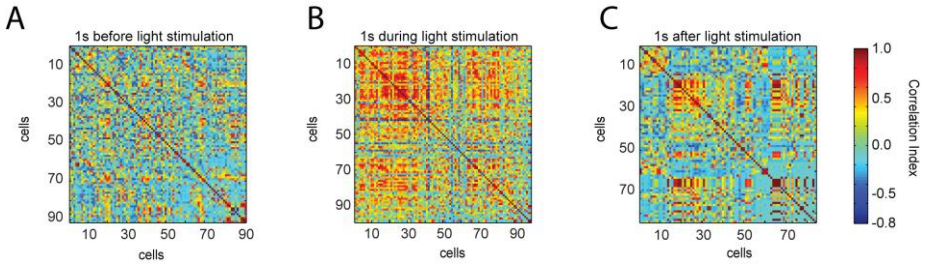

Figure 3.5 - Correlation plots for DAD-mediated light response reveals positive correlation for light-on and light-off RGC responses. Example of correlation of light responses in DAD-treated retina. **(A)** Correlation of RGC responses before light stimulation. **(B)** Correlation during light stimulation and **(C)** after switching off light. One second binning was applied. Red indicates high correlation while green indicates no correlation. During light stimulation most cells and after switching off light a fraction of cells show a positive correlation in RGC firing. Binning for correlation was set to 1 second. Figure adapted from (Laprell et al. 2015c).

3.1.3 DAD specifically activates bipolar cells upon illumination

In the next set of experiments the target cell type of DAD in the retina was determined. RGCs were synaptically isolated from the remaining retinal circuitry by blocking synaptic transmission with $CdCl_2$. Under these conditions DAD-mediated light-responses were completely abolished (PI = –0.015±0.094, n = 8 retinae, $p<0.05$, Wilcoxon rank sum test, compared to PI without blockers) (Figure 3.6 A). A similar effect was observed after the application of antagonists for NMDA and non-NMDA receptors (D-AP5 and NBQX, respectively), which block excitatory synaptic input from bipolar cells onto RGCs (–0.00213±0.012, n = 6 retinae) (Figure 3.6 B). These two experiments clearly indicate that, first, DAD is not directly activating RGCs and second, identify bipolar cells as the main target of DAD. However, to exclude major inputs from amacrine cells, a cocktail of $GABA_A$, $GABA_C$ and glycine receptors was applied (picrotoxin, TPMPA and strychnine, respectively).

After application of this cocktail, light-responses were still detectable and in contrast to AAQ, did not invert (PI = 0.32±0.03, n = 6 retinae, $spikes_{dark}$/s = 10.9±2.15, $spikes_{480}$/s = 19.9±4.16) (Figure 3.6 C). An inversion of the light response would have indicated a major input from inhibitory neurons rather than from bipolar cells (Polosukhina et al. 2012).

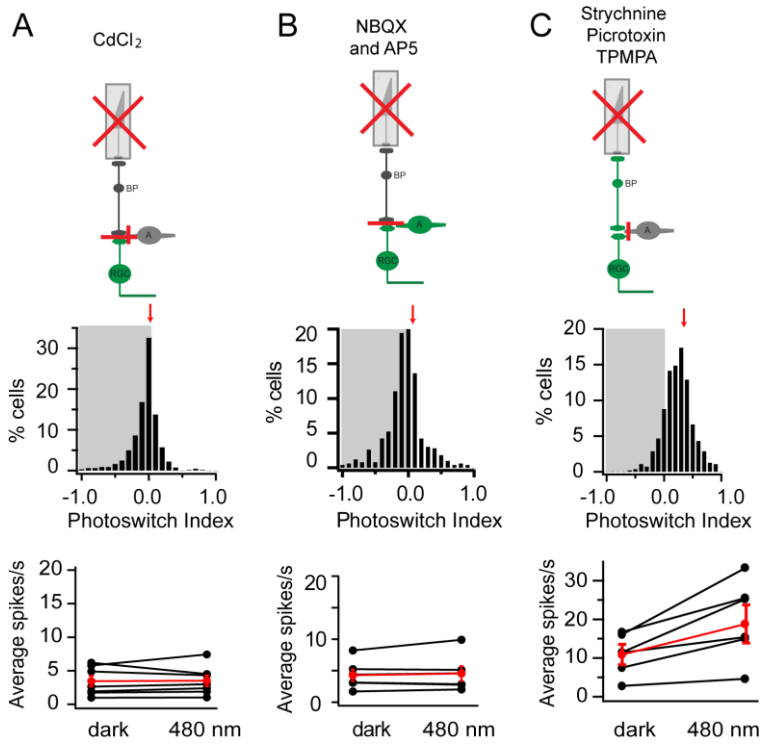

Figure 3.6 - Pharmacology in TKO retinae revealed bipolar cells as the cellular target of DAD. (A) Statistics of light responses in TKO retinae after wash in of $CdCl_2$. (Left) Distribution of PI for RGC populations (n = 688 cells). The red arrow indicates the average PI = –0.015±0.094 (n = 8 retinae. (Right) Average spiking rate in darkness and with 460 nm light (n = 8 retinae). **(B)** Statistics of light responses in TKO retinae after wash in of NBQX and D-AP5. (Left) Distribution of PI for RGC populations (n = 477 cells). The red arrow indicates the average PI = –0.00123±0.012 (n = 6 retinae). (Right) Average spiking rate in darkness and with 460 nm light. (Right). **(C)** Statistics of light responses in TKO retinae after wash in of strychnine, picrotoxine and TPMPA. (Left) Distribution of PI for RGC populations (n = 882 cells). The red arrow indicates the average PI = 0.32 ±0.030 (n = 6 retinae). Figure adapted from (Laprell et al. 2015c).

In addition to the pharmacological experiments on MEA, we performed patch-clamp experiments in retina whole mount preparations to confirm bipolar cells as the main cell type targeted by DAD. Isolation of the synaptic inputs onto RGCs was achieved by using an intracellular solution that blocked all intrinsic activity of the recorded RGC (*see* section 2.1.2). Application of 1 µM TTX in the extracellular solution blocked spontaneous activity of the retinal circuitry. Using this approach only excitatory and inhibitory postsynaptic potentials (EPSPs and IPSPs, respectively) mediated by DAD-activity onto bipolar and amacrine cells were recorded.

Before treatment with DAD the average EPSPs and IPSPs were negligible (average EPSP = –2.97±0.77 pA, n = 9 cells, average IPSP = 3.51±0.52 pA, n = 9 cells) (Figure 3.7 B and C). In contrast, after treatment in 94.1 % of all recorded RGCs light-dependent

EPSPs were recorded, and IPSPs in 82.4 % (EPSP = −76.97±8.65 pA, n = 17 cells, average IPSP = 135.24±41.73 pA, n = 16 cells) (Figure 3.7 D and E). Importantly, both EPSPs and IPSPs were significantly reduced by blocking excitatory input to RGCs by NBQX and D-AP5 (average EPSP = −10.87±5.47 pA, n = 11 cells, $p < 0.001$, average IPSP = 7.03±3.79 pA, n = 13 cells, $p = 0.01$, Wilcoxon rank sum test) (Figure 3.7 D and E, red traces. Quantification in figure 3.7 F). This indicates an indirect signal transduction from bipolar to amacrine onto RGCs. A simplified overview of the pathway for DAD activity in the retina is depicted in figure 3.7 G.

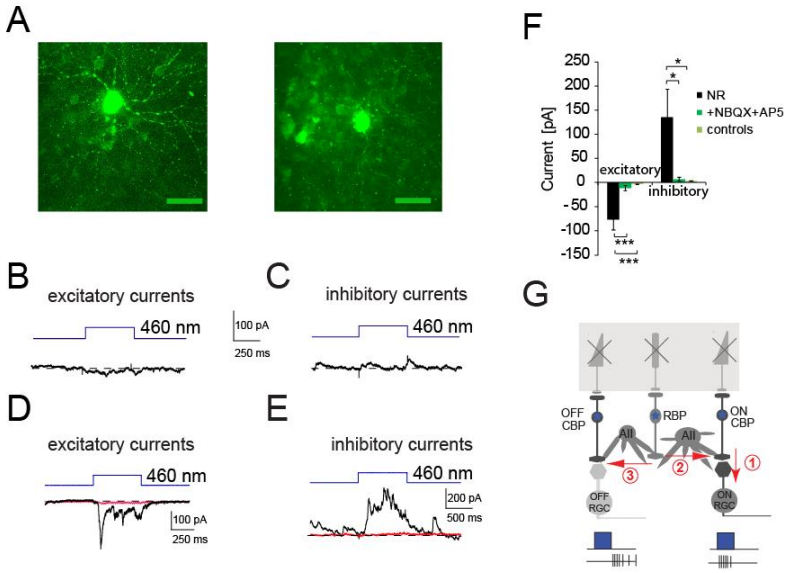

Figure 3.7 - DAD specifically photosensitizes bipolar cells in TKO retinae. **(A)** Immunofluorescence stainings of two example RGCs patched and filled with neurobiotin. Bar indicates 40 µm. **(B)** EPSP recording in whole-cell RGC patch clamp configuration at holding potential of −60 mV in TKO retinae before treatment with DAD. A blue line above the recorded trace indicates the light pulse with 460 nm. **(C)** IPSP recording in the same cell as in (B) at 0 mV holding potential. An error in holding potential was corrected (Manookin et al. 2010). A blue line above the recorded trace indicates the light pulse with 460 nm. **(D)** and **(E)** RGC patch-clamp recordings in DAD-treated TKO retina with the same light stimulation and holding potentials as in (A) and (B), respectively (black traces). After application of NBQX and D-AP5 both, excitatory and inhibitory postsynaptic potentials are inhibited (red traces). **(F)** Quantification of EPSPs and IPSPs in DAD-treated TKO RGCs, before and after inhibition of AMPA and NMDA receptors with NBQX and D-AP5, respectively (average EPSP = −10.87±5.47 pA, n = 11 cells, $p<0.001$, average IPSP = 7.03±3.79 pA, n = 13 cells, $p = 0.01$). **(G)** Graphical overview for three possible scenarios of DAD-mediated light-response pathways. Either cone bipolar cells (CBP) transmitting the signal onto RGCs directly (1), or rod bipolar cells (RBP) are activated signaling to AII amacrine cells, which synapse onto CBP (2). Off-light responses are most likely transmitted via the rod bipolar, AII amacrine pathway which synapse on off-RGCs (3). Figure modified from Figure modified from (Laprell et al. 2015c).

Taken together, the findings of MEA and patch-clamp experiments demonstrate that DAD does primarily activate bipolar cells rather than acting on amacrine or RGCs, thus utilizing the intrinsic retinal signaling pathways.

3.1.4 Visual acuity of DAD photoswitching in the retina

Visual acuity strongly relies on the precision of the stimulated retinal area. The smaller the illuminated area can be, the more precise the image can get. Also the duration of the pulse needed for significant increase of RGC spiking is critical for image formation. Therefore, different light pulse durations, light intensity threshold and also spatial acuity of DAD activity was tested.

Under bright light conditions (12.5 x 10^{15} photons cm^{-2} s^{-1}) pulses between 25 ms and 1000 ms have been applied to DAD-treated retinae. A short light pulse of 50 ms was able to trigger a significant increase in spiking frequency ($p<0.05$, n = 8 retinae) and the maximal spiking frequency was achieved with 500 ms to 1000 ms light stimulation (average PI = 0.49±0.03, n = 8 retinae) (Figure 3.8 A and B). After switching off light, the spiking frequency returns to baseline with τ_{off} = 621.4±51.3 ms (n = 8 retinae) (Data not shown). Thus, the off-response in retina is much slower compared to the recorded cortical slice data ($\tau_{darkness}$ = 0.201±0.012 s, Fig. 3.1 G). Yet, one has to keep in mind that the off-signal is a combination of cells responding with an increase in spiking frequency to light off and those, which go back to baseline firing immediately. Furthermore, the cells recorded (RGCs) are not the cells, which are stimulated by DAD (i.e. bipolar cells). This is in contrast to cortical slice preparations, in which the cell recorded is also the cell targeted by DAD. To accelerate the relaxation process and thereby achieve faster changes in spiking frequencies for on/off stimulation, green light could be used instead of darkness, as has been demonstrated in brain slice experiments (τ_{green} = 0.072±0.01 s) (Figure 3.1. G).

Next, DAD-mediated light-responses were compared with other PCLs in terms of the minimum light-intensity needed for activation. Together with Ivan Tochitsky (UC Berkeley, Prof. Richard Kramer's lab) the minimum light intensity for RGC responses was determined (3 x 10^{13} photons cm^{-2} s^{-1}) (Figure 3.8 C, indicated with *), and is therefore slightly lower compared to the threshold for DENAQ-treated rd1/rd1 retinae (Tochitsky et al. 2014), and similar to ChR2 and NpHR applications in vision restoration approaches (Pan et al. 2014, Busskamp et al. 2010). Furthermore, we determined the dynamic range of DAD-activity in the retina by increasing the light intensity over three orders of magnitude, from 10^{13} – 10^{16} photons cm^{-2} s^{-1}. The half-maximal response was achieved at a light intensity of 1 x 10^{14} photons cm^{-2} s^{-1} (Figure 3.8 C dashed line).

Spatial acuity and precisely patterned DAD-light stimulation is critical in order to restore shape recognition and natural scene perception (Reutsky-Gefen et al. 2013). We therefore determined the response properties of small spot stimulation (Figure 3.8 D). Small 90 µm spots were able to spatially increase spiking frequency in RGCs (PI = 0.41±0.15, n = 22 cells) with none of the surrounding, not illuminated RGCs, affected (PI = 0.00±0.11, n = 1206 cells, $p < 0.001$, Wilcoxon rank sum test) (Figure 3.8 E). Even a precise 30 µm spot stimulation led to an increase in almost all RGCs recorded. With increasing the diameter of the spot the RGC-light response saturated at a spot size of 240 µm, which is

close to the average dendritic field diameter of mouse RGCs (Figure 3.8 F) (Ren et al. 2010).

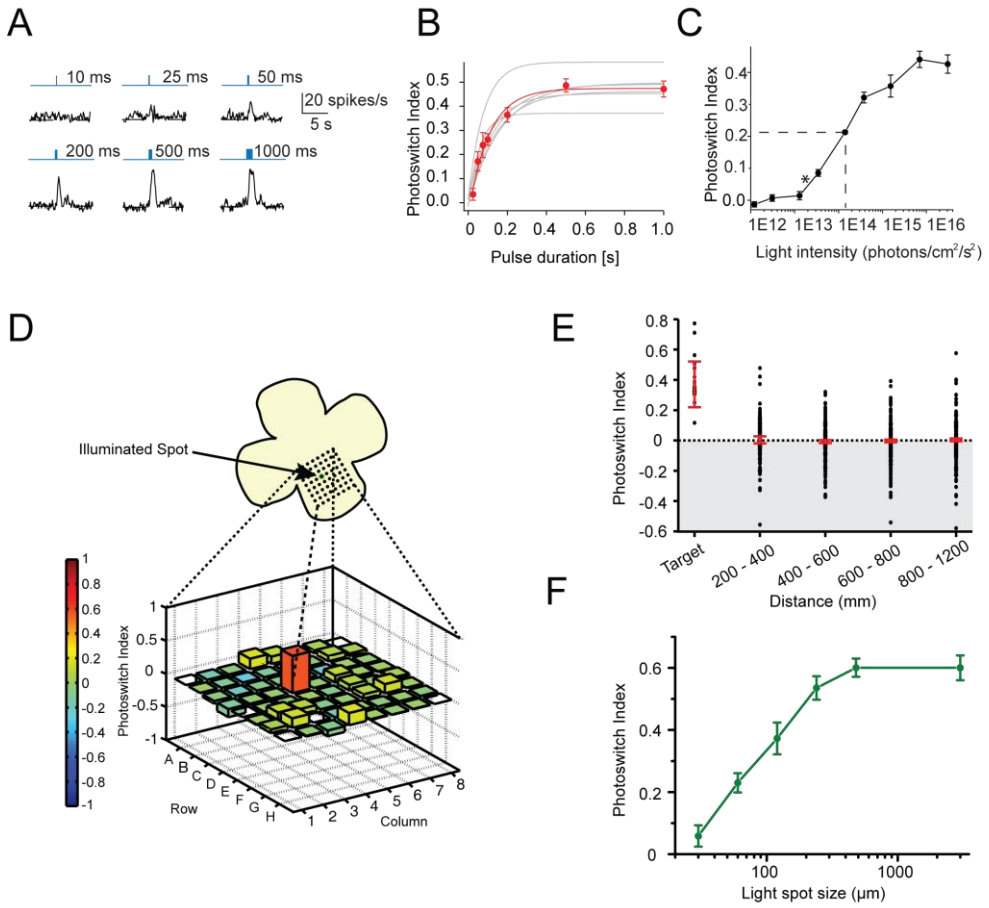

Figure 3.8 - Light sensitivity of DAD and small spot stimulation in TKO retinae. (A) Examples for short light-pulse stimulation (intensity = 12.5 x 10^{15} photons cm^{-2} s^{-1}) in DAD TKO treated retinae. **(B)** Quantification of light-pulse stimulation in DAD treated TKO retinae. 50 ms light pulses significantly increase spiking rate above background spiking ($p<0.05$, n = 8 retinae). Maximum stimulation is reached within 200-500 ms. **(C)** Light-intensity versus PI response curve for DAD treated TKO retinae (n = 5 retinae). Significant increase in spiking activity was achieved with 3x10^{13} photons cm^{-2} s^{-1} (marked with *) and reached maximum at 1 x 10^{16} photons cm^{-2} s^{-1} covering 4 log units of light intensity. **(D)** Small spot stimulation of an rd1/rd1 retina treated with 200 µM DAD. Illumination was centered on a single electrode (D4) with a diameter of 90 µm. A PI index was only detected from RGCs in the targeted area. **(E)** Quantification of experiment depicted in (A). RGCs in targeted area showed an increase, whereas surrounding RGCs were unaffected (PI= 0.41±0.15, n = 22 cells and PI = 0.00±0.11, n = 1206 cells, respectively). Single photoswitch indices are depicted as black circles as a function of distance from the targeted electrode. Binning of distance 200 µm. Mean±95% confidence intervals are shown in red. **(F)** Receptive field mapping experiment. Light responses of DAD-treated TKO retinae in respect to increasing diameter of light stimulation spots. Saturation of light response is achieved with 240 µm spot size. Data are mean±SEM, n = 16 cells). Figure modified from (Laprell et al. 2015c). Figures (C)-(F) by Ivan Tochitsky, University of California, Berkeley

Altogether, DAD light-sensitivity is comparable to other approaches in vision restoration and in principle, all RGCs can be independently controlled from one another in temporal and spatial precision, thus allowing the possibility of restoring high acuity vision.

3.1.5 DAD frequency stimulation

Vision relies on both, spatial and temporal precision. High spatial precision of DAD activation has been demonstrated in the previous section (3.1.4). In this section the temporal precision of DAD is elucidated. For slow stimulation patterns such as 0.2 or 0.5 Hz the RGC responses matches the light stimulation almost perfectly (Figure 3.9 A and B, respectively). However, when faster light stimulation protocols are applied, the retina is not able to match each light flash with an increase in RGC firing rate. For a 1 Hz stimulation 12±5 % of all light flashes is mismatched (Figure 3.9 C). This effect is dramatically increased for the application of 2 Hz light flashes (Figure 3.9 D). Here, 39±8 % are mismatched and the maximum spiking frequency is significantly reduced compared to 0.2 Hz (19.4±2.3 spikes/s and 35.3±5.9 spikes/s, respectively) (Figure 3.9 E and F).

Thus, a reliable light stimulation of DAD lies between 0.5 Hz and 1 Hz flashes in blind retinae. However, as for the τ_{off} (*see* section 3.1.1), high frequency pattern might be achieved better, when monochromatic green light would be used to actively switch DAD back to its *trans*-state.

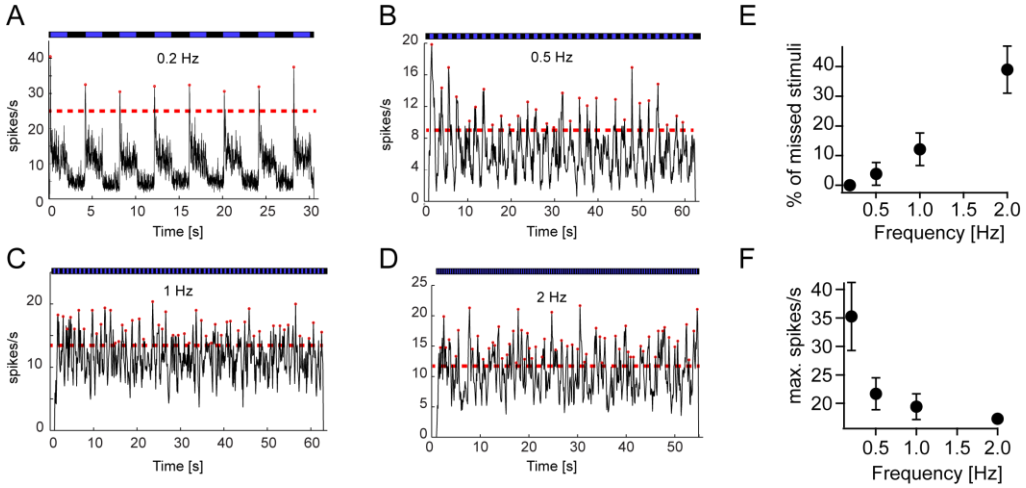

Figure 3.9 - DAD can follow light stimulation frequencies up to 1 Hz. (A)-(D) Histograms of a MEA recordings in TKO retinae after treatment with 200 µM DAD with different light stimulation frequencies. Threshold for spike detection indicated by the red line. **(A)** 0.2 Hz light stimulation. **(B)** 0.5 Hz light stimulation. **(C)** 1 Hz light stimulation and **(D)** with a 2 Hz light stimulation. The bar above the histogram indicates light/dark stimulation (blue: 460 nm, black: dark). **(E)** Quantification missed spikes depending on the light stimulation frequency. Results quantified from 6 independent experiments. **(F)** Analysis of maximal spiking frequency depending on the light stimulation protocol from the same experiments as in (E).

3.1.6 DAD only photosensitizes retinae undergoing degeneration

Retinal degeneration is a complex process involving *inter alia* synaptic remodeling and neural reprogramming (Marc et al. 2008, Jones et al. 2012). Dramatic changes, such as an increase in specific membrane-receptors, may lead to different accessibility or changed functionality of applied photoswitches. For instance, it has been previously demonstrated that expression levels of HCN-channels are strongly increased in RGCs of degenerating retina, but not in wt retinae or blind non-degenerating retinae. HCN-channels are the

primary target cell type of DENAQ, thereby only retinae undergoing degeneration are photosensitized (Tochitsky et al. 2014).

Preference analysis of DAD-mediated activation in degenerating versus non-degenerating retinae was performed in retinae from five different mouse lines: Two blind mouse lines undergoing retinal degeneration (cnga3$^{-/-}$, rho$^{-/-}$, opn4$^{-/-}$ and rd1/rd1; opn4$^{-/-}$), two mouse models for stationary night blindness, which do not undergo retinal degeneration (gnat1$^{-/-}$, gnat2$^{-/-}$, opn4$^{-/-}$ and tra$^{-/-}$, cnga3$^{-/-}$, opn4$^{-/-}$) (Chang et al. 2006) (Lyubarsky et al. 2002) (Panda et al. 2002), and in wt retinae under two different conditions (wt in ACSF and wt in presence of NBQX and L-AP4 to block synaptic transmission between photoreceptor cells and bipolar cells). A schematic overview of the experiments is depicted in figure 3.10 A.

In wt retinae DAD application had no significant effect. The overall light response was not changed (Fig. 3.10 B and C) and the strength of on- and off-light responses remained similar (difference in $PI(\Delta)_{wt}$ = 0.081±0.032, n = 5) (Fig. 3.10 D and E), as was the distribution of on- to off- light responses (Figure 3.11). However, the naturally occurring light responses in wt retinae may overlay the DAD-mediated light responses, therefore the experiments were performed again, but in the presence of the mGluR6 agonist L-AP4 and the AMPA/kainate antagonist NBQX. Using this cocktail, light-on and light-off responses in the wt retina are completely abolished (PI_{on} = –0.046±0.060, n = 5 retinae) (Slaughter and Miller 1981, DeVries and Schwartz 1999, DeVries 2000). The retinae were then treated with DAD, which was not able to recover light responses (PI_{on} = –0.052±0.067, n = 4 retinae, $\Delta_{wt+block}$ = 0.0043±0.059) (Figure 3.10. D and E). To demonstrate that NMDA receptor signaling is in principle sufficient to transmit DAD-induced light responses via the bipolar-RGC synapse, the same pharmacological approach was performed in TKO retinae resulting in large light-depending spiking patterns (PI = 0.505±0.108, n = 5 retinae, p = 0.05, Wilcoxon rank sum test) (Figure 3.12).

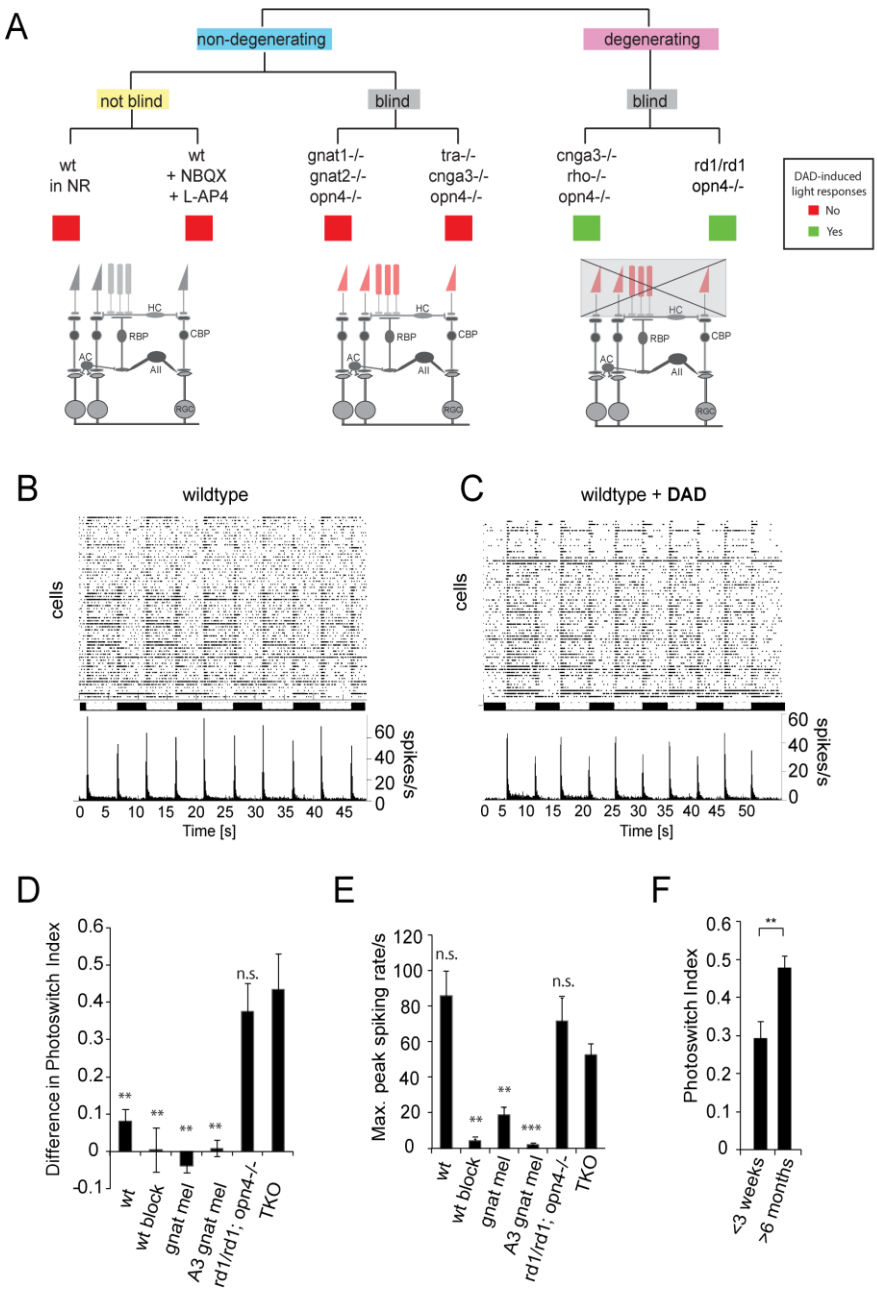

Figure 3.10 - DAD only photosensitizes retinae undergoing degeneration. (A) Overview of retinae tested for their ability to induce DAD-dependent changes in spiking frequency upon illumination. **(B)** Raster plot and histogram of a MEA recording in wt retinae before and (C) after treatment with 200µM DAD. The bar underneath the raster plot indicates light/dark stimulation (white: white light, black: darkness). **(C)** Difference in light responses before and after treatment with DAD of wt (Δspikes = 0.081±0.032, n = 5 retinae, p<0.5), wt in presence of NBQX and L-AP4 (wt+block, Δspikes = 0.004±0.059, n = 5 retinae, p<0.01), gnat1$^{-/-}$gnat2$^{-/-}$mel$^{-/-}$ (gnat mel, Δspikes= –0.039±0.017, n = 6, p<0.001), cnga3$^{-/-}$gnat1$^{-/-}$mel$^{-/-}$ (A3 gnat mel, Δspikes = 0.0087±0.022, n = 5, p<0.01), opn4$^{-/-}$rd/rd mice (mel rd, Δspikes = 0.38±0.075, n = 5 retinae, p>0.05) and TKO mice (Δspikes=0.44±0.095, n=13). Statistical tests were performed in respect to change in TKO mice (Wilcoxon rank sum test). **(D)** Maximum peak spiking frequencies of wt (85.6 spikes/s, n = 5, p>0.05), wildtype in presence of NBQX and L-AP4 (wt+block, 4.32 spikes/s, n=4, p<0.01), gnat1$^{-/-}$gnat2$^{-/-}$opn4$^{-/-}$ (gnat mel, 18.7 spikes/s, n = 6, p<0.01), cnga3$^{-/-}$gnat1$^{-/-}$opn4$^{-/-}$ (A3 gnat mel, 1.81 spikes/s, n = 5, p<0.001), opn4$^{-/-}$rd/rd mice (mel rd, 71.1 spikes/s, n=5, p>0.5) compared to TKO mice (52.6 spikes/s, n=13). Statistical tests were performed in respect to change in TKO mice (Wilcoxon ranks sum test). **(E)** PIs for DAD-treated TKO retinae from young (< 3 weeks, average PI = 0.29±0.01, n = 7 retinae) versus old mice (> 6 months) (average PI = 0.48±0.03, n = 6 retinae, p<0.01). Figure modified from (Laprell et al. 2015c).

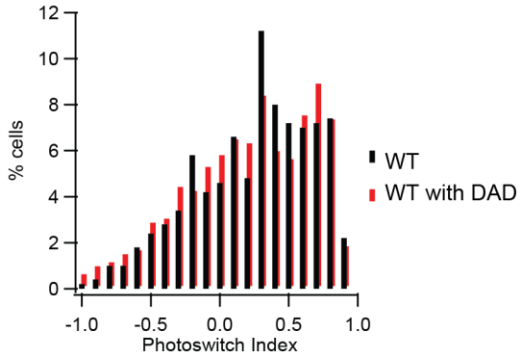

Figure 3.11 - DAD application to wild type retina does not influence single cell responses.
Distribution of PI for wild type RGC populations before (black) and after treatment (red) with 200 µM DAD (p = 0.46, Wilcoxon rank sum test). Figure adapted from (Laprell et al. 2015c).

In a next set of experiments DAD was tested on blind, but non-degenerating retinae, to investigate, whether loss of light-driven activity from photoreceptor cells alone is sufficient for DAD activity. In both blind, but structurally intact retinae, the gnat1$^{-/-}$,gnat2$^{-/-}$,opn4$^{-/-}$ (gnat-mel) and the tra$^{-/-}$,cnga3$^{-/-}$,opn4$^{-/-}$ (A3-gnat-mel), DAD was not able to photosensitize the retinae. The only responses detected were small remaining light-responses in gnat1$^{-/-}$,gnat2$^{-/-}$,opn4$^{-/-}$ mice, most likely due to alternative G-protein pathways (max firing rate$_{\text{gnat1-/-,gnat2-/-,opn4-/-}}$ = 18.7 spikes/s, TKO = 52.6 spikes/s, p <0.001, Wilcoxon rank sum test) (Figure 3.10 E) (Allen et al. 2010). However, this response was 2.5-fold smaller compared to DAD-induced light responses in TKO and could not be increased by application of DAD. Therefore, the difference of maximum spiking frequencies before and after application of DAD was negligible ($\Delta\text{spikes}_{\text{gnat-mel}}$ = –0.039±0.018, n = 6 retinae). In the second blind, but non-degenerating mouse line (tra$^{-/-}$,cnga3$^{-/-}$,opn4$^{-/-}$) no light responses were detected, neither before nor after treatment with DAD (max firing rate$_{\text{tra-/-,cnga3-/-,opn4-/-}}$ =1.8 spikes/s, $\Delta_{\text{A3-gnat-mel}}$ = 0.0087±0.022, n = 5 retinae) (Figure 3.10. D and E).

In addition, DAD was tested in retinae from a different mouse model also undergoing retinal degeneration (rd1/rd1; opn4$^{-/-}$) (Panda et al. 2003), to exclude the possibility that DAD specifically photosensitizes TKO retinae due to a mutation specific mechanism. The rd/rd, opn4$^{-/-}$ mouse line suffers from a null mutation in phosphodiesterase-6 (PDE-6) and lack melanopsin the ipRGCs (Bowes et al. 1990). The loss of PDE-6 result in elevated cGMP- and calcium levels leading to the apoptosis of rod photoreceptor cells and subsequent retinal degeneration starting within 2-3 weeks after birth (*see* section 1.3). These mice have lost all intrinsic light responses not only from rod photoreceptor cells, but also from cones within the first three months due to the effect called rod-cone dystrophy. After treatment with DAD, however, robust light-responses comparable to those in TKO mice were detected (PI = 0.39±0.067, $\Delta_{\text{mel-rd}}$ = 0.38±0.075, n = 5 retinae, p<0.001, Wilcoxon rank sum test, and Δ_{TKO} = 0.43±0.095, n = 6) (Figure 3.10. D and E).

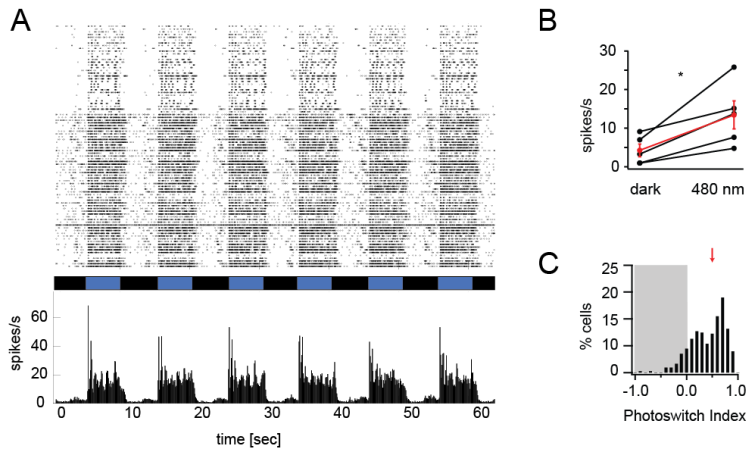

Figure 3.12 - Block of mGluR and AMPA signal transmission in TKO mice incubated with DAD. (A) Raster plot and histogram of DAD-treated TKO retina in presence of L-AP4 and NBQX. The bar underneath the raster plot indicates light/dark stimulation (blue: 460 nm, black: dark). **(B)** Statistics of light responses. Average spiking rate in darkness and with 460 nm light (n = 5 retinae). **(C)** Distribution of photoswitch index for RGC populations (n = 439 RGCs). The red arrow indicates the average PI = 0.51±0.11 (n = 5 retinae).

These six experiments demonstrate that in degenerating retinae, such as the TKO and rd1/rd1; opn4$^{-/-}$ mouse models, the death of rods and cones and the following changes in neurotransmitter release and increase in the activity of downstream retinal neurons, e.g. All amacrine cells (Borowska et al. 2011) and RGCs (Margolis et al. 2014, Stasheff 2008) is necessary for DAD-induced light responses.

The importance of retinal degeneration for the action of DAD is further substantiated by comparison of DAD-mediated effects in young versus old TKO retinae. In three week-old mice the retinae are structurally mostly intact, whereas in TKO mice older than 6 months the photoreceptor cells already did undergo severe degeneration and associated physiological changes (Claes et al. 2004). Maximum light-dependent spiking frequency after DAD application in retinae from young TKO mice were overall 62 % smaller compared to light responses in retinae from old TKO mice (3-week old and >6-month old) (PI_{old} = 0.48±0.03, n_{old} = 6 retinae, PI_{young} = 0.29±0.01, n_{young} = 7 retinae, p = 0.007, Wilcoxon rank sum test) (Figure 3.10.F). This result further highlights the importance of retinal degeneration for the effectiveness of DAD.

3.1.7 Towards the identification of the molecular target channel of DAD

DENAQ primarily acts on RGCs and more specifically on HCN channels, which are up-regulated in degenerated retinae (Tochitsky et al. 2014). Although DAD targets bipolar cells, the finding that DAD only photosensitizes retinae undergoing degeneration, hints towards a similar mode of action (Tochitsky et al. 2014). Therefore, additional experiments were performed to determine whether DAD acts on HCN-channels. Here, DAD was directly compared to the second generation compound PhENAQ (not published), which is very similar to DENAQ, in respect to the effect of the HCN-channel blockers on their light-induced spiking patterns. Two HCN-channel blockers were tested individually, ivabradine

and cilobradine (n = 1 retinae and n = 2 retinae, respectively). Both abolished light induced spiking patterns of PhENAQ (Example given for RGC light response with PhENAQ and PhENAQ+ivabradine in figure 3.13. A and B, respectively).

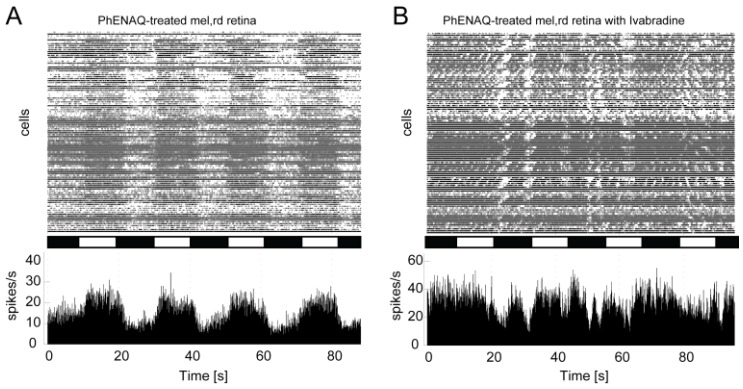

Figure 3.13 - HCN-channel blocker Ivabradine strongly affect PhENAQ induced light responses. (A) Raster plot and histogram of rd1/rd1;opn4$^{-/-}$ retina after incubation with PhENAQ. **(B)** Raster plot and histogram of the same retina as in (A), but after application of the specific HCN-channel blocker ivabradine (50 µM). The bar underneath the raster plot indicates light/dark stimulation (white: Xenon, black: dark).

In the case of DAD, the spiking pattern was altered, but not abolished by application of ivabradine or cilobradine (with experiment numbers n = 2 and n = 4, respectively). Examples for ivabradine and cilobradine application are given in figures 3.14 A,B and 3.14 C,D, respectively). The effect seen in DAD-treated retinae was probably induced by changed spontaneous spiking activity after application of HCN-channel blockers rather than by directly effecting DAD activation.

Taken together, the activation of bipolar rather than RGCs and the findings that HCN-channel blockers have no significant effect on DAD-activity suggest a very different mode of action for DAD compared to previous generation blockers, DENAQ and PhENAQ.

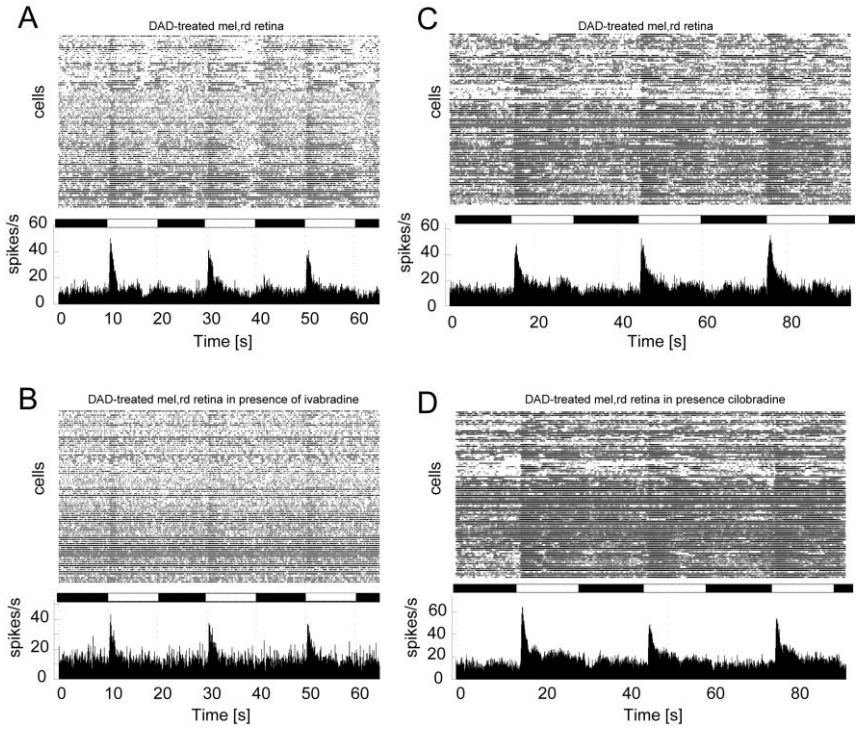

Figure 3.14 - HCN-channel blockers ivabradine and cilobradine only effect the spontaneous spiking activity, but not the DAD light response in rd1/rd1;opn4$^{-/-}$ retina. (A) Raster plot and histogram of rd1/rd1;opn4$^{-/-}$ retina after incubation with DAD and the same retina after wash-in of ivabradine (50 µM) **(B)**. **(C)** Raster plot and histogram of rd1/rd1;opn4$^{-/-}$ retina after incubation with DAD and after wash-in of cilobradine (50 µM) **(D).** The bar underneath the raster plot indicates light/dark stimulation (white: Xenon, black: dark).

3.1.8 Intravitreal injections of DAD and DAD-HCl

Ex-vivo MEA and patch-clamp experiments have demonstrated that DAD is able to light-activate the neural network of a blind degenerating retina. However, the experiments can only give little information about the accessibility of retinal tissue *in-vivo*. To determine whether DAD is able to penetrate the retina *in-vivo* and which concentrations are needed for behavioral experiments, 1 µL DAD at different concentrations were injected into the vitreal cavity of *rd1/rd1*; *opn4*$^{-/-}$ mice. After 4-24 hours mice were sacrificed, retinae dissected and retinal spiking was investigated on MEA. Dissected retinae after 4-6 hours showed the typical yellowish coloring by DAD, which was uniformly distributed over the whole tissue. Furthermore, analysis on MEA revealed that almost all RGCs showed light-dependent spiking activity after 4 and after 6 hours post injections (Figure 3.15 A and B, respectively). Retinae dissected 24 hours post injection did show no significant spiking differences between darkness and 460 nm light (data not shown). These results demonstrate that DAD is highly soluble in vitreous fluid (*see also* figure 2.2.) and that it is able to activate retinal neurons *in-vivo*.

For future *in-vivo* studies additional solvents (e.g. DMSO) need to be avoided. Therefore, DAD was also formulated as DAD-HCl salt, which was readily soluble in water or buffer (200 mM). The HCl formulation of DAD was at least as effective as DAD in DMSO (data not

shown) and was therefore used for all *in-vivo* experiments and also for *ex-vivo* experiments after it was confirmed that there was no difference in activity.

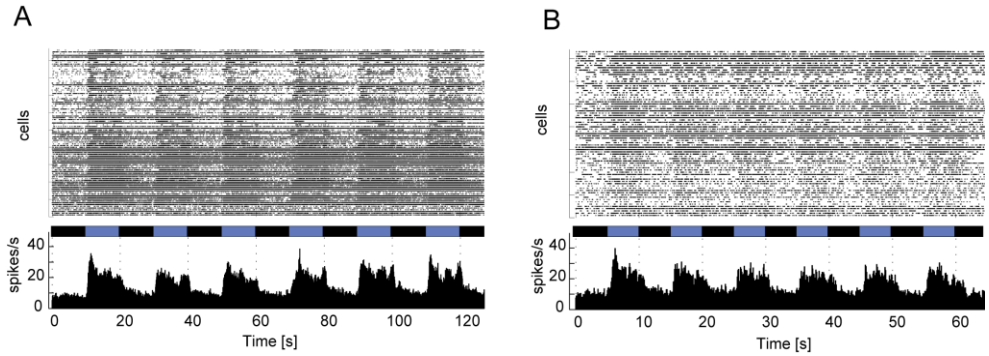

Figure 3.15 - MEA recordings after intravitreal injections of 5-7.5 mM DAD-HCl in *rd1/rd1*; *opn4*$^{-/-}$ mice. **(A)** Retina was dissected 4 hours post intravitreal injection of 7.5 mM DAD-HCl. Stimulation protocol was 10 s 460 nm light and 10 s darkness alternating. **(B)** Retina was dissected 6 hours post intravitreal injection of 5 mM DAD-HCl. Stimulation protocol was 5 s 460 nm light and 5 s darkness alternating.

3.1.9 Discussion DAD

DAD has been demonstrated to be a promising photochromic ligand approach for vision restoration in blind retinae. DAD can be activated using light in the visible range and thermodynamically relaxes back to its *trans*-configuration in the dark (*see* section 3.1). DAD can be dissolved in DMSO up to 200 mM or it can be formulated as an HCl-salt, to increase solubility in water and buffer (DAD-HCl); thereby possible DMSO effects can be circumvented. This may especially be important for *in-vivo* studies, in which higher concentrations need to be injected into the vitreous cavity due to possible wash-out effects and accessibility issues (*see* section 3.1.8). DAD and DAD-HCl have been shown to induce light-dependent spiking activity in RGCs after intravitreal injection of 5.0 – 7.5 mM and behavioral studies in rd1/rd1; opn4$^{-/-}$ mice are currently under investigation in the lab of Prof. Van Gelder (UW Washington, Seattle, USA). Intravitreal injections, however, have not only demonstrated that DAD and DAD-HCl are able to penetrate the retina and activate retinal bipolar cells (pharmacology data not shown), but also that it completely diffuses throughout the eye cup within 3 – 4 hours. The high diffusion rate and good penetration properties have good and bad aspects. On the negative side are possible absorption problems: DAD not only penetrates the retina, but also the lens when applied in very high concentrations, which will lead to loss of light intensity entering the eye (Figure 3.16 A inset). Calculations for the loss in light intensity are given in figure 3.16 B. At a final concentration of 0.4 mM DAD in the lens almost all light with an initial intensity of 300 W/m^2 will be absorbed by DAD (Figure 3.16 C). This effect, however, will be less dramatic in human applications due to a smaller lens relative to the eye size compared to mice (Figure 1.1 A and Figure 3.16 A, respectively). Furthermore, the lens can be easily removed during eye surgery and artificial lenses can be implanted instead. Depending on the

material these lenses may not be stained by DAD. Also, the working concentration of DAD lies between 100 and 200 µM and for human applications slow particle release approaches will be undertaken. Therefore high concentrations, such as 1 – 10 mM, will not occur in the vitreous.

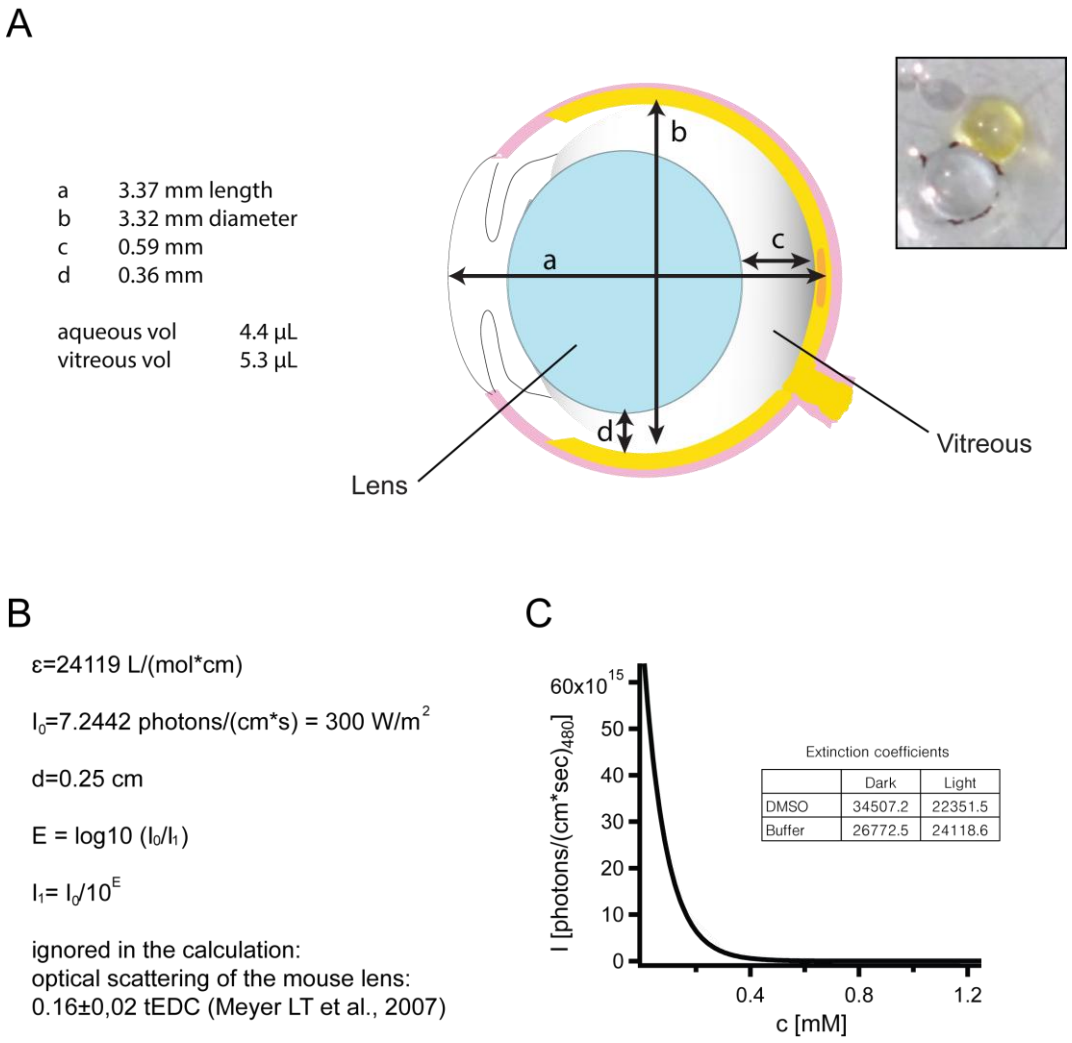

Figure 3.16 - Calculation for absorption of DAD after intravitreal injections in mice. (A) Schematic representation of a mouse eye. Figure modified from (Remtulla and Hallett 1985) and http://prometheus.med.utah.edu/~marclab/eyes.pdf (last accessed on 17 March 2015). Inset: Example of two lenses after intravitreal injection of vehicle only (white) and 15 mM DAD-HCl (yellow). Dissections were performed 4 hours post injection. **(B)** Calculation for DAD absorption in the mouse eye based on sizes of a mouse eye. Extinction coefficient ε was determined by UV/Vis spectroscopy at 460 nm light. Lengths of the lens was estimated with 0.25 cm and initiative light intensity was set to 300 W/m^2. **(C)** Graphical representation of calculations from figure B. Inset shows extinction coefficients determined in DMSO and ACSF in darkness and at 460 nm light. Calculations have been performed with the extinction coefficient at 460 nm in ACSF.

The high solubility of DAD has been shown by the good penetration into the retina and the lens, the latter one only at high concentrations. Furthermore, injections into macaque vitreous revealed good solubility properties, as has the short persistence after intravitreal injections. The solubility as well as the fast clearance is in stark contrast to previously

published less soluble photochromic blockers (e.g. DENAQ) and is advantageous for first clinical applications. In case of side effects treatment can be readily terminated. Furthermore, DAD penetrates the whole retina and not only a small portion due to diffusion limits and with this a more complex visual image might be achieved. And finally, the high solubility of DAD in water or buffer and the possibility of different formulations without changing the molecule's properties make it a perfect candidate for micro-particle release approaches. Small particle release approaches would also dramatically lower the concentration of DAD in the vitreous, because the working concentration lies between 100 µM and 200 µM. Therefore, the absorption problem will be limited in human patients.

Besides these pharmacokinetic properties, DAD has been shown to activate primarily bipolar cells in degenerating retinae. It is therefore the first diffusible photochromic ligand that selectively activates a specific cell type upstream from RGCs. Previous approaches with ChR2- and LiGluR-expression in on-bipolar cells revealed that utilizing the remaining neural network of the retina result in more complex output signals compared to the direct activation of RGCs (Mace et al. 2015, Gaub et al. 2014). The same effect holds true for DAD-induced light responses. Not only does DAD induce strong transient light-on responses, but it also leads to small transient light-off responses (*see* section 3.1.2). The same effect has been observed after ChR2-expression in on-bipolar cells of blind mice and has been attributed to lateral interactions between different bipolar cell types and amacrine cells (Mace et al. 2015). Although LiGluR-expression in on-bipolar cells should in principle induce the same light response, this effect has not been observed with this approach (Gaub et al. 2014). One explanation might be that ChR2 is localized throughout the whole plasma membrane of bipolar cells, whereas LiGluR expression is more localized to dendrites. Therefore, activation of ChR2 may lead to a much stronger depolarization compared to LiGluR activation. The same would hold true for DAD-induced activation, since potassium channels are not specifically localized to dendrites, but are rather distributed over the whole cell membrane. This stronger depolarization may contribute to the additional transient off-response in ChR2-expressing and DAD-treated retinae.

Genetic approaches have the advantage of being highly specific due to AAV-mediated delivery of the gene and promotor choice (i.e. mGluR6 promotor). This means that the genes can be targeted to only on-bipolar cells with no additional expression in off-bipolar cells or other retinal cell types. The PCL approach, on the other hand, is a simple pharmacological approach. Therefore, selectivity for on- versus off-bipolar cells cannot be guaranteed. It remains to be determined, whether DAD is more selective for one of the bipolar cell types. This, however, is a complicated task due to experimental limitations. First, DAD only acts on bipolar cells in degenerating retinae (*see* section 3.1.6). For clinical use this would be a great advantage, but for cell type identification DAD-activated cells cannot be compared to natural light responses. Second, DAD is a potassium channel blocker and therefore activation may depend on membrane potential. Studies in retinal

bipolar cells have demonstrated that retinal degeneration leads to changes in membrane potential in bipolar cells (Borowska et al. 2011). This might also explain why DAD only activates bipolar cells in degenerating retina. However, whole cell patch-clamp recordings and subsequent identification with immunohistochemistry of bipolar cells will not reveal the exact cell type activated by DAD, due to artificial changes in membrane potential. Two approaches that might reveal the exact bipolar cell type are currently under investigation. First, DAD-induced light responses in degenerating retinae are compared with CPPG application on MEA. CPPG is a selective antagonist for mGluR6, therefore RGCs activated by CPPG-stimulated on-bipolar cells can be identified. If DAD-mediated light responses would only be observed in the same RGCs as CPPG-induced responses, DAD would specifically activate on-bipolar cells. In a second approach, RGCs from DAD-treated retinae are patched with an intracellular solution containing neurobiotin (Neurobiotin tracer, vector laboratories, SP-1120). After detection of the light responses, the retinae are fixed with PFA and immunostained for neurobiotin and cholin acetyltransferase (ChAT). The ON and OFF ChAT bands in the IPL can then be used as landmarks for identifying stratification of bipolar cells and RGCs, which synapse in different layers depending on their type (Figure 3.17).

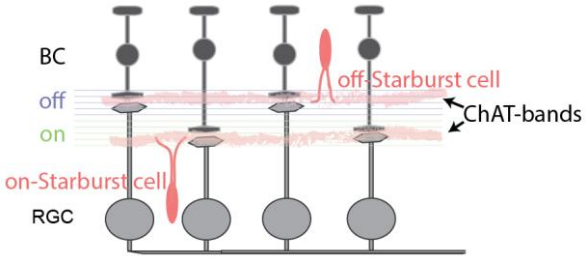

Figure 3.17 - Schematic representation of bipolar cell identification via ChAT bands. Starburst amacrine cells express high levels of cholin acetyltransferase (ChAT). Furthermore, they are divided into on- and off-starburst amacrine cells with distinct dendritic fields and are therefore useful as landmarks for bipolar cell stratification in the IPL.

This approach, however, may be limited due to retinal remodeling during the degeneration process (Marc et al. 2007, Marc et al. 2008). Recent studies further revealed that remodeling of the retina involves massive changes in glutamate receptor expression levels, i.e. on-bipolar cells exhibit high AMPA receptor expression levels (Chua et al. 2009, Dunn 2015, Jones et al. 2011, Marc et al. 2007). Furthermore, Lin et al. showed that not only the expression pattern, but also the AMPA receptor composition is changed after light-induced retinal degeneration (Lin et al. 2002).

Besides the identification of the exact target cell type, also the molecular target of DAD still remains unclear. HCN-channels, the target receptor of the second generation blockers DENAQ and PhENAQ, have shown to be up-regulated in degenerating retina (Tochitsky et al. 2014). However, application of ivabradine and cilobradine excluded HCN-channels as the molecular target of DAD.

Taken together, DAD has been shown to be a promising next-generation photochromic blocker for potassium channels in the retina. DAD targets cell types upstream from RGCs and in contrast to previous blocker generations (e.g. AAQ and DENAQ) is highly soluble in water and physiological buffer.

3.2 ATA: a selective photochromic AMPA receptor agonist for vision restoration

In the previous section DAD has been shown to be a promising candidate for vision restoration. In this section I want to demonstrate that not only photochromic channel blockers, but also photochromic receptor ligands are powerful molecules for restoring light-sensitivity to blind retinae. ATA is a selective photochromic AMPA receptor agonist in the dark and can be inactivated using blue light (440 nm–480 nm) (Figure 4.1 A). Its specificity and photopharmacological properties have been investigated in detail in cell culture and cortical neurons (Stawski et al. 2012).

Because photochromic receptor ligands are very different from channel blockers they might be a good complementary approach for vision restoration. Until today, no freely diffusible photochromic receptor ligand has been tested in blind retinae.

3.2.1 ATA conveys light-sensitivity to blind retinae

The functional properties of ATA were characterized in blind TKO retina using MEA recordings to monitor the spiking behavior of RGCs. Prior to the experiments retinae were incubated for a three minute period with 25 µM ATA. When switching between blue light (460 nm) and darkness robust light responses were detected (Figure 4.1 B) for hours without a significant rundown (data not shown). As in studies by Stawski et al. (2012) ATA was also active in the thermodynamically more stable *trans*-configuration in the retina and therefore induced significantly increased spiking rates in RGCs in the dark (dark: 22.9±6.36 spikes/s and 460 nm: 7.01±2.49 spikes/s, Figure 4.1 D). This spiking activity resulted in an overall negative PI of –0.50±0.05 (n = 10 retinae, Figure 4.1 C, red arrow).

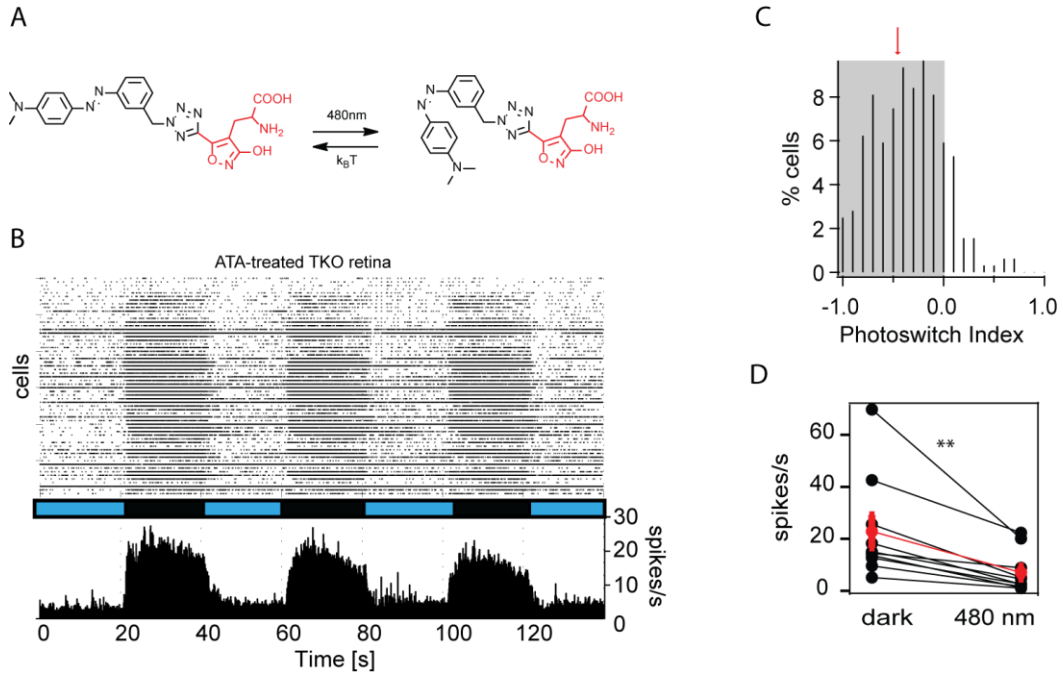

Figure 4.1 - ATA induces robust light-responses in genetically blind TKO retinae. (A) Molecular structure of ATA. Highlighted in red is the molecular structure of AMPA. Switching from *trans*- to *cis*-configuration is achieved using 460 nm light (Stawski et al. 2012). **(B)** Raster plot and histogram of MEA recording of ATA-treated TKO retina. The bar underneath the raster plot indicate the light stimulation protocol. **(C)** Statistics of light responses in ATA-treated TKO retinae. Distribution of PI for RGC populations (n = 962 cells). The red arrow indicates the mean PI for all recorded cells (PI = –0.50±0.05). **(D)** Average spiking rate in darkness and with 460 nm light; mean indicated in red (n = 10 retinae). Significance level $p < 0.01$ calculated using the Wilcoxon rank sum test. Figure adapted from (Laprell et al. 2015a).

Although the overall response was dark active, on single cell level the light-dependent responses showed a strong diversity, indicating an upstream effect of ATA in the retina. This hypothesis is further supported by the different ATA-induced light responses in the RGC layer (Figure 4.1 C and 4.2).

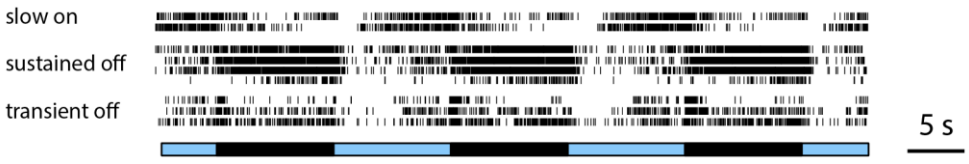

Figure 4.2 - ATA induces different light responses on single cell level. Raster plot of example RGCs showing slow on-light responses, sustained and transient off-light responses. The bar underneath the raster plot indicate the light stimulation protocol. Figure adapted from (Laprell et al. 2015a).

The pharmacological profile of ATA was the same in the retina as in previous studies in cortical neurons (Stawski et al. 2012). Application of the AMPA receptor antagonist NBQX (25 µM) completely blocked light-dependent firing in RGCs confirming that ATA is also a selective agonist for AMPA receptors in the retina. Background spiking during light and dark cycles was unchanged and the overall PI was –0.06±0.004 with 2.74±0.44 spikes/s and 3.56±0.41 spikes/s in light and dark, respectively (n = 8 retinae) (Figure 4.3).

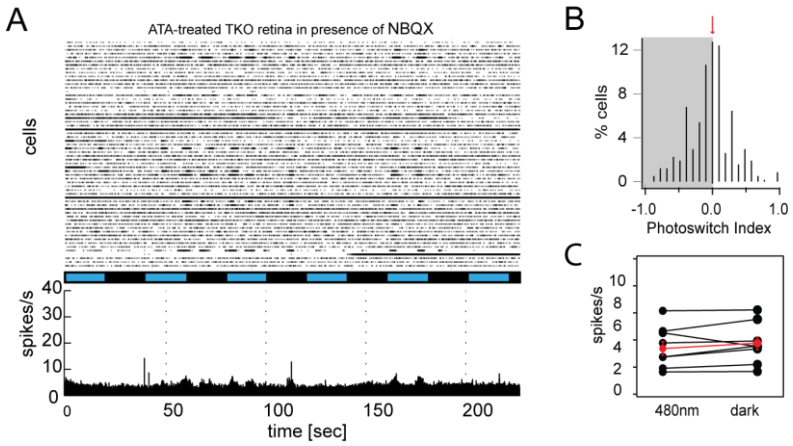

Figure 4.3 - ATA exclusively light-sensitizes AMPA receptors in the degenerating retina. (A) Raster plot and histogram of MEA recording of ATA-treated TKO retina in presence of 25 µM NBQX. **(B)** Statistics of light responses in ATA-treated TKO retinae. Distribution of photoswitch index for RGC populations (n = 286 cells). The red arrow indicates the mean photoswitch index for all recorded cells (Photoswitch Index = –0.06±0.004). **(C)** Average spiking rate in darkness and with 460 nm light (n = 8 retinae). Average is presented as MEAN±SEM. Figure adapted from (Laprell et al. 2015a).

3.2.2 Various cell types shape the ATA-induced light response

AMPA receptors are expressed in a wide variety of retinal cell types (Gilbertson et al. 1991, Zhou et al. 1993, Boos et al. 1993, Cohen and Miller 1994, Yu and Miller 1995). To intentify the main target cell types of ATA pharmacological experiments were undertaken. In the first set of experiments $CdCl_2$ was applied to isololate RGC light responses. The light response in presence of $CdCl_2$ was significantly altered. Instead of a sustained light-off response (Figure 4.4 A), a strong transient light-off response with a following slower sustained response was observed in all experiments (Figure 4.4 B). The background spiking activity, however, was unchanged, resulting in a lower PI compared to retinae without blockers (PI (w/$CdCl_2$) = –0.60±0.09, n = 6 retinae). Interestingly, in a few experiments the application of $CdCl_2$ resulted in a brief transient light-on response in addition to the transient and sustained off-light responses (Figure 4.5). This effect is possibly induced by gap junctions generating homologous RGC-RGC as well as heterologous RGC-amacrine cell interactions (Bloomfield and Volgyi 2009). The slower onset of the sustained off-response is most likely due to the desensitization of AMPA receptors.

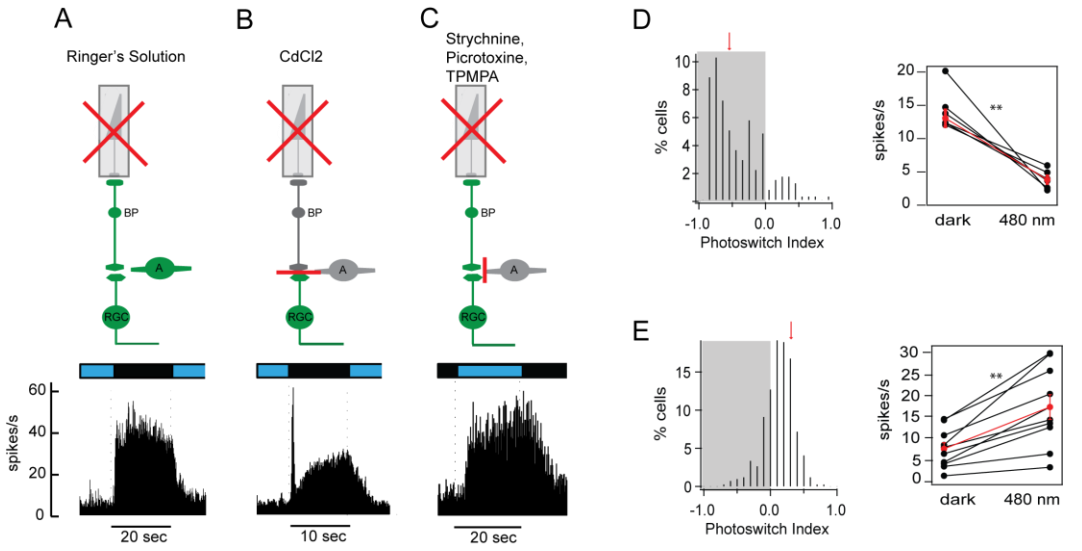

Figure 4.4 - Pharmacological approaches reveal that ATA mediates its light-responses primarily through RGCs and amacrine cells.
(A-C) Top:: Schematic drawing of retinal cell types. Cells depicted in green may contribute to the light-dependent effect of ATA on RGC-output . Bottom: Histogram of ATA3-induced light-response. **(A)** No blockers are applied, therefore all retinal cell types may contribute to RGC output. **(B)** Synaptic inputs from amacrine and bipolar cells are blocked using $CdCl_2$. Therefore, RGCs are synaptically isolated from the remaining retina. **(C)** Inhibitory input on RGCs are specifically blocked by strychnine, picrotoxine and TPMPA. RGC signal output consists of bipolar cell- and RGC-mediated components. **(D)** Statistical analysis of light responses in ATA-treated TKO retinae in presence of 500 µM $CdCl_2$. (Left) Distribution of PI for RGC populations (n = 797 cells). The red arrow indicates the mean PI for all recorded cells (PI = –0.6±0.09). (Right) Average spiking rate in darkness and with 460 nm light (n = 6 retinae). Average is presented as mean±sem. **(E)** Statistical analysis of light responses in ATA-treated TKO retinae in presence of strychnine, picrotoxine and TPMPA. (Left) Distribution of photoswitch index for RGC populations (n = 418 cells). The red arrow indicates the mean PI for all recorded cells (PI = 0.36±0.03). (Right) Average spiking rate in darkness and with 460 nm light (n=10 retinae). Average is presented as mean±sem. Significance level $p < 0.01$ calculated using the Wilcoxon rank sum test. Figure adapted from (Laprell et al. 2015a).

Together, the strong transient off-response and the slower sustained response in presence of $CdCl_2$ demonstrate that ATA has its primary effects on RGCs. However, the different shape of light response further indicates a more complex mode of action. To determine, which other cell types shape the overall response, the inhbititory input from amacrine cells to RGCs was blocked using a combination of strychnine (1 µM), picrotoxin (5 µM) and TPMPA (10 µM). Thereby, only bipolar cell to RGC signal transmission was recorded. Interestingly, the light response was inverted when inhibitory inputs were blocked (PI = 0.36±0.03, n = 10 retinae) (Figure 4.4 C). This cannot be explained by a simple computational model of the retina, since ATA should have the same effect on all retinal cell types, i.e. it activates AMPA receptors in the dark. In this scenario, however, ATA would activate bipolar cells in light to a stronger extend than RGCs in darkness. In addition to the inversion the light-on response was slightly delayed compared to the light response in buffer (Figure 4.4 A).

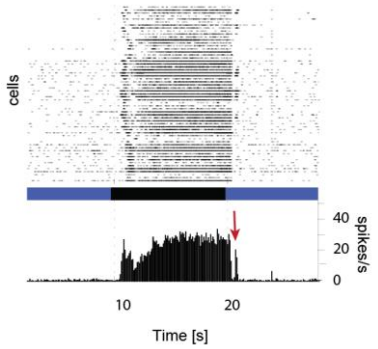

Figure 4.5 - ATA induces small light-on responses in some TKO retinae after application of $CdCl_2$. In rare cases $CdCl_2$ did not only induce transient light-off responses, but also transient light on-responses in comparable RGC spiking frequencies. Figure adapted from (Laprell et al. 2015a)

Summarized, these results indicate that inputs from all three major cell types shape the overall output of ATA-mediated light response. The most prominent effects, however, result from a combination of amacrine cells and especially RGCs light activation.

3.2.3 Intravitreal injections of ATA

MEA recordings after intravitreally administered ATA were performed to demonstrate that the molecule is able to penetrate the retina and to induce light-responses after injection *in-vivo*.

Together with Arshan Perrera (LMU Munich, AK Prof. Biel), 1 µL of 1 mM ATA (Na^+) in PBS was injected into the vitreal cavity in anaesthetized TKO mice. After 6 hours the animals were sacrificed and the retinae dissected. All injected animals did show ATA-mediated light responses on MEA (n = 5 retinae). Surprisingly, the spiking frequency was increased when light was switched on in contrast to the *ex-vivo* experiments (Figure 4.6) (section 3.2.1). Furthermore, in a few retinae the overall shape of the light response was altered to a more transient peak-response compared to the slow sustained light responses after short incubation times *ex-vivo*. The inversion of the light response may be due to desensitization of neurons, which are activated in the dark. However, it remains to be elucidated, which cell types are responsible for the light-on responses in RGCs (see also section 3.2.2).

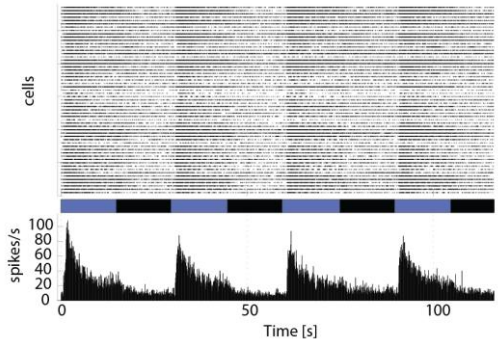

Figure 4.6 - ATA-mediated light responses show a transient light-on response after intravitreal injections. Raster plot and histogram of a MEA recording 6 hours post injection.

3.2.4 Discussion ATA

Although ATA has a broader action on different retinal cells and a less pronounced light-response compared to DAD, it is yet a promising PCL for vision restoration. This molecule is the first diffusible photochromic receptor agonist, which has been tested in blind retinae. Therefore, ATA expands the range of molecule classes for the photopharmacological approach of vision restoration.

ATA bears important new features compared to previous generation blockers, such as AAQ and DENAQ. First, ATA is highly solubility in water (200 mM when formulated as the Na^+-salt) and second, it activates cells from the extracellular site. Therefore, ATA does not need to be taken up by the cell and the ATA-induced stimulation resembles a more natural stimulus by mimicking excitatory synaptic transmission rather than blocking and unblocking potassium channels.

ATA has been shown to be actively switched off using visible light in the blue range (440-480 nm), but white light has been demonstrated to be as efficient as blue light (PI = –0.38±0.03, n = 11 retinae) (Figure 4.7). In addition, working concentrations of ATA are very low (25 µM), only require short incubation times (3-5 minutes) and the light responses remain over several hours without significant rundown. This effect can likely be attributed to the hydrophobicity of the azobenzene photoswitch, serving as a reservoir in the membrane. This hypotheses is further supported by the yellow coloring of the retina after incubation, which last throughout the experiment.

In pharmacological experiments it was demonstrated that primarily amacrine cells and RGCs shape the overall ATA-induced light response. However, the experiments with $CdCl_2$ revealed that ATA can act on RGCs alone. This might be beneficial for patients with advanced retinal degeneration, in which PCLs for upstream cell targets might not work.

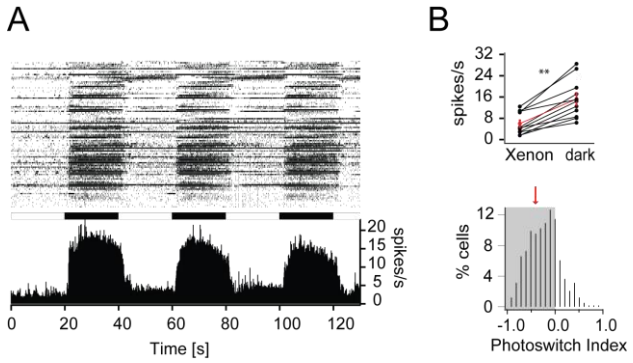

Figure 4.7 - ATA-induced light responses with Xenon light source. (A) Raster plot and histogram of MEA recording of ATA-treated TKO retina with white light application. Bar underneath the histogram represents dark and Xenon illumination. **(B)** Average spiking rate in darkness and with 460 nm light for individual experiments (n = 11 retinae, $p < 0.01$). The overall average is presented as mean±sem (red). **(C)** Statistics of light responses in ATA-treated TKO retinae. Distribution of PI for RGC populations (n = 577 cells). The red arrow indicates the mean PI for all recorded cells (PI = –0.38±0.04). Figure adapted from (Laprell et al. 2015a).

Taken together the pharmacological experiments revealed the molecular and the cellular targets of ATA. However, the effect of ATA in the absence of inhibitory input cannot be easily explained. It is clear that amacrine cell input inhibits signal transmission from bipolar to RGCs, by which the ATA response of RGCs prevails. Yet, the exact mechanism of bipolar cell light-activation cannot be clarified with this experiment. A simple explanation of the inversion in bipolar cells would have been the activation of metabotropic glutamate receptors in on-bipolar cells (such as mGluR6), which was ruled out by the NBQX experiments. Recent studies, however, demonstrated dramatic changes of iGluR expression levels in degenerating retinae. Studies of retinal remodeling in rd1/rd1 mice showed that at postnatal day 15 on-bipolar cells exhibit poor activation of mGluR6 and show an increased expression level of iGluRs, thereby shifting its functionality from on- to off-bipolar cells (Chua et al. 2009). A different study revealed that as long as remaining cones are present, although non-functional, the distribution of off- to on-cone bipolar cells and rod-bipolar cells is shifted from 40:30:30 to nearly 80:15:05 (Marc et al. 2007, Jones et al. 2011). Loss of mGluR6 after photoreceptor ablation further substantiate this finding of change in cell fate (Dunn 2015). Further complicating matters, Lin et al. could demonstrate that AMPA receptor composition is dramatically changed in retina after light-induced retinal degeneration (Lin et al. 2002). These physiological effects are only a few examples of the severe alterations happening through retinal degeneration. Remodeling not only affects expression levels of specific receptors, but lead to dramatic changes in the overall synaptic transmission, which further revises the fundamental topology of the retina (Jones et al. 2012). These substantial changes in retinal architecture make it hard to predict and evaluate specific activation patters for ATA. However, retinal remodeling may not only influence PCL approaches, but also strongly impact genetic approaches using ChR2 or LiGluR.

Taken together, ATA is the first freely diffusible photochromic receptor ligand used for restoration of light perception in blind retinae. It can be inactivated using blue or white light and most importantly, it was demonstrated that ATA is able to directly photosensitize RGCs, regardless of the effects on bipolar, amacrine cells and effects of retinal remodeling.

3.3 Restoration of transient light-on and light-off responses using a combination therapy approach

DAD and ATA have been shown to exhibit very different properties. In the retina, DAD strongly increases spiking frequency in RGCs upon illumination with blue light, whereas ATA is active in the dark-adapted *trans*-state and needs to be actively switched off with light. Furthermore, DAD primarily targets bipolar cells, while RGCs and amacrine cells are the major target cell types of ATA.

These different features made the molecules good candidates for a combinatorial approach to see whether strong on- and off-light responses can be restored using different PCLs. After a short 3-minute incubation with both compounds (100 µM DAD and 25 µM ATA), the same light stimulation protocol was applied to the retinae as in previous experiments with only one compound. Alternating blue light and dark stimulation was able to induce both light-on and -off responses (Figure 5.1). Interestingly, light-off responses, which can be attributed to ATA-activation, were transient rather than sustained. ATA application alone did only result in slow sustained light-off responses (*see* section 3.2.1). However, these transient light-off responses cannot be attributed to DAD, since it is much more pronounced compared to the light-off responses in retinae treated with DAD only (PI_{on} = 0.52±0.06 and PI_{off} = 0.26±0.06, n = 6 retinae) (Figure 5.1 A-D and 2.3 B, respectively). Furthermore, a complex signal output can be observed on single RGC level. In 42 % of all RGCs both, transient light-on and transient light-off responses, were detected. From the remaining cells 37 % of RGCs exhibited transient light-on responses and only 21 % of RGCs showed transient light-off responses (n = 412 RGCs) (Figure 5.1 E). For comparison, in retinae treated with DAD only, the distribution was 22 % on-off, 66 % only on- and 12 % only light-off responses (*see* section 3.1.3). The combination of DAD with ATA showed similar distributions of RGCs to wild type at postnatal day 13 (ON-RGC: 35.0 %, OFF-RGC: 10.8 % and ON-OFF-RGC: 54.1 %, (Liu et al. 2009). The shift in light-responses compared to DAD- or ATA-treatment alone is further supported by the PI distribution of TKO retinae treated with both, which spanned a range similar to the PI distribution of wt retinae (Figure 5.1 F).

The shift from on-light responses to on-off light responses was further investigated by analysis of RGC spike correlation (Figure 5.2). Prior illumination RGC spiking activity was not correlated (Figure 5.2 A; blue-green), while activation of DAD and inactivation of ATA with blue light induced a strong positive correlation within the RGC layer (Figure 5.2 B). After switching light off many RGCs exhibit a transient increase in spiking frequency again, which led to a positive correlation within the first second in the dark (Figure 5.2 C). Importantly, this light-off correlation is much more pronounced when compared to correlation experiments with DAD alone (Figure 3.5 *see* section 3.1.2).

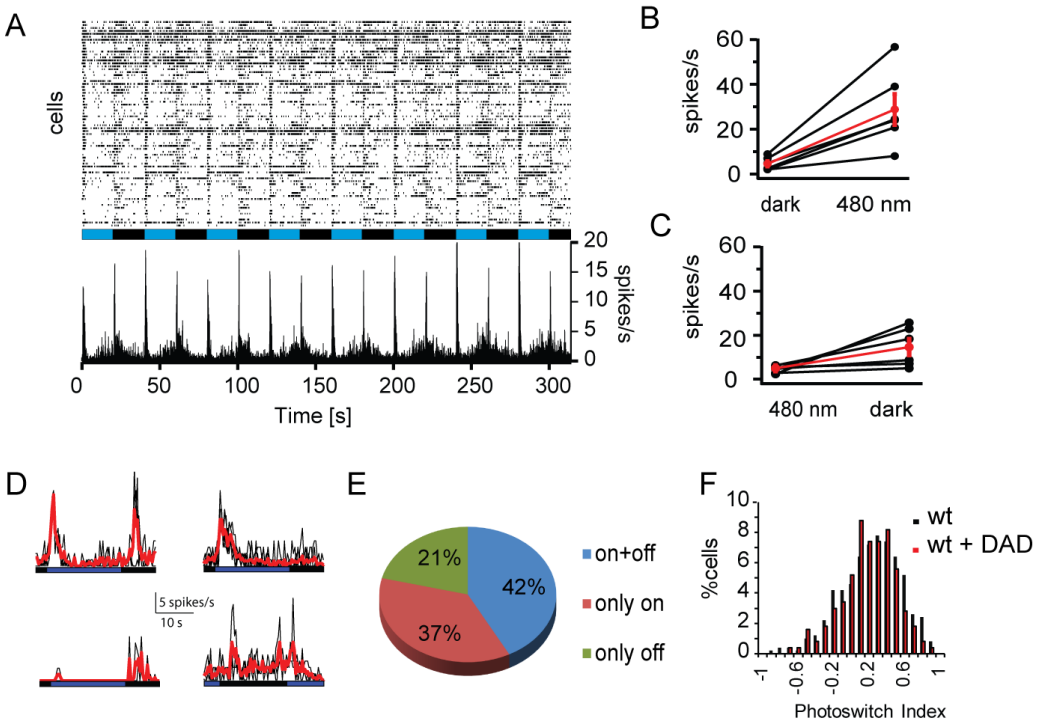

Figure 5.1 - Combination therapy induce transient light-on and light-off responses in blind retinae. (A) Raster plot and histogram of a MEA recording in a TKO retina after treatment with 200 µM DAD and 25 µM ATA. The bar underneath the raster plot indicates light/dark stimulation (blue: 460 nm, black: dark). **(B)** Average spiking rates upon onset of 460 nm light (n = 6 retinae). Average is presented as mean±sem. **(C)** Average spiking rates upon offset of 460 nm light (n = 6 retinae). Average is presented as mean±sem. **(D)** Example histograms for DAD and ATA treated TKO RGC light responses. The bars underneath the histograms indicate the light stimulation protocol. **(E)** Percentage distribution of DAD and ATA mediated light responses. 42 % of all recorded RGCs in TKO mice show both, on- and off-light responses. 37 % only show only on- and 21 % solely off-responses (n = 412 cells in 6 retinae). **(F)** Distribution of photoswitch index for RGC populations with combination therapy in TKO retinae (red) compared to wild type retinae (black) (n = 11 TKO retinae and n = 7 wt retinae). Figure adapted from (Laprell et al. 2015c).

Taken together, the combination experiments demonstrated that PCLs are able to induce light responses similar to those in wt retinae. Although DAD, like ChR2 or LiGluR, is in principle able to restore both light-on and -off responses, the additional application of ATA revealed an even more pronounced effect. The exact working mode of the combinatorial approach needs to be further investigated, especially in respect to the shift from sustained to transient light-off responses. However, ATA has been the first photochromic receptor ligand applied to blind retinae and with novel next-generation molecules developed an even higher specificity may be achieved. To date, the only optochemical approaches able to restore both, light-on and -off responses, were to either targeting ChR2 or NpHR to remaining cones or on-bipolar cells (Busskamp et al. 2010, Werblin 2011, Mace et al. 2015). Here, a novel photopharmacological approach for restoration of transient on- and off-responses is presented, which does not require any genetic manipulation.

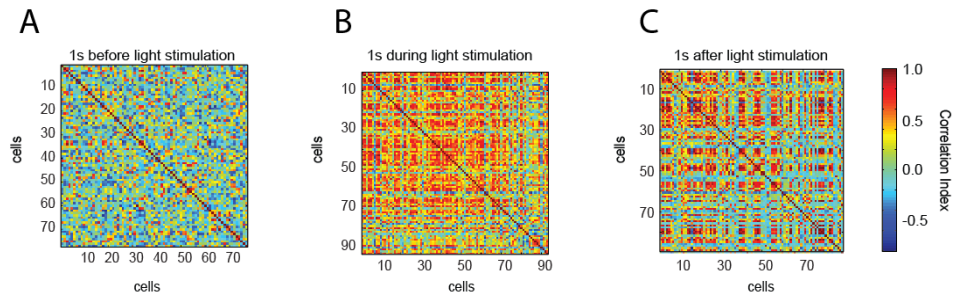

Figure 5.2 - Example of correlation of light responses in DAD/ATA-treated retina. (A) Correlation of RGC responses 1 s before light stimulation. **(B)** Correlation during the first second of light stimulation. **(C)** Correlation within the first second after switching off light. One second binning was applied. Red indicates high correlation while green indicates no correlation (Scale bar at the right). During light stimulation most cells and after switching off light a fraction of cells show a positive correlation in RGC firing. Figure adapted from (Laprell et al. 2015c).

3.4 Conclusion: Vision restoration

Degenerative diseases of the outer retina, such as RP and AMD, lead to visual impairment and eventually to complete blindness with no cure currently available. In the past decade several approaches towards restoration of vision have been investigated (*see* section 1.2). Opto-electronic devices, such as Argus II and alpha-IMS, as well as the still more experimental optogenetic approaches are promising strategies for the restoration of vision (*see* section 1.4). However, both exhibit specific limitations. Introduction of retinal implants is highly invasive and may lead to severe scarring of ocular tissue. Furthermore, the durability of the devices is limited due to corrosion of material and the density of stimulation electrodes is not only restricted by the size, but also by safe levels of extracellular current. In principle, this approach is reversible and would allow exchange for novel devices, but scarring of tissue and high costs may limit the realization.

Optogenetic approaches are invasive on a different level than opto-electronic devices. The introduction of the genes may have no effect on ocular tissue in respect to scarring. However, it remains to be seen, whether adding new genes (especially non-human genes) may induce undesirable side effects. Furthermore, optogenetic approaches are irreversible and cannot be readily terminated or exchanged for next-generation approaches. The introduction of modified channels, such as LiGluR, may circumvent some of these limitations as it is not 'xenogenetic' and the ligand would be interchangeable, nevertheless the target protein would remain the same (Gaub et al. 2014, Caporale et al. 2011).

In this chapter three different photopharmacological approaches towards restoration of vision were presented. The first approach is based on the photochromic potassium channel blocker DAD, which selectively targets bipolar cells in the degenerating retina (*see* section 3.1). In the second approach the photochromic excitatory amino acid, ATA, was applied to blind retinae. This is the very first example of a freely diffusible PCL based on a receptor ligand applied for vision restoration (*see* section 3.2). As such, it complements previous pharmacological approaches based on photochromic channel blockers. The potential of photopharmacology in vision restoration is further increased by the possibility to combine PCLs with different properties. Using this strategy robust light-on as well as light-off responses can be induced similar to those in wt retinae (*see* section 3.3). These photopharmacological approaches circumvent almost all drawback mentioned for the implantation or optogenetic approaches by being a mere pharmacological strategy. PCLs can be added or removed from the system as required without the need of genetic modification. This not only allows to stop treatment in case of side effects, but its reversibility also rises the opportunity to develop better molecules and to adjust the treatment to the needs of the patient. Furthermore, the photopharmacological approach is not limited to a specific stage of disease onset. DAD has been shown to effect only degenerating retinae, however, it already induces light sensitivity in young mice in which

only parts of the retinae were degenerated (*see* section 3.1.6). Opto-electronic devices and optogenetics would always target both, healthy and degenerated tissue, thereby interfering with the remaining vision during early onset of disease. Additionally, the photopharmacological approach is adaptable to the progress of the disease by targeting different cell types. During early onset photochromic ligands for the activation of bipolar cells could be applied, while late stage patients would receive ligands that primarily target the remaining RGCs.

Taken together, the photopharmacological approach using freely diffusible photochromic ligands is not only minimally invasive and cheaper, but it is also flexible in its application.

In respect to previous photopharmacological approaches, DAD and ATA have been shown to be advantageous in terms of application. Both molecules, when formulated as salts, are highly soluble in physiological buffers giving the opportunity for sustained drug release using nano-/microparticle approaches (Rowe-Rendleman et al. 2014, London et al. 2011). Furthermore, DAD and ATA both need substantially shorter incubation times. This may be likely attributed to the molecular structures, i.e. both compounds are non-permanently charged. Another advantage of DAD and ATA over previous generation photochromic ligands is the activation of upstream cell targets. Thereby, the remaining retinal circuitry is utilized, which will most likely lead to higher image resolution and increased information transferred to higher brain regions.

4 PCL characterization

4.1 ATG

4.1.1 Introduction ATG

Ionotropic glutamate receptors (iGluR) form non-selective cation channels that mediate fast excitatory synaptic transmission. The group of iGluRs can be subdivided according to their specific agonist, i.e. AMPA, kainate and NMDARs. They are ubiquitously expressed throughout the nervous system where they are responsible for the excitatory synaptic transmission between neurons. In this chapter I will focus on NMDARs, which are associated with synaptic plasticity, i.e. long-term depression and potentiation (Paoletti et al. 2013). In addition, many diseases have been linked to NMDARs dysfunction, such as Alzheimer's and Huntington's diseases.

NMDARs are composed of four subunits as hetero-oligomeric membrane proteins. GluN1 subunits are obligatory for receptor formation and the binding of the co-agonist, i.e. glycine or D-serine, whereas glutamate binds to the GluN2 subunits.

Recently, a functional tetrameric receptor structure has been described, which will provide deep insights into specific receptor function and disease mechanisms (Karakas and Furukawa 2014, Lee et al. 2014). However, most NMDAR properties were obtained through electrophysiological recordings, demonstrating the relevance of these experiments. To probe the function of iGluRs in the brain several variants of caged agonists and antagonists have been developed, which take advantage of the spatio-temporal precision of light. Compounds like caged glutamate, caged NMDA or caged MK-801 have been proven to be useful elucidate the function of glutamate receptors in synaptic transmission (Gee et al. 1999, Maier et al. 2005, Rodriguez-Moreno et al. 2011, Kramer et al. 2009, Thompson 2005). Caged compounds, however, entail one major drawback: Although receptor activation can be precisely timed, they cannot actively be switched off and therefore the deactivation remains diffusion limited (DiGregorio et al. 2007).

PCLs circumvent this limitation and can be called 'reversibly caged' ligands. They can repeatedly be switched between their active and inactive state. Furthermore, PCLs do not generate photochemical byproducts, which may have toxic side effects when accumulated. In this section azobenzene-triazole-glutamate (ATG), a novel photoswitchable glutamate derivate will be described (Figure 6.1 A).

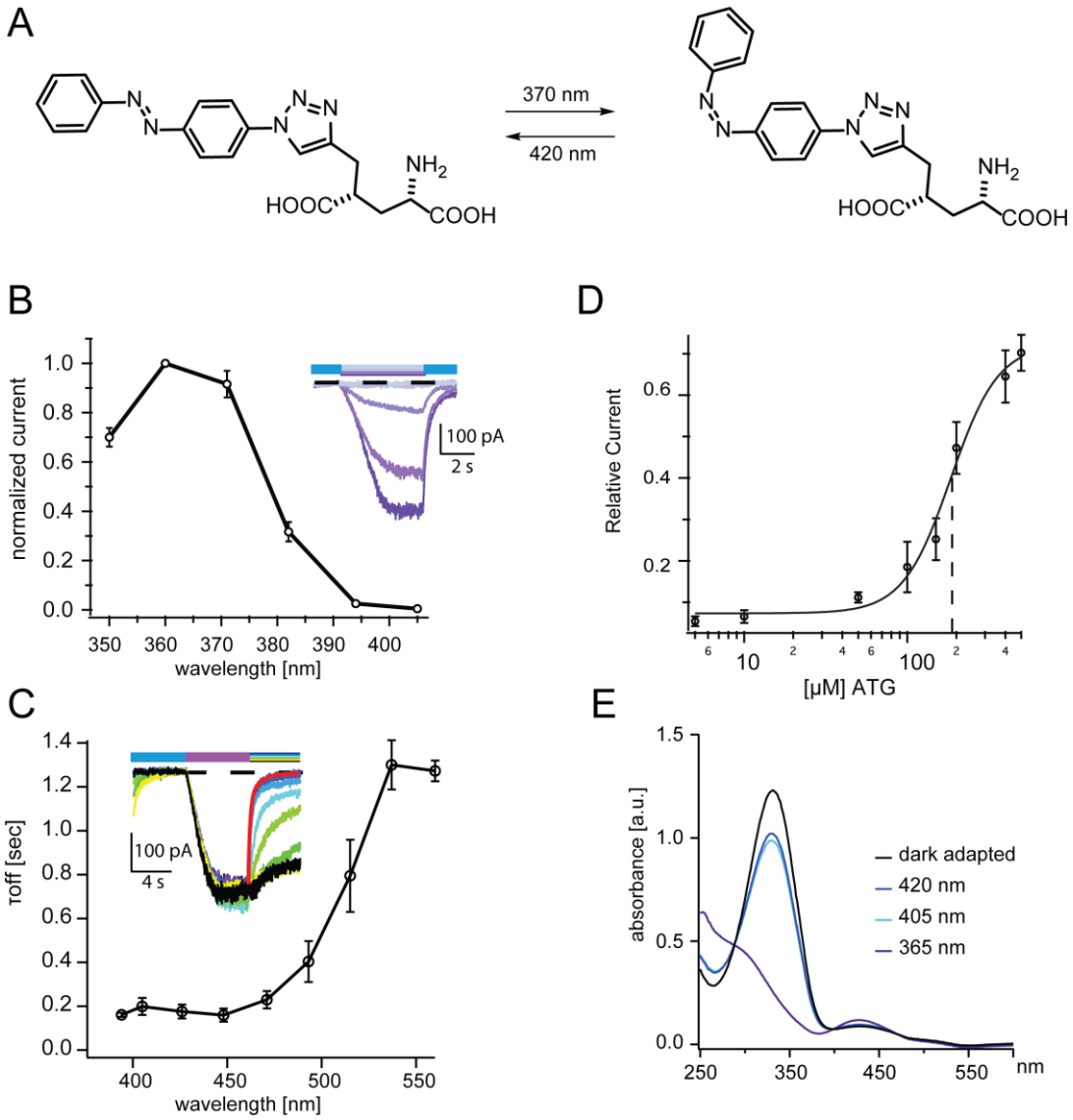

Figure 6.1 - Action spectrum, kinetics and dose-response curve. (A) Molecular structure of ATG. *Trans*- to *cis*- and *cis*- to *trans*-conversion can be achieved using near UV and blue light, respectively. **(B)** Wavelength screening for activation of ATG-mediated currents. Current amplitude was measured after 5 s light stimulation with the respective wavelength and normalized to the maximal current amplitude at 360 nm. Inset: Raw data traces for 5 s light stimulation from 360 nm to 410 nm light (dark to light violet. **(C)** Wavelength screening for τ_{off} kinetics of ATG-mediated currents. Measurement of τ_{off} kinetics for wavelengths between 400 nm and 540 nm light. Inset: Raw data traces showing the off-kinetics after a 5 s light-stimulation with 370 nm. Best τ_{off} kinetics were achieved at 425-450 nm light (red trace: exponential fit). **(D)** Dose-response relationship of ATG-mediated currents in cortical slice preparations. Concentrations from 1 to 500 µM were tested. The EC_{50} is 185 µM and was calculated using the Hill-equation. **(E)** UV/vis spectra of ATG in the dark-adapted state and during illumination with 370, 405 and 420 nm light. Figure modified from (Laprell et al. 2015b).

4.1.2 ATG: a selective PCLs for NMDA receptors

Characterization of ATG was performed in mouse layer 2/3 cortical neurons. Perfusion with 200 µM ATG allowed photo-control of neural activity by toggling between 360-370 nm and 420 nm light (Figure 6.1). ATG is inactive in its thermodynamically stable *trans*-configuration and induces large currents after switching to *cis*-configuration with near UV-

light, in contrast to previously published glutamate receptor agonists, e.g. GluAzo and ATA (Volgraf et al. 2007, Stawski et al. 2012). Lambda screen experiments revealed that wavelengths between 350 nm and 370 nm were best for receptor activation (Figure 6.1 B) and that τ_{off} was fastest using 420 nm light (τ_{off} = 0.17 s ± 0.03; n = 16, Figure 6.1 C). These findings are in accordance with measured UV/vis spectra, in which 365 nm was best for *trans*- to *cis*-isomerization and 405 nm–420 nm wavelengths were best for switching back (Figure 6.1 E). If no light is applied after *trans*- to *cis*-isomerization, thermal relaxation into the *trans*-isoform was very slow in physiological buffer solution (Figure 6.2).

Together with the lab of Prof. DiGregorio (Institute Pasteur, Paris) we could further show that ATG can also be two-photon activated (720 nm), which allows high spatio-temporal precision, such as single spine activation (Laprell et al. 2015b).

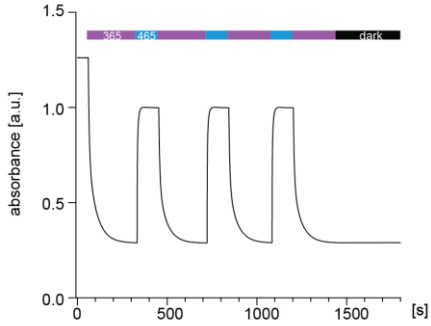

Figure 6.2 - Thermal stability of ATG. Kinetics of the conversion of *trans*- to *cis*-ATG during illumination with 460 nm and 365 nm light (high power LEDs) measured at the maximal absorption wavelength of *trans*-ATG (330 nm). Figure adapted from (Laprell et al. 2015b).

In current-clamp mode switching to *cis*-configuration using 370 nm light induced strong action potential firing (Figure 6.3 A), which was readily terminated after switching back to 420 nm light. Furthermore, using dose-response experiments an EC_{50}-value of 185 µM for *cis*-ATG was determined (Figure 6.1 D).

The molecular target receptors of ATG were identified in various pharmacological experiments. Photosensitization of cortical neurons was completely abolished in presence of D-AP5, a competitive NMDAR antagonist (Figure 6.2 B). Current-voltage relationships further substantiated the finding that ATG selectively activates NMDARs. The ATG-induced IV-relationship was directly compared to an NMDA puff induced IV-relationship. In presence of ATG alone, currents had the characteristic J-shaped relationship attributable to the magnesium (Mg^{2+}) block of the NMDAR pore at membrane resting potential (Dingledine et al. 1999) (Figure 6.3 C). In absence of Mg^{2+} the IV-relationship was found to be linear and the reversal potential was close to 0 mV, as it is expected for a non-selective cation channel. IV-relationships showed no current in presence of the NMDAR antagonist D-AP5 or MK-801, a pore blocker of NMDARs (Figure 6.4, green and blue traces, respectively). NBQX on the other hand, had no significant effect on the IV-relationship (Figure 6.4, red trace). Taken together, the pharmacological experiments and the IV-relationships

demonstrate that ATG selectively activates NMDARs and has no effect on AMPA or kainate receptors in mouse cortical neurons.

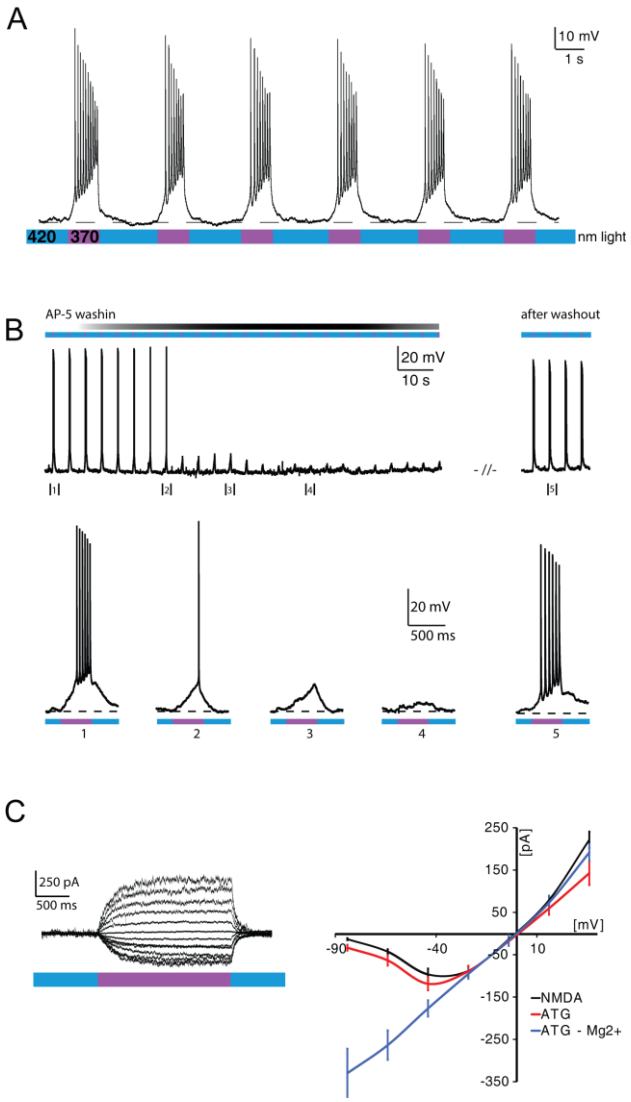

Figure 6.3 - Photopharmacology of ATG. (A) Current-clamp recording of a cortical neuron in an acute slice preparation. Irradiation with 370 nm light (violet) induces robust action potential firing that is terminated by irradiation with 420 nm light (blue). **(B)** Washing in AP-5 (50 µM), an NMDA-specific antagonist, blocks the ATG-mediated light-dependent action potential firing. **(C)** Current-voltage relationships indicative of NMDARs as targets for ATG. Black: Current-voltage relationship of puff-applied NMDA currents (n = 12 cells). Red: Current-voltage relationship of ATG-mediated currents under 370 nm light (n = 10 cells). Blue: Current-voltage relationship of ATG-mediated currents in the absence of Mg^{2+} ions (n = 10 cells). Error bars indicate SEM. Figure adapted from (Laprell et al. 2015b).

In collaboration with Jan Terhag (Prof. Michael Hollmann, Ruhr-University Bochum, Germany) we investigated, whether ATG is NMDAR-subtype selective. We therefore heterologously expressed different heterotetramers of GluN1 with GluN2A-D in *Xenopus* oocytes. Here, ATG was able to light-activate NMDARs equally for all subtype compositions, however, to a much smaller extent than glutamate (max. 9 % of glutamate-evoked currents (Laprell et al. 2015b). This finding demonstrates that ATG-activation is less efficient when receptors are heterologously expressed.

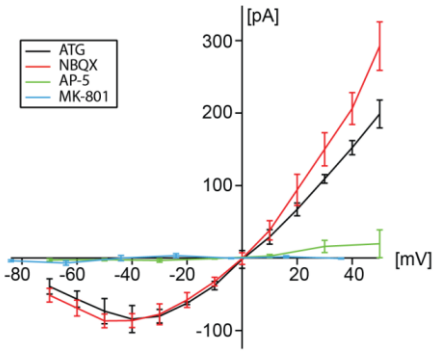

Figure 6.4 - Current-voltage relationship of ATG-mediated currents (370 nm) in the presence of NMDAR and AMPAR antagonists in cortical neurons. 200 µM ATG was used for all experiments. Black: control Red: 25 µM NBQX (n=8 cells), a selective AMPAR antagonist. Green: 40 µM AP-5, a selective NMDAR antagonist (n = 3 cells). Blue: 50 µM MK-801, a selective NMDAR blocker (n = 5 cells). Single data points represent mean±SEM. Modified from (Laprell et al. 2015b).

4.1.3 Calcium imaging

In contrast to AMPA and kainate receptors, NMDARs are highly permeable to Ca^{2+} and are therefore important mediators for intracellular calcium signaling. Ca^{2+} influx through NMDARs is in particular associated with postsynaptic alterations, such as glutamate receptor expression, thereby influencing synaptic plasticity (Dingledine et al. 1999). To investigate whether ATG-mediated currents are large enough to increase intracellular Ca^{2+} levels, imaging experiments were performed using the fluorescent Ca^{2+}-indicator Quest-Fluo-8-AM. Acute brain slices were incubated with the membrane-permeable indicator and TTX was added to the perfusion to prevent calcium entry through spontaneous network activity (Figure 6.5). After light activation of ATG large calcium-transients were detected ($\Delta F/F = 20\pm3$ %, n = 18 cells) (Figure 6.5 B left). Since the activation of NMDARs depolarizes the membrane, a fraction of the calcium signal can be attributed to calcium entry through voltage-gated calcium channels. Therefore, felodipine a VGCC-blocker was applied which significantly reduced the calcium signal ($\Delta F/F = 13\pm3$ %, n = 10 cells, $p < 0.05$, Wilcoxon rank sum test, Figure 6.5 B right), leaving the remaining Ca^{2+} transients exclusively evoked by ATG-mediated NMDAR activation (Figure 6.5 B inset).

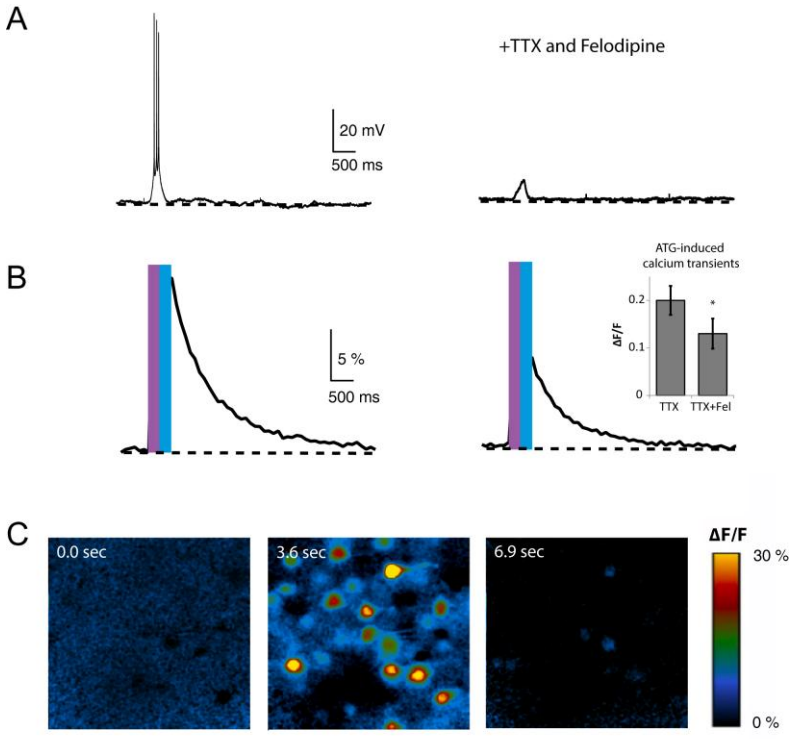

Figure 6.5 - Calcium imaging using ATG in hippocampal neurons. (A) ATG-mediated electrical signals elicited with 370 nm light and terminated with 420 nm (250 ms light pulse). right – in the presence of 40 µM Felodipine (Fel) and 1 µM TTX. **(B)** Corresponding calcium transients to (a). Bar graph: Quantification of calcium transients (ATG+TTX: n = 18 and ATG+TTX+Felodipine: n=10). *p < 0.05, Wilcoxon rank-sum test. Error bars indicate SEM. **(C)** Changes in fluorescence (ΔF/F) at different time points of the calcium transient; prior to light stimulation, immediately after illumination and after returning to basal calcium levels. Figure adapted from (Laprell et al. 2015b).

4.1.4 Mimicking synaptic coincidence detection with ATG

NMDARs are coincidence detectors of post- and presynaptic activity due to their physiological properties. Activation of NMDARs not only require binding of two agonists, glutamate and an allosteric modulator (i.e. glycine or D-serine), but also the Mg^{2+} block needs to be removed from the pore by an initial depolarization through AMPARs (Nevian and Sakmann 2004). This Mg^{2+} block endows NMDARs with a voltage-dependent gating mechanism. Therefore, NMDARs can act as 'coincidence detector', as they require both glutamate release from the presynaptic terminal and simultaneous postsynaptic depolarization to fully activate. To test whether ATG-activated NMDARs are also able to act as coincidence detectors a combined light-electrical stimulus protocol was applied. Here, an antidromic stimulation of the axon hillock, i.e. depolarization of the postsynaptic cell, was paired with 370 nm light activation (black and violet lines, respectively) (Figure 6.6 A-C). The electric stimulation was set sub-threshold and only in the case of coincidence with light stimulation, action potential firing was induced (Figure 6.6 A-C center). When light stimulation was applied before electrical stimulation, the threshold was not exceeded (Figure 6.6 A-C right). The spiking rate was also significantly reduced when the interval

between electrical and light stimulation was too long (Figure 6.6 B, C left). The statistical analysis of the experiments summarized in figure 6.6 D clearly show that ATG-activated NMDARs can operate as coincidence detectors.

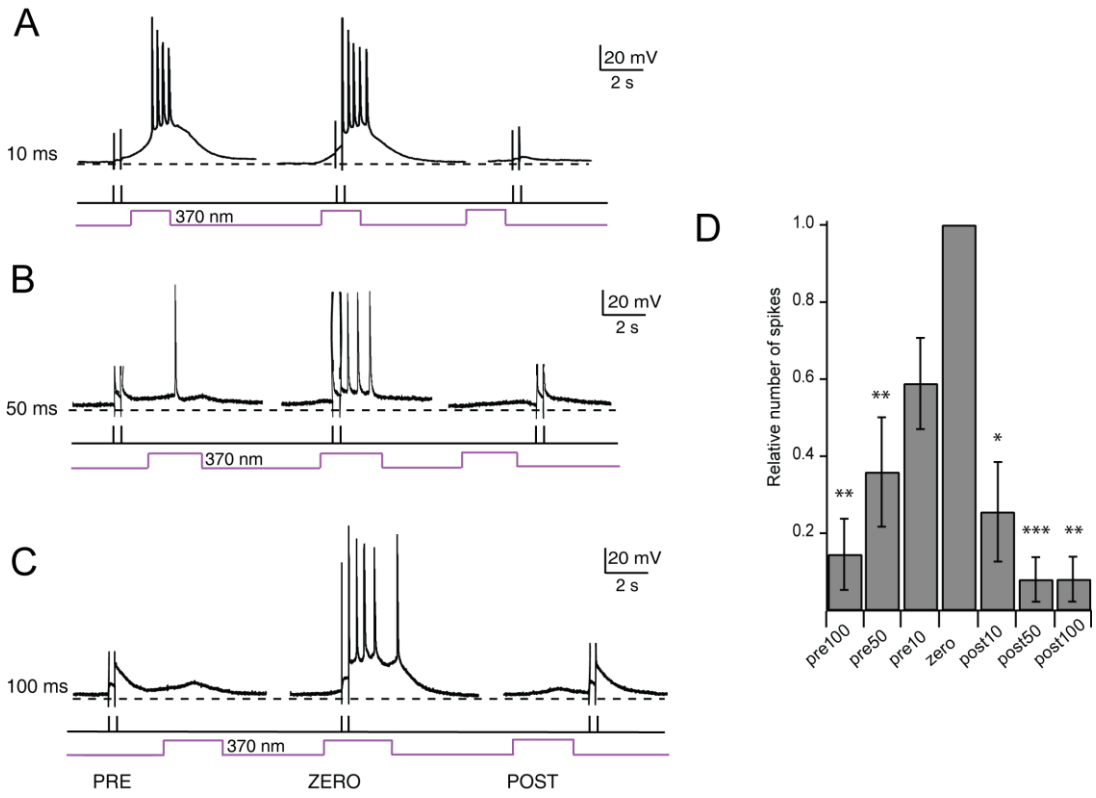

Figure 6.6 - Coincidence detection using ATG. Coincidence detection of light-induced ATG current paired with antidromic stimulation. **(A)** Antidromic stimulation (black bars) of the postsynaptic cell 10 ms prior to, simultaneous and 10 ms after the light stimulation (violet trace). **(B)** Same experiment as in (A) with 50 ms interval between pre and post stimulus. **(C)** Same experiment as in (A) and (B) with 100 ms interval between pre and post stimulus. **(D)** Quantification of coincidence detection. Relative number of spikes compared to condition ZERO, when both stimuli were applied together (n = 11 cells). Statistics calculated using Wilcoxon rank sum test. (*p < 0.05, **p < 0.01, ***p < 0.001). Figure adapted from (Laprell et al. 2015b).

4.1.5 *cis*-STG: a selective NMDAR agonist

Stilbenes are thermally stable molecules of an ethene double bond substituted with a phenyl ring on both ends of the double bond. The molecular structure resembles that of an azobenzene and the stilbene can also exist in either *trans*- or *cis*-configuration. However, stilbenes are not photoswitchable. The *cis*-stable stilbene version of ATG, *cis*-STG, can be used as a model for and exhibits a similar pharmacological profile as *cis*-ATG. Patch clamp experiments in cortical neurons could show that puff application of *cis*-STG (200 µM) was able to induce action potential firing. In addition, the J-shaped IV relationship and the sensitivity towards a block by D-AP5 (*cis*-STG current in presence of D-AP5 and TTX −1.45±0.09 pA; <15 % of *cis*-STG-currents in absence D-AP5) indicate the same selectivity

of *cis*-STG for NMDARs (Figure 6.7 A and B, respectively). Taken together, *cis*-STG represents a novel class of selective, synthetic NMDAR agonists.

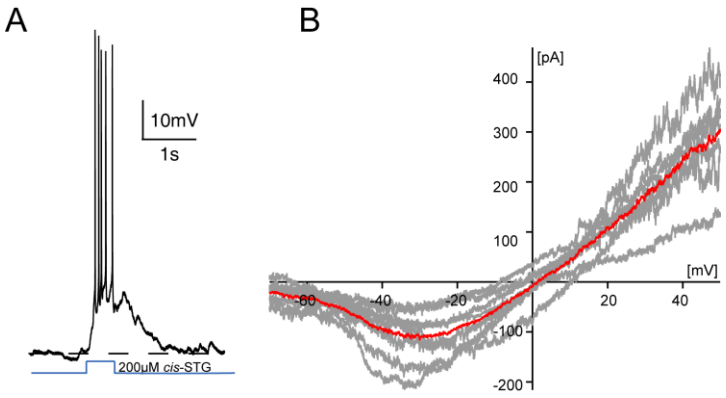

Figure 6.7 - Characterization of *cis*-STG. (A) Current-clamp recording in cortical neuron with *cis*-STG. Puff-application of 200 µM *cis*-STG for 500 ms result in robust action potential firing. **(B)** Current-voltage relationship of *cis*-STG in cortical neurons. Ramps were performed between −70 mV and 50 mV. Single cell recordings are depicted in grey (n = 5), average trace of all experiments is shown in red. Figure adapted from (Laprell et al. 2015b)

4.1.6 ATG-mediated currents in murine Purkinje cells

It was thought for a long time that cerebellar Purkinje cells do not express functional NMDARs (Perkel et al. 1990, Llano et al. 1991). In the past decade, however, significant evidence was found that NMDARs are postsynaptically expressed at the climbing fiber to Purkinje cell synapse. The expression of NMDARs in Purkinje cells show a late developmental onset and are barely detectable until postnatal week four (Piochon et al. 2007). Therefore, Purkinje cells from mice postnatal day 15 to 17 would provide a good negative control for ATG specificity, because no NMDAR currents should be detectable. Application of 200 µM ATG (in presence of 1 µM TTX) to mouse cerebellar slices, however, induced large light-dependent currents (Figure 6.8 A, B) (−283.4±10.5 pA), as did puff application of NMDA (Figure 6.8 A, B, −440±183.4 pA). To elucidate the molecular target of these currents pharmacological experiments were performed. NMDA puff induced currents were completely blocked using D-AP5, which indicates that mice older than two weeks already express substantial levels of NMDARs (Figure 6.8 C, −8.33±0.33 pA). However, currents induced by ATG were insensitive to the NMDAR antagonist D-AP5 (50 µM) and to the NMDAR pore blocker MK-801 (1 mM) (Figure 6.8 C) (−273.6±18.6 pA and −343.5±15.5 pA, respectively). Blockers for AMPARs (NBQX), mGluRI (YM298198, 50 µM) and mGluRII/III (CPPG, 300 µM) were also not able to block ATG-mediated currents. NBQX application, however, reduced leak currents, which led to a relative increase in ATG-mediated currents (Figure 6.8, −624.00±26.66 pA). The reduction of leak currents by NBQX might be due to residual activation of AMPARs by *trans*-ATG in cerebellar Purkinje cells. Furthermore, blocking synaptic transmission using $CdCl_2$ had only a minor effect on ATG-mediated currents, excluding the possibility of primarily activating cells presynaptic to Purkinje cells (−498.55±13.42 pA in presence of ATG, NBQX and $CdCl_2$) (Figure 6.8).

Two more experiments were performed to confirm that *cis*-ATG induced currents are not mediated through NMDARs in cerebellar Purkinje cells. First, the concentration of the allosteric modulator D-serine (10 µM) was increased and second, extracellular Ca^{2+} was depleted. Application of D-serine led to slightly increased ATG-mediated currents, whereas depletion of Ca^{2+} had no effect (Figure 6.8, −370.63±21.27 pA and −267.00±5.85 pA, respectively).

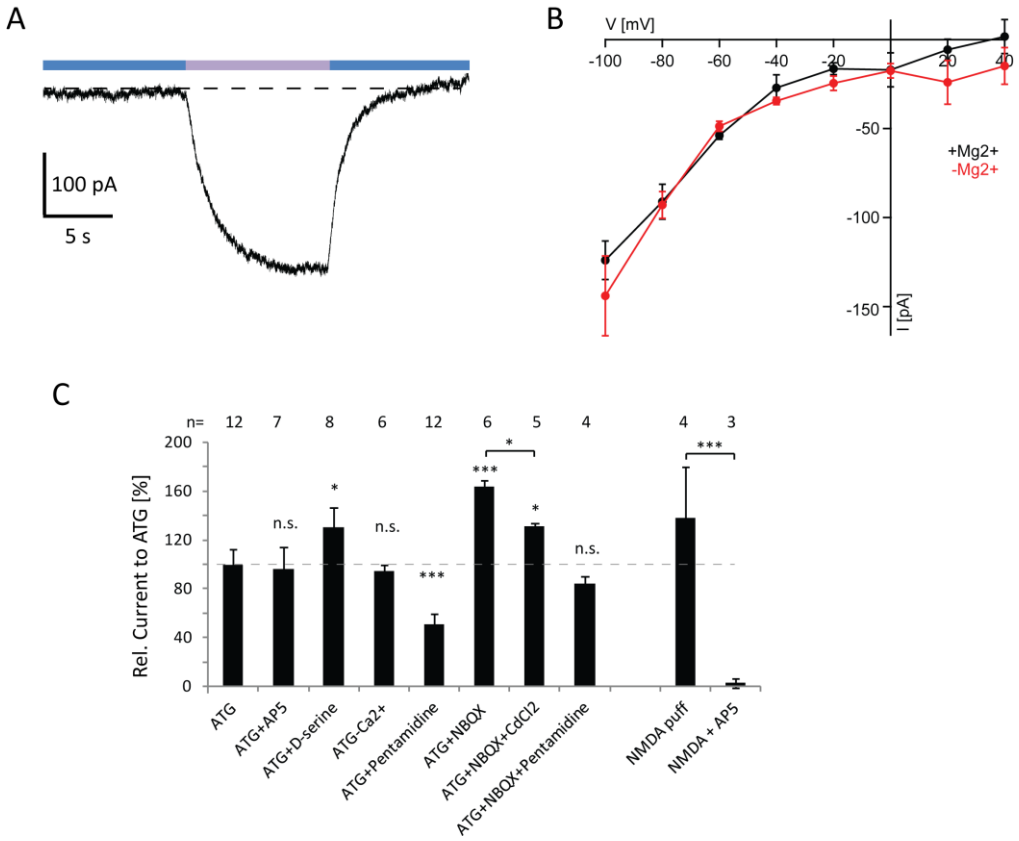

Figure 6.8 - Characterization of ATG-mediated currents in Purkinje cells. (A) Raw data trace for ATG-light activated current at −60 mV holding potential. Blue bar represents 420 nm illumination and violet 370 nm. **(B)** Current-voltage (IV) relationship of ATG-induced currents in Purkinje cells. Black: IV-relationship in ACSF . Red: IV-relationship without Mg^{2+}. Holding potentials larger than −20 mV may not be exact due to the size of Purkinje cells ('space clamp'). **(C)** Pharmacology of ATG- and NMDA-induced currents. Currents were normalized to ATG-currents and statistical analysis was performed using Student's t-test. *p < 0.05, **p < 0.01, ***p < 0.001. Error bars represent SEM.

In conclusion, these results indicate that ATG does not activate common NMDARs, but an unknown receptor in cerebellar Purkinje cells and has only little effect on AMPARs in *trans*-configuration. These findings were unexpected, since ATG has been shown to be a selective NMDAR agonist and induced no significant leak currents in mouse cortical neurons (*see* section 4.1.2).

Interestingly, receptors composed of GluN1 and GluN3 subunits have been shown to be unaffected by glutamate or NMDA, resistant to the intrinsic Mg^{2+} block and to specific NMDAR blockers, such as MK-801, or competitive antagonists. These receptor combinations only respond to glycine and are inhibited by D-serine (Chatterton et al. 2002). Whether it is this receptor combination that ATG is able to activate remains to be

investigated. However, as expression levels in the cerebellum are low and as they do not respond to glutamate it seems unlikely that ATG could activate these NMDARs.

The only receptor that is highly expressed in Purkinje cells and exhibits a similar structure to glutamate receptors is the orphan receptor GluRδ2. This receptor has been shown to be almost exclusively expressed in Purkinje cells of the cerebellum and plays a crucial role in synaptic plasticity and motor coordination (Zuo et al. 1997, Kakegawa et al. 2007a, Kakegawa et al. 2007b, Lomeli et al. 1993). Due to structural similarities to other glutamate receptors, such as NMDARs and AMPARs, several studies have been undertaken to identify agonists or antagonists of the receptor. Zuo et al. (1997) reported that addition of 100 µM AP5, 100 µM CNQX or 100 µM 7-chlorokynurenic acid, a blocker of the glycine binding site of NMDARs, did not alter holding current or membrane conductance. Furthermore, application of 1 mM glutamate, 1 mM aspartate or 0.1 mM kainate in presence of 10 µM glycine failed to open the GluRδ2 pore. However, evidence exists that the channel pore of Gluδ2 is functional (Kohda et al. 2000, Schmid and Hollmann 2008, Schmid et al. 2009). A recent study also demonstrated that Gluδ2 is activated by mGluRI activation (Ady et al. 2014). To date, most information about GluRδ2 function has been obtained from a gain of function mutation in lurcher (Lc) mice, in which a highly conserved alanine is replaced by a threonine residue in the third hydrophobic protein segment (Vogel et al. 2007). This point mutation renders the receptor constitutively open and leads to ataxia in heterozygous and early death in homozygous lurcher mice. As for the wt receptor also the lurcher mutant receptor does not respond to any NMDAR- or AMPAR-blockers. GluRδ2^{Lc}-mediated currents were only considerably reduced by the application of pentamidine (10 µM), an NMDAR blocker (Williams et al. 2003), or 1-naphthyl acetyl spermine (NASP; 10 µM), a polyamine analog of *Joro* spider toxin, an open-channel blocker of AMPA and kainate receptors (Kohda et al. 2000). Furthermore, D-serine and glycine had reducing effects on membrane currents similar to NASP, when applied at high concentrations (Naur et al. 2007).

To investigate whether ATG may activate GluRδ2 receptors in Purkinje cells, pentamidine (50 µM) was applied to cerebellar slices in presence of ATG. The application of pentamidine significantly reduced light-induced currents by ATG (Figure 6.8), but also leak currents were substantially reduced (ATG-mediated currents in presence of pentamidine −127.41±11.24 pA, $p < 0.001$ and leak currents before and after application of pentamidine, respectively −878.8.41±68.1 pA and −426.5±49.8 pA, $p < 0.001$). The reduction of ATG-mediated currents by 50 % is similar to the results in lurcher mice and indicates that ATG might activate GluRδ2 receptors in mouse Purkinje cells (Williams et al. 2003). To further substantiate this finding, light-induced IV-relationships with ATG were performed. The ATG-mediated IV-relationship resembles the IV recorded in Purkinje cells of lurcher mice (Figure 6.8 B, black trace) (Naur et al. 2007). Furthermore, the absence of Mg^{2+} had no effect on the shape of the IV (Figure 6.8 B, red trace). Thus, ATG-mediated

activation of NMDARs in Purkinje cells of the cerebellum plays a minor role and an activation of GluRδ2 seems to be more likely.

To further investigate ATG's activity on GluRδ2 receptors, both, GluRδ2 and NMDARs were heterologously expressed in HEK cells. Surprisingly, neither GluRδ2 nor NMDARs could be activated by ATG after heterologous expression (data not shown), which might be due to low channel number (see section 4.1.2). Therefore, investigation of ATG-mediated activation of GluRδ2 will concentrate on the GluRδ2 knockout animal, Hotfoot-Nancy, in which a lack of ATG-mediated currents would ultimately proof GluRδ2 specificity in Purkinje cells (Lalouette et al. 2001).

4.1.7 Red-shifted ATG

Application of UV light to neural tissue may have undesirable side effects. Therefore, many PCLs have been red-shifted by attaching an additional dimethylamine group in para-position to the azo-group (N=N), e.g. ATA. This red-shifting effect is induced by the electron-donating group and can be further enhanced by an electron-withdrawing group on the other end of the molecule ('push-pull' azobenzenes) (Mourot et al. 2011) (Sadovski et al. 2009). Besides red-shifting the absorption spectrum these modifications have the additional effect of an increased rate of thermal relaxation from *cis* to *trans*, which are further influenced by polar protic solvents (Whitten et al. 1971). However, depending on the photoswitch and its target receptor modifications can have dramatic effects on its functionality, positively and negatively. In case of ATG, this small modification led to the complete loss of ATG's activity in cortical neurons (Figure 6.9). Patch-clamp experiments in layer 2/3 cortical neurons revealed that red shifted-ATG (rs-ATG) had neither influence on leak currents, nor did it elicit light-induced currents (data not shown). This result indicates that ATG is completely enclosed by the clamshell domain of NMDARs, which may be the reason for its high selectivity for NMDARs in cortical neurons. In Purkinje cells, however, rs-ATG was able to induce light-dependent currents. Here, the molecule was *trans*-active, therefore induced currents in the dark, and could effectively be switched off using light between 480 nm and 500 nm (Figure 6.9 B, C). Not only was the polarity of activation inverted, but also the currents induced by rs-ATG were much smaller compared to ATG (–92.24±7.17 pA and –283.4±10.5 pA, respectively). Although no pharmacological experiments have been performed in the cerebellum yet, these results indicate a completely different functionality of rs-ATG compared to ATG.

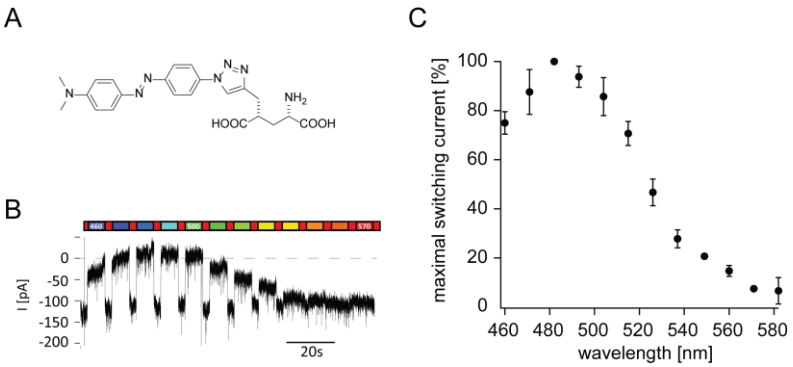

Figure 6.9 - Characterization of red-shifted ATG (rs-ATG) in cerebellar Purkinje cells. (A) Structure of *trans*-rs-ATG. **(B)** Raw data trace of lambda screen for best inactivation wavelengths. **(C)** Data analysis of lambda screens. Maximal switching current in % for *cis*- to *trans*-isomerization. Best inactivation is achieved using wavelengths between 480 nm and 500 nm. Data points represent mean±SEM (n = 5 experiments).

4.1.8 Discussion ATG

ATG is a freely diffusible photochromic ligand that selectively activates NMDARs in mouse cortical neurons. It has the unique features of being inactive in its thermodynamically stable

trans-configuration and can be quickly switched to its active state using near UV light (360-370 nm). As such, it is not excitotoxic when applied to neural networks in the dark. Furthermore, it is the first diffusible photoswitch that can be activated using two-photon (2-P) activation (720-740 nm). Until today only photochromic tethered ligands (PTLs) have been shown to be excitable by two-photon activation (Carroll et al. 2015). In contrast to caged-NMDAR agonists ATG has the advantage that it can be switched back to its inactive state using blue light (405-420 nm). Rapid laser experiments furthermore demonstrated that photoswitching occurs in the timescale of intrinsic receptor deactivation (Laprell et al. 2015b).

Calcium-imaging and coincidence detection experiments revealed that ATG selectively activates NMDARs in the mouse cortical neurons and two-photon excitation of ATG result in high spatio-temporal precision of NMDAR activation (Laprell et al. 2015b). These results demonstrate that ATG is a useful tool for the study of NMDARs in cortical neurons. In addition, *cis*-STG has been shown to represent a new class of selective synthetic NMDAR agonists. Only red-shifting the PCL did not lead to NMDAR currents; most likely, because ATG may be completely enclosed in the clamshell leaving no room for modifications.

In cerebellar Purkinje cells ATG seems to elicit its action through a different type of receptor. Here, in contrast to NMDA application, ATG activation could not be eliminated by D-AP5 application. Furthermore, antagonists for AMPA, mGluR I and mGluR II/III did not prevent light-induced currents. On the other hand the open channel blocker pentamidine has shown to reduce ATG-mediated currents significantly. Similar results have been obtained for the orphan receptor GluRδ2^{Lc}. Also the IV-relationship of ATG-mediated currents in Purkinje cells were comparable to those in lurcher mice. Only the relative increase in ATG-mediated currents by application of 10 µM D-serine does not fit into the overall picture. Naur et al. (2007) demonstrated that D-serine reduce the GluRδ2^{Lc} currents with an EC_{50} of 182±11 µM. However, these results may be different in native GluRδ2, which share strong structural similarities with NMDARs, who's currents are also potentiated by D-serine application.

Taken together, pharmacological experiments as well as the comparison of IV-relationships indicate that ATG activates the orphan receptor GluRδ2 in cerebellar Purkinje cells. On the other hand, GluRδ2 heterologously expressed in HEK cells as well as in *Xenopus* oocytes did not show ATG-mediated currents. This, however, seems to be a general problem for ATG-mediated currents. ATG-activation on heterologously expressed NMDAR compositions was not able to provoke membrane currents in HEK cells and only significantly smaller currents compared to glutamate- or NMDA-induced currents were observed after expression of NMDARs in *Xenopus* oocytes (Laprell et al. 2015b).

The only way to ultimately prove an ATG specificity towards GluRD2 in Purkinje cells is to do the same experiments in a GluRD2 knockout animal, e.g. Hotfoot-Nancy. We are currently waiting for them to breed in the lab of our collaborator. These mice bear deletions

in the GluRδ2 encoding gene, lacking the channel pore and the ligand binding domain (Mendoza et al. 2010, Lalouette et al. 2001, Ady et al. 2014). Lack of ATG-mediated currents in these mice would ultimately proof a GluRD2 specificity and would lead to the first ever published agonist of these receptors.

4.2 GluAzo and red-shifted GluAzo

In 2007 Volgraf et al. published a reversible caged glutamate (GluAzo) for activation of ionotropic glutamate receptors (Volgraf et al. 2007). Studies in HEK cells expressing iGluR5 and iGluR6 showed that GluAzo is able to activate non-NMDA receptors with an EC_{50} of 9 µM under 500 nm and an approximately 10-fold reduced EC_{50} under 380 nm illumination. Furthermore, experiments with 25 µM GluAzo in dissociated rat hippocampal neurons revealed that GluAzo induces action potential firing in its dark adapted *trans*-isoform and can be actively switched off using green light. Application of 10 µM DNQX, a selective non-NMDAR antagonist, was able to prevent light-induced action potential firing (Volgraf 2008).

Further evaluation of GluAzo selectivity has not been undertaken. Therefore, experiments in acute murine coronal brain slice were performed using 25 µM GluAzo (Figure 7.1). Surprisingly, GluAzo induced action potential firing in its *cis*-isoform in contrast to previous results from dissociated rat hippocampal cells (Figure 7.1 B). Further experiments in whole-cell voltage clamp mode showed that *cis*-GluAzo induced currents were significantly reduced by 50 µM D-AP5 (−67.77±10.13 pA and −18.31±8.15 pA, respectively) (Figure 7.1 C and D). These results indicate that GluAzo is more selective for NMDA receptors in acute brain slices as opposed to non-NMDA receptors in cultured neurons or HEK cells. This finding is further supported by the typical J-shaped IV-relationship induced by the Mg^{2+} block in acute brain slices (Figure 7.1 E). As ATG was able to elicit light-dependent currents in cerebellar Purkinje cells, the same experiment was performed using GluAzo. In presence of 25 µM GluAzo inward-currents could be detected under 380 nm light (−96.05±13.77 pA, n = 3 cells), however, considerable smaller than ATG-induced currents (*see* section 4.1.6). Similarly to ATG, these currents could not be blocked by application of 1 mM MK-801 in the intracellular solution (−75.89±10.18 pA, n = 3 cells).

Since GluAzo showed similar functionalities to ATG, we tried to 'red-shift' this molecule in order to prevent UV-irradiation of the tissue. The same approach as for ATG was undertaken, i.e. attaching an additional dimethylamine group in para-position to the azo-group (N=N) yielding rs-GluAzo (Figure 7.1 F). As previously for ATG, GluAzo-mediated activity was prevented by this modification (Figure 7.1 G).

Taken together, these data demonstrate that in acute coronal brain slices GluAzo is a *cis*-active NMDAR selective agonist and that it can activate cerebellar Purkinje neurons in a similar fashion as ATG.

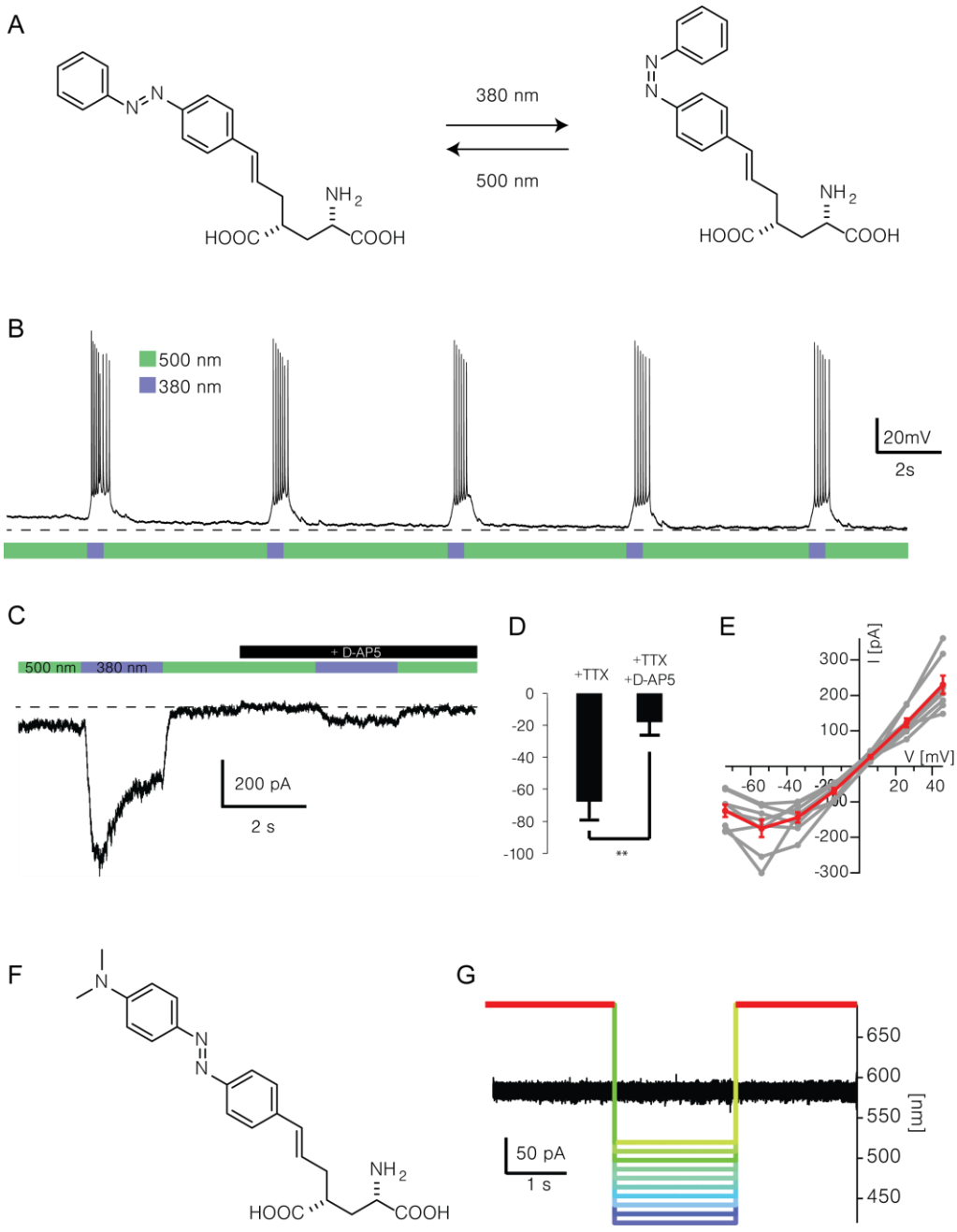

Figure 7.1 - GluAzo is a selective *cis*-active NMDAR agonist in acute coronal brain slices. **(A)** Molecular structure of GluAzo in *trans*- and *cis*-configuration. Switching between the two states is achieved using 380 nm and 500 nm, respectively. **(B)** Current-clamp recording in a layer 2/3 cortical neuron. Light-dependent action potential firing occurs at 380 nm. **(C)** Whole cell voltage-clamp recording of a layer 2/3 cortical neuron displaying large inward currents at 380 nm, which can significantly reduced by application of the selective NMDAR antagonist, D-AP5. **(D)** Quantification of GluAzo experiments in absence and presence of D-AP5. **(E)** Current-voltage relationship of GluAzo under 380 nm light shows the typical J-shaped form due to Mg^{2+} block of NMDA receptors. **(F)** Molecular structure of rs-GluAzo in *trans*-configuration. **(G)** Lambda screen between 430 nm and 510 nm in voltage-clamp mode showed no light-induced currents in layer 2/3 cortical neurons. Overlay of all 10 traces.

4.3 AzoCholine

Acetylcholine is an important neurotransmitter involved in a variety of neural functions such as movement and cognition (Kalamida et al. 2007, Lemoine et al. 2012). Acetylcholine receptors (AChRs) can be divided into two main classes, muscarinic and nicotinic AChRs (*see* section 1.1.4). Due to the large distribution and combinatorial diversity optical control of AChRs would be favorable. Therefore, acetylcholine was modified in such a way that it contains a light-switchable azobenzene moiety yielding AzoCholine (Damijonaitis et al. 2015). AzoCholine is a freely diffusible PCL bearing not only resemblance to acetylcholine, but also to the α7 specific antagonist MG624 (Figure 8.1 A). Experiments in HEK cells revealed that AzoCholine specifically activates α7 nicotinic AChRs in its dark-adapted *trans*-configuration and can be actively switched off using UV-light (Damijonaitis et al. 2015).

More detailed information about the working mode of AzoCholine in neural networks was obtained in multielectrode recordings from acute hippocampal brain slice preparations (Figure 8.1 B). After mounting the brain slice, recordings were performed in presence and absence of 50 µM AzoCholine (Figure 8.1 C and D, respectively). To increase the baseline spiking activity the potassium concentration was increased to 7.5 mM. Before AzoCholine application no light-dependent spiking pattern was observed by switching between 370 nm and 440 nm light (Figure 8.1 G). After wash-in of AzoCholine the bursting pattern in hippocampal neurons followed the light stimulation protocol, i.e. an increase in spiking rate upon illumination with 440 nm light (Figure 8.1 C and E). As in the HEK cells experiments bursting was induced in *trans*-configuration and was suppressed by 370 nm illumination (n = 6 experiments, 173 with bursting cells) (Figure 8.1 E). Application of MG624 further revealed that AzoCholine is specifically activating α7 nicotinic AChRs in acute brain slice, as light-dependent bursting activity was prevented (Figure 8.1 D and F). Control experiments were done using brain slices not treated with AzoCholine and slices in the presence of AzoCholine, but without light stimulation. These experiments demonstrated that the observed effects were all due to light activation of α7 nicotinic AChRs (Figure 8.1 G and H).

Taken together, these results demonstrate that AzoCholine is a promising tool for the light activation of α7 nicotinic AChRs. Besides the described experiments, Damijonaitis et al. (2015) further showed that AzoCholine is not only functional in brain slices *ex-vivo*, but that it also functions on rat primary afferent DRG neurons and effects thrashing behavior in *C. elegans in-vivo* (Damijonaitis et al. 2015).

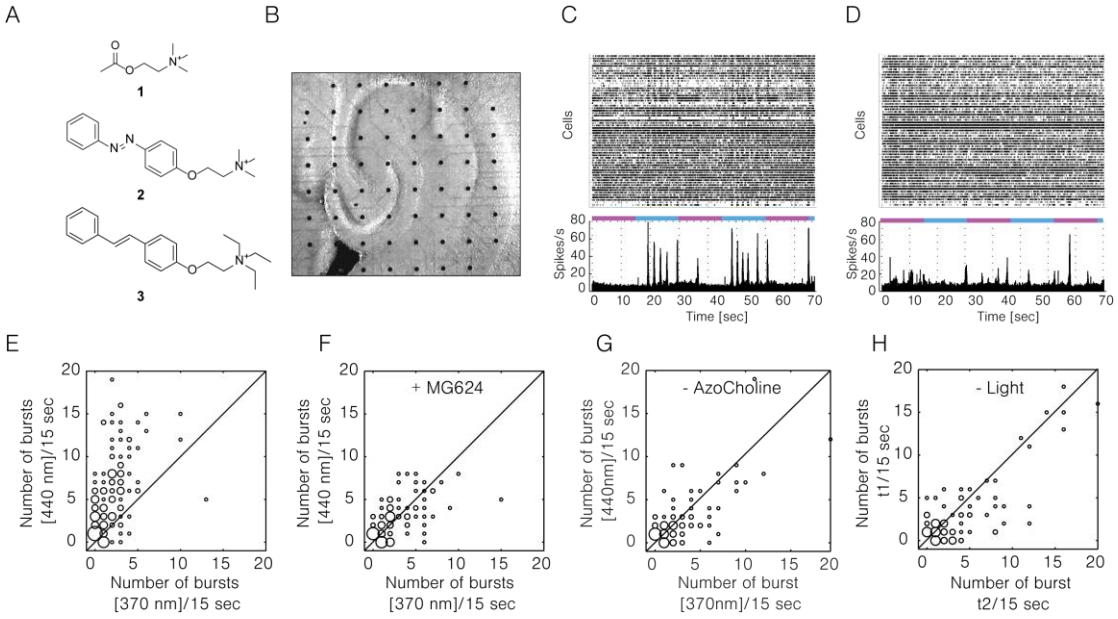

Figure 8.1 - AzoCholine activates α7 nicotinic AChRs in acute hippocampal brain slices. (A) Molecular structures of Acetylcholine (1), AzoCholine (2) and MG624 (3). **(B)** Image of an acute hippocampal brain slice mounted on the 8x8 MEA. **(C)** MEA recording of an acute hippocampal brain slice. Top: Raster plot. Bottom: Histogram and light stimulation protocol. Switching between 370 nm and 440 nm modulates bursting activity. **(D)** Same brain slice as in (C) in presence of 5 µM MG624. **(E)-(H)** Analysis of MEA experiments. (E) in presence of 50 µM AzoCholine (n = 6 experiments, 173 cells, $p < 0.001$, Student's t-test). (F) in presence of 50 µM AzoCholine and 5 µM MG624 (n = 6 experiments, 121 cells, $p > 0.05$, Student's t-test). (G) in absence of AzoCholine (n = 6 experiments, 103 cells, $p > 0.05$, Student's t-test) and (H) in presence of 50 µM AzoCholine without light stimulation (n = 4 experiments, 98 cells, $p > 0.05$ Student's t-test). The bursting activity was analyzed in Matlab for the whole light stimulation of 15 s for each wavelength. The circle size is related to the number of cells responding, i.e. a larger circle indicates a higher number of cells responding with the same bursting activities at 370 nm and 440 nm, and vice versa. Figure modified from (Damijonaitis et al. 2015).

5 Summary

The experiments performed and the outcomes of this dissertation are summarized in the following four tables.

Table 8 - **Part 1: DAD, a photochromic potassium channel blocker for vision restoration**

MOTIVATION	EXPERIMENTAL PROCEDURE	RESULT
First tests in acute coronal brain slices	Patch-clamp in layer 2/3 cortical neurons	DAD can be switched using blue light and blocks in the dark
Pharmacology in acute coronal brain slices	Patch-clamp in layer 2/3 cortical neurons	DAD is a potassium channel blocker
First tests in blind retinae (TKO)	Multielectrode-array (MEA) recordings in blind retinae	DAD activates the retina during light and is inactive in the dark
Identification of target cell type (general)	Pharmacology in blind retinae on MEA	DAD specifically targets bipolar cells
Identification of synaptic transmission pathways	Patch-clamp experiments in whole mount preparations from blind retinae	DAD utilizes the remaining retinal circuitry: Excitation via BC-RGC and inhibitory inputs via BC-amacrine cell-RGC signal transmission
Experiments in different mouse models	MEA recordings in five different mouse lines: 1. TKO 2. rd1/rd1, opn4$^{-/-}$ 3. gnat1$^{-/-}$,gnat2$^{-/-}$, opn4$^{-/-}$ 4. cnga3$^{-/-}$, gnat1$^{-/-}$, opn4$^{-/-}$ 5. wt w/ and w/o L-AP4 and NBQX	DAD only targets cell types in blind and degenerating retinae, healthy tissue is not affected.
Light sensitivity*	MEA recordings with light-intensities between 10^{12} and 10^{16} photons cm^{-2} s^{-1}	DAD can be activated under bright daylight conditions, with blue and white light (10^{14} photons cm^{-2} s^{-1})
Spatial precision*	MEA recordings with increasing light spot size	DAD can activate RGCs with small spot stimulation (30 µm)
Temporal precision	MEA recordings with increasing frequency of light stimulation	DAD can follow 1 Hz light stimulation with a mismatch of only 12 %
Intravitreal injections	MEA recordings after intravitreal injections in anaesthetized mice using different concentrations and different time points	5-10 mM DAD activates blind retina 2-8 hours post injection
In-vivo behavioral experiments **	Intravitreal injection of 5 mM DAD and light-dark shuttle box test after 2-6 hours	DAD is capable of restoring light-dependent visual responses to blind mice

* Experiments performed by Dr. Ivan Tochitsky (Prof. Richard Kramer, University of California, Berkeley, USA)
** Experiments performed with Dr. Kuldeep Kaur (Prof. Russell Van Gelder, University of Washington, Seattle, USA)

Table 9 - **Part 2: ATA, a photochromic AMPA receptor agonist for vision restoration**

MOTIVATION	EXPERIMENTAL PROCEDURE	RESULT
First tests in dissociated neurons and acute hippocampal brain slices[#]	Patch-clamp in hippocampal neurons	ATA can be switched using blue light and is active in the dark
Pharmacology in brain slices[#]	Patch-clamp in hippocampal neurons	ATA is an AMPA receptor specific agonist
First tests in blind retinae (TKO)	Multielectrode-array (MEA) recordings in blind retinae	ATA activates the retina in the dark and is inactive during light application
Identification of target cell type (general)	Pharmacology in blind retinae on MEA	ATA targets primarily amacrine cells and retinal ganglion cells
Light sensitivity	MEA recordings with different light-intensities	ATA can be inactivated under bright daylight conditions, with blue and white light (10^{14} photons cm^{-2} s^{-1})
Intravitreal injections[##]	MEA recordings after intravitreal injections in anaesthetized mice using different concentrations and different time points	1 mM ATA activates blind retina 2-8 hrs post injection

Table 10 - **Part 3: Combination therapy restores on- and off-light responses similar to wildtype**

MOTIVATION	EXPERIMENTAL PROCEDURE	RESULT
Test of photoswitch combination in blind retinae	Multielectrode-array (MEA) recordings in blind retinae	ATA and DAD restore transient light-on and light-off responses in blind retinae similar to wildtype

Table 11 - **Part 4: Characterization of the NMDA receptor specific PLC, ATG, in acute murine brain slices**

MOTIVATION	EXPERIMENTAL PROCEDURE	RESULT
Basic characterizations and wavelengths-screenings	Patch-clamp in layer 2/3 cortical neurons	ATG is a *cis*-active iGluR agonist that can be switched from *trans*- to *cis*- with 360 nm and with 420 nm from *cis*- to *trans*-configuration
Pharmacology in brain slices	Patch-clamp in layer 2/3 cortical neurons	ATG is NMDA receptor specific
Calcium imaging	Patch-clamp and imaging in hippocampal neurons	ATG can be combined with calcium imaging experiments
Coincidence detection	Patch-clamp in layer 2/3 cortical neurons	ATG-activated NMDA receptors function as coincidence detectors
2-P activation[†]	Patch-clamp in hippocampal neurons	ATG can be 2-P activated
Single spine[†]	Patch-clamp in hippocampal neurons	ATG can be activated in a local precise manner

Experiments shown in Stawski et al. 2012
Experiments performed with Arshan Perrera (Prof.Martin Biel, Ludwig-Maximilians-University, Munich, Germany)
† Experiments performed by Emilienne Repak and Nelson Rebola (Dr. David DiGregorio, Institute Pasteur, Paris, France)

6 Literature

ADAMS AJ, VERDON WA AND SPIVEY BE 2013. Color Vision. In*:* TASMAN, WJ, A.E. (Ed.) Duane's Ophthalmology: Lippincott Williams & Wilkins.

ADY V, PERROY J, TRICOIRE L, PIOCHON C, DADAK S, CHEN X, DUSART I, FAGNI L, LAMBOLEZ B AND LEVENES C. 2014. Type 1 metabotropic glutamate receptors (mGlu1) trigger the gating of GluD2 delta glutamate receptors. EMBO reports 15: 103-109.

AGE-RELATED EYE DISEASE STUDY RESEARCH G. 2000. Risk factors associated with age-related macular degeneration. A case-control study in the age-related eye disease study: Age-Related Eye Disease Study Report Number 3. Ophthalmology 107: 2224-2232.

AKIYAMA K, NAKANISHI S, NAKAMURA NH AND NAITO T. 2008. Gene expression profiling of neuropeptides in mouse cerebellum, hippocampus, and retina. Nutrition 24: 918-923.

ALDRICH RW. 2001. Fifty years of inactivation. Nature 411: 643-644.

ALFORD S AND GRILLNER S. 1990. CNQX and DNQX block non-NMDA synaptic transmission but not NMDA-evoked locomotion in lamprey spinal cord. Brain research 506: 297-302.

ALLEN AE, CAMERON MA, BROWN TM, VUGLER AA AND LUCAS RJ. 2010. Visual responses in mice lacking critical components of all known retinal phototransduction cascades. PLoS One 5: e15063.

AMTHOR FR, OYSTER CW AND TAKAHASHI ES. 1984. Morphology of on-off direction-selective ganglion cells in the rabbit retina. Brain research 298: 187-190.

AMTHOR FR, TAKAHASHI ES AND OYSTER CW. 1989. Morphologies of rabbit retinal ganglion cells with complex receptive fields. The Journal of comparative neurology 280: 97-121.

ANDERSEN PH, GINGRICH JA, BATES MD, DEARRY A, FALARDEAU P, SENOGLES SE AND CARON MG. 1990. Dopamine receptor subtypes: beyond the D1/D2 classification. Trends in pharmacological sciences 11: 231-236.

ARIKKATH J AND CAMPBELL KP. 2003. Auxiliary subunits: essential components of the voltage-gated calcium channel complex. Current opinion in neurobiology 13: 298-307.

ARMSTRONG CM AND MATTESON DR. 1985. Two distinct populations of calcium channels in a clonal line of pituitary cells. Science 227: 65-67.

AUDO I ET AL. 2009. TRPM1 is mutated in patients with autosomal-recessive complete congenital stationary night blindness. American journal of human genetics 85: 720-729.

AUGUSTINE GJ. 1990. Regulation of transmitter release at the squid giant synapse by presynaptic delayed rectifier potassium current. The Journal of physiology 431: 343-364.

BAGNOLI P, DAL MONTE M AND CASINI G. 2003. Expression of neuropeptides and their receptors in the developing retina of mammals. Histology and histopathology 18: 1219-1242.

BALSE E, TESSIER LH, FORSTER V, ROUX MJ, SAHEL JA AND PICAUD S. 2006. Glycine receptors in a population of adult mammalian cones. The Journal of physiology 571: 391-401.

BANSAL A, SINGER JH, HWANG BJ, XU W, BEAUDET A AND FELLER MB. 2000. Mice lacking specific nicotinic acetylcholine receptor subunits exhibit dramatically altered spontaneous activity patterns and reveal a limited role for retinal waves in forming ON and OFF circuits in the inner retina. The Journal of neuroscience : the official journal of the Society for Neuroscience 20: 7672-7681.

BAUMGART J AND PEREZ-REYES E 2010. Voltage-gated calcium channels In*:* KEW, J AND DAVIES, A (Eds.) Ion channels from structure to function, Oxford University Press, p. 104-129.

BAYLOR DA, FUORTES MG AND O'BRYAN PM. 1971. Lateral interaction between vertebrate photoreceptors. Vision research 11: 1195-1196.

BEAN BP. 1985. Two kinds of calcium channels in canine atrial cells. Differences in kinetics, selectivity, and pharmacology. The Journal of general physiology 86: 1-30.

BEAULIEU JM AND GAINETDINOV RR. 2011. The physiology, signaling, and pharmacology of dopamine receptors. Pharmacological reviews 63: 182-217.

BEECH DJ AND BARNES S. 1989. Characterization of a voltage-gated K+ channel that accelerates the rod response to dim light. Neuron 3: 573-581.

BERRIDGE MJ, LIPP P AND BOOTMAN MD. 2000. The versatility and universality of calcium signalling. Nature reviews Molecular cell biology 1: 11-21.

BETTLER B, KAUPMANN K, MOSBACHER J AND GASSMANN M. 2004. Molecular structure and physiological functions of GABA(B) receptors. Physiological reviews 84: 835-867.

BETZ H AND LAUBE B. 2006. Glycine receptors: recent insights into their structural organization and functional diversity. Journal of neurochemistry 97: 1600-1610.

BI A, CUI J, MA YP, OLSHEVSKAYA E, PU M, DIZHOOR AM AND PAN ZH. 2006. Ectopic expression of a microbial-type rhodopsin restores visual responses in mice with photoreceptor degeneration. Neuron 50: 23-33.

BIEL M AND MICHALAKIS S. 2007. Function and dysfunction of CNG channels: insights from channelopathies and mouse models. Molecular neurobiology 35: 266-277.

BISCHOFBERGER J, ENGEL D, LI L, GEIGER JR AND JONAS P. 2006. Patch-clamp recording from mossy fiber terminals in hippocampal slices. Nature protocols 1: 2075-2081.

BLAZYNSKI C AND PEREZ MT. 1991. Adenosine in vertebrate retina: localization, receptor characterization, and function. Cellular and molecular neurobiology 11: 463-484.

BLOOMFIELD SA AND DACHEUX RF. 2001. Rod vision: pathways and processing in the mammalian retina. Progress in retinal and eye research 20: 351-384.

BLOOMFIELD SA AND VOLGYI B. 2009. The diverse functional roles and regulation of neuronal gap junctions in the retina. Nature reviews Neuroscience 10: 495-506.

BOOS R, SCHNEIDER H AND WASSLE H. 1993. Voltage- and transmitter-gated currents of all-amacrine cells in a slice preparation of the rat retina. The Journal of neuroscience : the official journal of the Society for Neuroscience 13: 2874-2888.

BOROWSKA J, TRENHOLM S AND AWATRAMANI GB. 2011. An intrinsic neural oscillator in the degenerating mouse retina. The Journal of neuroscience : the official journal of the Society for Neuroscience 31: 5000-5012.

BOWES C, LI T, DANCIGER M, BAXTER LC, APPLEBURY ML AND FARBER DB. 1990. Retinal degeneration in the rd mouse is caused by a defect in the beta subunit of rod cGMP-phosphodiesterase. Nature 347: 677-680.

BOWMAKER JK. 1998. Evolution of colour vision in vertebrates. Eye (Lond) 12 (Pt 3b): 541-547.

BRAKE AJ AND JULIUS D. 1996. Signaling by extracellular nucleotides. Annual review of cell and developmental biology 12: 519-541.

BRANDLE U, GUENTHER E, IRRLE C AND WHEELER-SCHILLING TH. 1998. Gene expression of the P2X receptors in the rat retina. Brain research Molecular brain research 59: 269-272.

BRANDSTATTER JH, KOULEN P, KUHN R, VAN DER PUTTEN H AND WASSLE H. 1996. Compartmental localization of a metabotropic glutamate receptor (mGluR7): two different active sites at a retinal synapse. The Journal of neuroscience : the official journal of the Society for Neuroscience 16: 4749-4756.

BRECHA N, JOHNSON D, PEICHL L AND WASSLE H. 1988. Cholinergic amacrine cells of the rabbit retina contain glutamate decarboxylase and gamma-aminobutyrate immunoreactivity. Proceedings of the National Academy of Sciences of the United States of America 85: 6187-6191.

BRIGGMAN KL, HELMSTAEDTER M AND DENK W. 2011. Wiring specificity in the direction-selectivity circuit of the retina. Nature 471: 183-188.

BROICHHAGEN J, JURASTOW I, IWAN K, KUMMER W AND TRAUNER D. 2014a. Optical control of acetylcholinesterase with a tacrine switch. Angewandte Chemie 53: 7657-7660.

BROICHHAGEN J ET AL. 2014b. Optical control of insulin release using a photoswitchable sulfonylurea. Nature communications 5: 5116.

BRUUN A AND EHINGER B. 1993. NPY-induced neurotransmitter release from the rabbit and chicken retina. Acta ophthalmologica 71: 590-596.

BUELL G, COLLO G AND RASSENDREN F. 1996. P2X receptors: an emerging channel family. The European journal of neuroscience 8: 2221-2228.

BUSSKAMP V ET AL. 2010. Genetic reactivation of cone photoreceptors restores visual responses in retinitis pigmentosa. Science 329: 413-417.

CAJAL S. 1893. La rétine des vertébrés. Cellule 9: 121-255.

CAPORALE N, KOLSTAD KD, LEE T, TOCHITSKY I, DALKARA D, TRAUNER D, KRAMER R, DAN Y, ISACOFF EY AND FLANNERY JG. 2011. LiGluR restores visual responses in rodent models of inherited blindness. Molecular therapy : the journal of the American Society of Gene Therapy 19: 1212-1219.

CARROLL EC, BERLIN S, LEVITZ J, KIENZLER MA, YUAN Z, MADSEN D, LARSEN DS AND ISACOFF EY. 2015. Two-photon brightness of azobenzene photoswitches designed for glutamate receptor optogenetics. Proceedings of the National Academy of Sciences of the United States of America 112: E776-785.

CASINI G. 2005. Neuropeptides and retinal development. Archives italiennes de biologie 143: 191-198.

CATTERALL WA. 2000. Structure and regulation of voltage-gated Ca2+ channels. Annual review of cell and developmental biology 16: 521-555.

CATTERALL WA, GOLDIN AL AND WAXMAN SG. 2005. International Union of Pharmacology. XLVII. Nomenclature and structure-function relationships of voltage-gated sodium channels. Pharmacological reviews 57: 397-409.

CHANG B, DACEY MS, HAWES NL, HITCHCOCK PF, MILAM AH, ATMACA-SONMEZ P, NUSINOWITZ S AND HECKENLIVELY JR. 2006. Cone photoreceptor function loss-3, a novel mouse model of achromatopsia due to a mutation in Gnat2. Invest Ophthalmol Vis Sci 47: 5017-5021.

CHANG B, HAWES NL, HURD RE, DAVISSON MT, NUSINOWITZ S AND HECKENLIVELY JR. 2002. Retinal degeneration mutants in the mouse. Vision research 42: 517-525.

CHANG B ET AL. 2007. Two mouse retinal degenerations caused by missense mutations in the beta-subunit of rod cGMP phosphodiesterase gene. Vision research 47: 624-633.
CHATTERTON JE ET AL. 2002. Excitatory glycine receptors containing the NR3 family of NMDA receptor subunits. Nature 415: 793-798.
CHAUDHURI A 2011. The Visual System: Retinal Processing and Early Vision. Fundamentals of sensory perception: Oxford University Press, p. 272-311.
CHAUDHURI D, ISSA JB AND YUE DT. 2007. Elementary mechanisms producing facilitation of Cav2.1 (P/Q-type) channels. The Journal of general physiology 129: 385-401.
CHEBIB M AND JOHNSTON GA. 1999. The 'ABC' of GABA receptors: a brief review. Clinical and experimental pharmacology & physiology 26: 937-940.
CHEN C AND CANNON SC. 1995. Modulation of Na+ channel inactivation by the beta 1 subunit: a deletion analysis. Pflugers Archiv : European journal of physiology 431: 186-195.
CHERRY TJ, TRIMARCHI JM, STADLER MB AND CEPKO CL. 2009. Development and diversification of retinal amacrine interneurons at single cell resolution. Proceedings of the National Academy of Sciences of the United States of America 106: 9495-9500.
CHOW AY. 1993. Electrical stimulation of the rabbit retina with subretinal electrodes and high density microphotodiode array implants. Invest Ophtalmol Vis Sci (Suppl) 34: 835.
CHOW AY AND CHOW VY. 1997. Subretinal electrical stimulation of the rabbit retina. Neuroscience letters 225: 13-16.
CHOW AY, PARDUE MT, PERLMAN JI, BALL SL, CHOW VY, HETLING JR, PEYMAN GA, LIANG C, STUBBS EB, JR. AND PEACHEY NS. 2002. Subretinal implantation of semiconductor-based photodiodes: durability of novel implant designs. Journal of rehabilitation research and development 39: 313-321.
CHUA J, FLETCHER EL AND KALLONIATIS M. 2009. Functional remodeling of glutamate receptors by inner retinal neurons occurs from an early stage of retinal degeneration. The Journal of comparative neurology 514: 473-491.
CHUANG AT, MARGO CE AND GREENBERG PB. 2014. Retinal implants: a systematic review. The British journal of ophthalmology 98: 852-856.
CLAES E, SEELIGER M, MICHALAKIS S, BIEL M, HUMPHRIES P AND HAVERKAMP S. 2004. Morphological characterization of the retina of the CNGA3(-/-)Rho(-/-) mutant mouse lacking functional cones and rods. Investigative ophthalmology & visual science 45: 2039-2048.
CLAPHAM DE. 2007. Calcium signaling. Cell 131: 1047-1058.
COETZEE WA ET AL. 1999. Molecular diversity of K+ channels. Annals of the New York Academy of Sciences 868: 233-285.
COHEN ED. 2001. Voltage-gated calcium and sodium currents of starburst amacrine cells in the rabbit retina. Visual neuroscience 18: 799-809.
COHEN ED AND MILLER RF. 1994. The role of NMDA and non-NMDA excitatory amino acid receptors in the functional organization of primate retinal ganglion cells. Visual neuroscience 11: 317-332.
COLAMARTINO G, MENINI A AND TORRE V. 1991. Blockage and permeation of divalent cations through the cyclic GMP-activated channel from tiger salamander retinal rods. The Journal of physiology 440: 189-206.
COLTHURST MJ, WILLIAMS RL, HISCOTT PS AND GRIERSON I. 2000. Biomaterials used in the posterior segment of the eye. Biomaterials 21: 649-665.
CONN PJ AND PIN JP. 1997. Pharmacology and functions of metabotropic glutamate receptors. Annual review of pharmacology and toxicology 37: 205-237.
CORRINGER PJ, LE NOVERE N AND CHANGEUX JP. 2000. Nicotinic receptors at the amino acid level. Annual review of pharmacology and toxicology 40: 431-458.
CURCIO CA, SLOAN KR, KALINA RE AND HENDRICKSON AE. 1990. Human photoreceptor topography. The Journal of comparative neurology 292: 497-523.
DA CRUZ L ET AL. 2013. The Argus II epiretinal prosthesis system allows letter and word reading and long-term function in patients with profound vision loss. The British journal of ophthalmology 97: 632-636.
DAMANN N, VOETS T AND NILIUS B. 2008. TRPs in our senses. Current biology : CB 18: R880-889.
DAMIJONAITIS A ET AL. 2015. AzoCholine Enables Optical Control of Alpha 7 Nicotinic Acetylcholine Receptors in Neural Networks. ACS chemical neuroscience.
DANCIGER M, BLANEY J, GAO YQ, ZHAO DY, HECKENLIVELY JR, JACOBSON SG AND FARBER DB. 1995. Mutations in the PDE6B gene in autosomal recessive retinitis pigmentosa. Genomics 30: 1-7.
DEN HOLLANDER AI, BLACK A, BENNETT J AND CREMERS FP. 2010. Lighting a candle in the dark: advances in genetics and gene therapy of recessive retinal dystrophies. J Clin Invest 120: 3042-3053.
DEVRIES SH. 2000. Bipolar cells use kainate and AMPA receptors to filter visual information into separate channels. Neuron 28: 847-856.

DEVRIES SH AND SCHWARTZ EA. 1999. Kainate receptors mediate synaptic transmission between cones and 'Off' bipolar cells in a mammalian retina. Nature 397: 157-160.

DIB-HAJJ S AND PRIESTLEY T 2010. Voltage-gated sodium channels. In*:* KEW, J AND DAVIES, C (Eds.) Ion channels from structure to function, Oxford University Press, p. 131-171.

DIGREGORIO DA, ROTHMAN JS, NIELSEN TA AND SILVER RA. 2007. Desensitization Properties of AMPA Receptors at the Cerebellar Mossy Fiber Granule Cell Synapse. Journal of Neuroscience 27: 8344-8357.

DINGLEDINE R, BORGES K, BOWIE D AND TRAYNELIS SF. 1999. The glutamate receptor ion channels. Pharmacological reviews 51: 7-61.

DONEVAN SD AND ROGAWSKI MA. 1993. GYKI 52466, a 2,3-benzodiazepine, is a highly selective, noncompetitive antagonist of AMPA/kainate receptor responses. Neuron 10: 51-59.

DOROUDCHI MM ET AL. 2011. Virally delivered channelrhodopsin-2 safely and effectively restores visual function in multiple mouse models of blindness. Molecular therapy : the journal of the American Society of Gene Therapy 19: 1220-1229.

DUBOCOVICH ML AND WEINER N. 1985. Pharmacological differences between the D-2 autoreceptor and the D-1 dopamine receptor in rabbit retina. The Journal of pharmacology and experimental therapeutics 233: 747-754.

DUNN FA. 2015. Photoreceptor ablation initiates the immediate loss of glutamate receptors in postsynaptic bipolar cells in retina. The Journal of neuroscience : the official journal of the Society for Neuroscience 35: 2423-2431.

EMERIT MB, RIAD M AND HAMON M. 1992. Trophic effects of neurotransmitters during brain maturation. Biology of the neonate 62: 193-201.

EVANS RJ, DERKACH V AND SURPRENANT A. 1992. ATP mediates fast synaptic transmission in mammalian neurons. Nature 357: 503-505.

FAIN GL, QUANDT FN, BASTIAN BL AND GERSCHENFELD HM. 1978. Contribution of a caesium-sensitive conductance increase to the rod photoresponse. Nature 272: 466-469.

FAMIGLIETTI EV. 1987. Starburst amacrine cells in cat retina are associated with bistratified, presumed directionally selective, ganglion cells. Brain research 413: 404-408.

FAMIGLIETTI EV. 1991. Synaptic organization of starburst amacrine cells in rabbit retina: analysis of serial thin sections by electron microscopy and graphic reconstruction. The Journal of comparative neurology 309: 40-70.

FAMIGLIETTI EV, JR. AND KOLB H. 1975. A bistratified amacrine cell and synaptic cirucitry in the inner plexiform layer of the retina. Brain research 84: 293-300.

FEHRENTZ T, SCHONBERGER M AND TRAUNER D. 2011. Optochemical genetics. Angewandte Chemie 50: 12156-12182.

FEIGENSPAN A AND BORMANN J. 1994. Facilitation of GABAergic signaling in the retina by receptors stimulating adenylate cyclase. Proceedings of the National Academy of Sciences of the United States of America 91: 10893-10897.

FEIGENSPAN A, GUSTINCICH S, BEAN BP AND RAVIOLA E. 1998. Spontaneous activity of solitary dopaminergic cells of the retina. The Journal of neuroscience : the official journal of the Society for Neuroscience 18: 6776-6789.

FEIGENSPAN A, WASSLE H AND BORMANN J. 1993. Pharmacology of GABA receptor Cl- channels in rat retinal bipolar cells. Nature 361: 159-162.

FEIGENSPAN A AND WEILER R. 2004. Electrophysiological properties of mouse horizontal cell GABAA receptors. Journal of neurophysiology 92: 2789-2801.

FELLER MB. 2002. The role of nAChR-mediated spontaneous retinal activity in visual system development. Journal of neurobiology 53: 556-567.

FESENKO EE, KOLESNIKOV SS AND LYUBARSKY AL. 1985. Induction by cyclic GMP of cationic conductance in plasma membrane of retinal rod outer segment. Nature 313: 310-313.

FLETCHER EL, JOBLING AI, VESSEY KA, LUU C, GUYMER RH AND BAIRD PN. 2011. Animal models of retinal disease. Progress in molecular biology and translational science 100: 211-286.

FORTIN DL ET AL. 2008. Photochemical control of endogenous ion channels and cellular excitability. Nat Methods 5: 331-338.

FOSTER RG, PROVENCIO I, HUDSON D, FISKE S, DE GRIP W AND MENAKER M. 1991. Circadian photoreception in the retinally degenerate mouse (rd/rd). J Comp Physiol A 169: 39-50.

FOUNDATIONFIGHTINGBLINDNESS. 2015. Available: https://www.blindness.org/content/rod-cone-dystrophy [Accessed 06.01.2015 2015].

FRINGS S, LYNCH JW AND LINDEMANN B. 1992. Properties of cyclic nucleotide-gated channels mediating olfactory transduction. Activation, selectivity, and blockage. The Journal of general physiology 100: 45-67.

FRINGS S, SEIFERT R, GODDE M AND KAUPP UB. 1995. Profoundly different calcium permeation and blockage determine the specific function of distinct cyclic nucleotide-gated channels. Neuron 15: 169-179.

FU Y 2011. The Retina and its Disorders Phototransduction: Phototransduction in Rods: Academic Pr Inc.

FYK-KOLODZIEJ B AND POURCHO RG. 2007. Differential distribution of hyperpolarization-activated and cyclic nucleotide-gated channels in cone bipolar cells of the rat retina. The Journal of comparative neurology 501: 891-903.

GARGINI C, TERZIBASI E, MAZZONI F AND STRETTOI E. 2007. Retinal organization in the retinal degeneration 10 (rd10) mutant mouse: a morphological and ERG study. The Journal of comparative neurology 500: 222-238.

GAUB BM ET AL. 2014. Restoration of visual function by expression of a light-gated mammalian ion channel in retinal ganglion cells or ON-bipolar cells. Proceedings of the National Academy of Sciences of the United States of America 111: E5574-5583.

GAUSS R, SEIFERT R AND KAUPP UB. 1998. Molecular identification of a hyperpolarization-activated channel in sea urchin sperm. Nature 393: 583-587.

GEE KR, NIU L, SCHAPER K, JAYARAMAN V AND HESS GP. 1999. Synthesis and photochemistry of a photolabile precursor of N-methyl-D-aspartate (NMDA) that is photolyzed in the microsecond time region and is suitable for chemical kinetic investigations of the NMDA receptor. Biochemistry 38: 3140-3147.

GEKELER F AND ZRENNER E. 2005. [Status of the subretinal implant project. An overview]. Der Ophthalmologe : Zeitschrift der Deutschen Ophthalmologischen Gesellschaft 102: 941-949.

GILBERTSON TA, SCOBEY R AND WILSON M. 1991. Permeation of calcium ions through non-NMDA glutamate channels in retinal bipolar cells. Science 251: 1613-1615.

GILLIAM JC AND WENSEL TG. 2011. TRP channel gene expression in the mouse retina. Vision research 51: 2440-2452.

GOLDIN AL. 2003. Mechanisms of sodium channel inactivation. Current opinion in neurobiology 13: 284-290.

GOLDSTEIN JM AND LITWIN LC. 1993. NBQX is a selective non-NMDA receptor antagonist in rat hippocampal slice. Molecular and chemical neuropathology / sponsored by the International Society for Neurochemistry and the World Federation of Neurology and research groups on neurochemistry and cerebrospinal fluid 18: 145-152.

GRABSCH H ET AL. 1999. Immunohistochemical detection of alpha1E voltage-gated Ca(2+) channel isoforms in cerebellum, INS-1 cells, and neuroendocrine cells of the digestive system. The journal of histochemistry and cytochemistry : official journal of the Histochemistry Society 47: 981-994.

GREEN WR. 1999. Histopathology of age-related macular degeneration. Molecular vision 5: 27.

GREENWOOD D, YAO WP AND HOUSLEY GD. 1997. Expression of the P2X2 receptor subunit of the ATP-gated ion channel in the retina. Neuroreport 8: 1083-1088.

HAGEMANN GS. Age-Related Macular Degeneration (AMD) [Online]. Available: http://webvision.med.utah.edu/book/part-xii-cell-biology-of-retinal-degenerations/age-related-macular-degeneration-amd/ [Accessed 25.02.2015 2015].

HAMPSON EC, VANEY DI AND WEILER R. 1992. Dopaminergic modulation of gap junction permeability between amacrine cells in mammalian retina. The Journal of neuroscience : the official journal of the Society for Neuroscience 12: 4911-4922.

HAN J, DINCULESCU A, DAI X, DU W, SMITH WC AND PANG J. 2013. Review: the history and role of naturally occurring mouse models with Pde6b mutations. Molecular vision 19: 2579-2589.

HARTONG DT, BERSON EL AND DRYJA TP. 2006. Retinitis pigmentosa. Lancet 368: 1795-1809.

HARTVEIT E. 1999. Reciprocal synaptic interactions between rod bipolar cells and amacrine cells in the rat retina. Journal of neurophysiology 81: 2923-2936.

HAYNES L AND YAU KW. 1985. Cyclic GMP-sensitive conductance in outer segment membrane of catfish cones. Nature 317: 61-64.

HOON M, OKAWA H, DELLA SANTINA L AND WONG RO. 2014. Functional architecture of the retina: Development and disease. Prog Retin Eye Res 42: 44-84.

HOSHI T, ZAGOTTA WN AND ALDRICH RW. 1990. Biophysical and molecular mechanisms of Shaker potassium channel inactivation. Science 250: 533-538.

HOSHI T, ZAGOTTA WN AND ALDRICH RW. 1991. Two types of inactivation in Shaker K+ channels: effects of alterations in the carboxy-terminal region. Neuron 7: 547-556.

HOYER D AND BARTFAI T. 2012. Neuropeptides and neuropeptide receptors: drug targets, and peptide and non-peptide ligands: a tribute to Prof. Dieter Seebach. Chemistry & biodiversity 9: 2367-2387.

ICHINOSE T, SHIELDS CR AND LUKASIEWICZ PD. 2005. Sodium channels in transient retinal bipolar cells enhance visual responses in ganglion cells. The Journal of neuroscience : the official journal of the Society for Neuroscience 25: 1856-1865.

ISHII M, HORIO Y, TADA Y, HIBINO H, INANOBE A, ITO M, YAMADA M, GOTOW T, UCHIYAMA Y AND KURACHI Y. 1997. Expression and clustered distribution of an inwardly rectifying potassium channel, KAB-2/Kir4.1, on mammalian retinal Muller cell membrane: their regulation by insulin and laminin signals. The Journal of neuroscience : the official journal of the Society for Neuroscience 17: 7725-7735.

JAN LY AND JAN YN. 1997. Voltage-gated and inwardly rectifying potassium channels. The Journal of physiology 505 (Pt 2): 267-282.

JAVAHERI M, HAHN DS, LAKHANPAL RR, WEILAND JD AND HUMAYUN MS. 2006. Retinal prostheses for the blind. Annals of the Academy of Medicine, Singapore 35: 137-144.

JAZWA A, FLORCZYK U, JOZKOWICZ A AND DULAK J. 2013. Gene therapy on demand: site specific regulation of gene therapy. Gene 525: 229-238.

JOHNSTON GA. 1996. GABAA receptor pharmacology. Pharmacology & therapeutics 69: 173-198.

JOHNSTON GA, CHEBIB M, HANRAHAN JR AND MEWETT KN. 2003. GABA(C) receptors as drug targets. Current drug targets CNS and neurological disorders 2: 260-268.

JONES BW, KONDO M, TERASAKI H, LIN Y, MCCALL M AND MARC RE. 2012. Retinal remodeling. Jpn J Ophthalmol 56: 289-306.

JONES BW, KONDO M, TERASAKI H, WATT CB, RAPP K, ANDERSON J, LIN Y, SHAW MV, YANG JH AND MARC RE. 2011. Retinal remodeling in the Tg P347L rabbit, a large-eye model of retinal degeneration. The Journal of comparative neurology 519: 2713-2733.

KAKEGAWA W, KOHDA K AND YUZAKI M. 2007a. The delta2 'ionotropic' glutamate receptor functions as a non-ionotropic receptor to control cerebellar synaptic plasticity. The Journal of physiology 584: 89-96.

KAKEGAWA W, MIYAZAKI T, HIRAI H, MOTOHASHI J, MISHINA M, WATANABE M AND YUZAKI M. 2007b. Ca2+ permeability of the channel pore is not essential for the delta2 glutamate receptor to regulate synaptic plasticity and motor coordination. The Journal of physiology 579: 729-735.

KALAMIDA D, POULAS K, AVRAMOPOULOU V, FOSTIERI E, LAGOUMINTZIS G, LAZARIDIS K, SIDERI A, ZOURIDAKIS M AND TZARTOS SJ. 2007. Muscle and neuronal nicotinic acetylcholine receptors. Structure, function and pathogenicity. The FEBS journal 274: 3799-3845.

KARAKAS E AND FURUKAWA H. 2014. Crystal structure of a heterotetrameric NMDA receptor ion channel. Science 344: 992-997.

KARSCHIN A AND WASSLE H. 1990. Voltage- and transmitter-gated currents in isolated rod bipolar cells of rat retina. Journal of neurophysiology 63: 860-876.

KAUPP UB AND SEIFERT R. 2002. Cyclic nucleotide-gated ion channels. Physiological reviews 82: 769-824.

KEBABIAN JW AND CALNE DB. 1979. Multiple receptors for dopamine. Nature 277: 93-96.

KIEN T, MAUL T AND BARGIELA A. 2012. A review of retinal prosthesis approaches. International Journal of Modern Physics: Conference Series 9: 209-231.

KLAVER CC, WOLFS RC, ASSINK JJ, VAN DUIJN CM, HOFMAN A AND DE JONG PT. 1998. Genetic risk of age-related maculopathy. Population-based familial aggregation study. Archives of ophthalmology 116: 1646-1651.

KLEIN R, KLEIN BE, TOMANY SC, MEUER SM AND HUANG GH. 2002. Ten-year incidence and progression of age-related maculopathy: The Beaver Dam eye study. Ophthalmology 109: 1767-1779.

KLUMPP DJ, SONG EJ, ITO S, SHENG MH, JAN LY AND PINTO LH. 1995. The Shaker-like potassium channels of the mouse rod bipolar cell and their contributions to the membrane current. The Journal of neuroscience : the official journal of the Society for Neuroscience 15: 5004-5013.

KOHDA K, WANG Y AND YUZAKI M. 2000. Mutation of a glutamate receptor motif reveals its role in gating and delta2 receptor channel properties. Nature neuroscience 3: 315-322.

KOLB H, CUENCA N AND DEKORVER L. 1991. Postembedding immunocytochemistry for GABA and glycine reveals the synaptic relationships of the dopaminergic amacrine cell of the cat retina. The Journal of comparative neurology 310: 267-284.

KOLB H AND DEKORVER L. 1991. Midget ganglion cells of the parafovea of the human retina: a study by electron microscopy and serial section reconstructions. The Journal of comparative neurology 303: 617-636.

KOLB H AND MARSHAK D. 2003. The midget pathways of the primate retina. Documenta ophthalmologica Advances in ophthalmology 106: 67-81.

KOLB H, NELSON R, AHNELT P AND CUENCA N. 2001. Cellular organization of the vertebrate retina. Progress in brain research 131: 3-26.

KOLB H, NELSON R AND MARIANI A. 1981. Amacrine cells, bipolar cells and ganglion cells of the cat retina: a Golgi study. Vision research 21: 1081-1114.

KOULEN P, KUHN R, WASSLE H AND BRANDSTATTER JH. 1997. Group I metabotropic glutamate receptors mGluR1alpha and mGluR5a: localization in both synaptic layers of the rat retina. The Journal of neuroscience : the official journal of the Society for Neuroscience 17: 2200-2211.

KOULEN P, MALITSCHEK B, KUHN R, WASSLE H AND BRANDSTATTER JH. 1996. Group II and group III metabotropic glutamate receptors in the rat retina: distributions and developmental expression patterns. The European journal of neuroscience 8: 2177-2187.

KRAMER RH, FORTIN DL AND TRAUNER D. 2009. New photochemical tools for controlling neuronal activity. Current Opinion in Neurobiology 19: 544-552.

KUISLE M AND LUETHI A 2010. Hyperpolarization-activated cation channels. In*:* KEW, J AND DAVIES, C (Eds.) Ion channels from structure to function, Oxford University Press, p. 183-206.

KVANTA A, ALGVERE PV, BERGLIN L AND SEREGARD S. 1996. Subfoveal fibrovascular membranes in age-related macular degeneration express vascular endothelial growth factor. Investigative ophthalmology & visual science 37: 1929-1934.

LAGALI PS, BALYA D, AWATRAMANI GB, MUNCH TA, KIM DS, BUSSKAMP V, CEPKO CL AND ROSKA B. 2008. Light-activated channels targeted to ON bipolar cells restore visual function in retinal degeneration. Nature neuroscience 11: 667-675.

LALOUETTE A, LOHOF A, SOTELO C, GUENET J AND MARIANI J. 2001. Neurobiological effects of a null mutation depend on genetic context: comparison between two hotfoot alleles of the delta-2 ionotropic glutamate receptor. Neuroscience 105: 443-455.

LAM DM. 1997. Neurotransmitters in the vertebrate retina. Investigative ophthalmology & visual science 38: 553-556.

LAPRELL L, HÜLL K, STAWSKI P, SCHOEN C, MICHALAKIS S, SUMSER M AND TRAUNER D. 2015a. Restoring light sensitivity in blind retinae using a photochromic AMPA receptor agonist. Neuropharmacology under review.

LAPRELL L, REPAK E, FRANCKEVICIUS V, HARTRAMPF F, TERHAG J, HOLLMANN M, SUMSER M, REBOLA N, DIGREGORIO D AND TRAUNER D. 2015b. Optical control of NMDA-receptors with a diffusible photoswitch. Nature communications resubmitted.

LAPRELL L ET AL. 2015c. Restoring visual responses with a photoswitch that targets bipolar cells in blind mice. Neuron Manuscript in preparation.

LE NOVERE N, CORRINGER PJ AND CHANGEUX JP. 2002. The diversity of subunit composition in nAChRs: evolutionary origins, physiologic and pharmacologic consequences. Journal of neurobiology 53: 447-456.

LEE CH, LU W, MICHEL JC, GOEHRING A, DU J, SONG X AND GOUAUX E. 2014. NMDA receptor structures reveal subunit arrangement and pore architecture. Nature 511: 191-197.

LEHMANN-HORN F AND JURKAT-ROTT K. 1999. Voltage-gated ion channels and hereditary disease. Physiological reviews 79: 1317-1372.

LEMOINE D, JIANG R, TALY A, CHATAIGNEAU T, SPECHT A AND GRUTTER T. 2012. Ligand-gated ion channels: new insights into neurological disorders and ligand recognition. Chemical reviews 112: 6285-6318.

LIN M, ZHU MX AND RIKIHISA Y. 2002. Rapid activation of protein tyrosine kinase and phospholipase C-gamma2 and increase in cytosolic free calcium are required by Ehrlichia chaffeensis for internalization and growth in THP-1 cells. Infection and immunity 70: 889-898.

LINDSTROM J, ANAND R, GERZANICH V, PENG X, WANG F AND WELLS G. 1996. Structure and function of neuronal nicotinic acetylcholine receptors. Progress in brain research 109: 125-137.

LIU X, ROBINSON ML, SCHREIBER AM, WU V, LAVAIL MM, CANG J AND COPENHAGEN DR. 2009. Regulation of neonatal development of retinal ganglion cell dendrites by neurotrophin-3 overexpression. The Journal of comparative neurology 514: 449-458.

LLANO I, MARTY A, ARMSTRONG CM AND KONNERTH A. 1991. Synaptic- and agonist-induced excitatory currents of Purkinje cells in rat cerebellar slices. The Journal of physiology 434: 183-213.

LOMELI H, SPRENGEL R, LAURIE DJ, KOHR G, HERB A, SEEBURG PH AND WISDEN W. 1993. The rat delta-1 and delta-2 subunits extend the excitatory amino acid receptor family. FEBS letters 315: 318-322.

LONDON NJ, CHIANG A AND HALLER JA. 2011. The dexamethasone drug delivery system: indications and evidence. Adv Ther 28: 351-366.

LOPEZ PF, SIPPY BD, LAMBERT HM, THACH AB AND HINTON DR. 1996. Transdifferentiated retinal pigment epithelial cells are immunoreactive for vascular endothelial growth factor in surgically excised age-related macular degeneration-related choroidal neovascular membranes. Investigative ophthalmology & visual science 37: 855-868.

LUDWIG A, ZONG X, JEGLITSCH M, HOFMANN F AND BIEL M. 1998. A family of hyperpolarization-activated mammalian cation channels. Nature 393: 587-591.

LUKASIEWICZ PD. 1996. GABAC receptors in the vertebrate retina. Molecular neurobiology 12: 181-194.

LUKASIEWICZ PD. 2005. Synaptic mechanisms that shape visual signaling at the inner retina. Progress in brain research 147: 205-218.

LUKASIEWICZ PD, EGGERS ED, SAGDULLAEV BT AND MCCALL MA. 2004. GABAC receptor-mediated inhibition in the retina. Vision research 44: 3289-3296.

LUNDBERG JM. 1996. Pharmacology of cotransmission in the autonomic nervous system: integrative aspects on amines, neuropeptides, adenosine triphosphate, amino acids and nitric oxide. Pharmacological reviews 48: 113-178.

LUTTRELL LM ET AL. 1999. Beta-arrestin-dependent formation of beta2 adrenergic receptor-Src protein kinase complexes. Science 283: 655-661.

LUTTRELL LM AND GESTY-PALMER D. 2010. Beyond desensitization: physiological relevance of arrestin-dependent signaling. Pharmacological reviews 62: 305-330.

LUTTRELL LM AND LEFKOWITZ RJ. 2002. The role of beta-arrestins in the termination and transduction of G-protein-coupled receptor signals. Journal of cell science 115: 455-465.

LYUBARSKY AL, LEM J, CHEN J, FALSINI B, IANNACCONE A AND PUGH EN, JR. 2002. Functionally rodless mice: transgenic models for the investigation of cone function in retinal disease and therapy. Vision Res 42: 401-415.

MA YP, CUI J, HU HJ AND PAN ZH. 2003. Mammalian retinal bipolar cells express inwardly rectifying K+ currents (IKir) with a different distribution than that of Ih. Journal of neurophysiology 90: 3479-3489.

MACE E ET AL. 2015. Targeting Channelrhodopsin-2 to ON-bipolar Cells With Vitreally Administered AAV Restores ON and OFF Visual Responses in Blind Mice. Molecular therapy : the journal of the American Society of Gene Therapy 23: 7-16.

MACKINNON R AND YELLEN G. 1990. Mutations affecting TEA blockade and ion permeation in voltage-activated K+ channels. Science 250: 276-279.

MAIER W, CORRIE JE, PAPAGEORGIOU G, LAUBE B AND GREWER C. 2005. Comparative analysis of inhibitory effects of caged ligands for the NMDA receptor. J Neurosci Methods 142: 1-9.

MANOOKIN MB, WEICK M, STAFFORD BK AND DEMB JB. 2010. NMDA receptor contributions to visual contrast coding. Neuron 67: 280-293.

MARC R, PFEIFFER R AND JONES B. 2014. Retinal Prosthetics, Optogenetics, and Chemical Photoswitches. ACS chemical neuroscience.

MARC RE, JONES BW, ANDERSON JR, KINARD K, MARSHAK DW, WILSON JH, WENSEL T AND LUCAS RJ. 2007. Neural reprogramming in retinal degeneration. Investigative ophthalmology & visual science 48: 3364-3371.

MARC RE, JONES BW, WATT CB, VAZQUEZ-CHONA F, VAUGHAN DK AND ORGANISCIAK DT. 2008. Extreme retinal remodeling triggered by light damage: implications for age related macular degeneration. Molecular vision 14: 782-806.

MARGOLIS DJ, GARTLAND AJ, SINGER JH AND DETWILER PB. 2014. Network oscillations drive correlated spiking of ON and OFF ganglion cells in the rd1 mouse model of retinal degeneration. PLoS One 9: e86253.

MASLAND RH. 2001. The fundamental plan of the retina. Nature neuroscience 4: 877-886.

MASU M ET AL. 1995. Specific deficit of the ON response in visual transmission by targeted disruption of the mGluR6 gene. Cell 80: 757-765.

MAYER ML, WESTBROOK GL AND GUTHRIE PB. 1984. Voltage-dependent block by Mg2+ of NMDA responses in spinal cord neurones. Nature 309: 261-263.

MCCORMICK KA, ISOM LL, RAGSDALE D, SMITH D, SCHEUER T AND CATTERALL WA. 1998. Molecular determinants of Na+ channel function in the extracellular domain of the beta1 subunit. The Journal of biological chemistry 273: 3954-3962.

MCCORMICK KA, SRINIVASAN J, WHITE K, SCHEUER T AND CATTERALL WA. 1999. The extracellular domain of the beta1 subunit is both necessary and sufficient for beta1-like modulation of sodium channel gating. The Journal of biological chemistry 274: 32638-32646.

MCFARLANE S AND POLLOCK NS. 2000. A role for voltage-gated potassium channels in the outgrowth of retinal axons in the developing visual system. The Journal of neuroscience : the official journal of the Society for Neuroscience 20: 1020-1029.

MCLAUGHLIN ME, EHRHART TL, BERSON EL AND DRYJA TP. 1995. Mutation spectrum of the gene encoding the beta subunit of rod phosphodiesterase among patients with autosomal recessive retinitis pigmentosa. Proceedings of the National Academy of Sciences of the United States of America 92: 3249-3253.

MENDOZA J, PEVET P, FELDER-SCHMITTBUHL MP, BAILLY Y AND CHALLET E. 2010. The cerebellum harbors a circadian oscillator involved in food anticipation. The Journal of neuroscience : the official journal of the Society for Neuroscience 30: 1894-1904.

MENGER N, POW DV AND WASSLE H. 1998. Glycinergic amacrine cells of the rat retina. The Journal of comparative neurology 401: 34-46.

MILLER RF, STENBACK K, HENDERSON D AND SIKORA M. 2002. How voltage-gated ion channels alter the functional properties of ganglion and amacrine cell dendrites. Archives italiennes de biologie 140: 347-359.

MISONOU H, MOHAPATRA DP AND TRIMMER JS. 2005. Kv2.1: a voltage-gated k+ channel critical to dynamic control of neuronal excitability. Neurotoxicology 26: 743-752.

MOEHLER H, BENKE D, RUDOLPH U AND FRITSCHY J-M 2010. GABAA Receptors. In*:* KEW, J AND C., D (Eds.) Ion Channels from structure to function: Oxford University Press, p. 263-272.

MORETTI M, VAILATI S, ZOLI M, LIPPI G, RIGANTI L, LONGHI R, VIEGI A, CLEMENTI F AND GOTTI C. 2004. Nicotinic acetylcholine receptor subtypes expression during rat retina development and their regulation by visual experience. Molecular pharmacology 66: 85-96.

MORGANS CW, BAYLEY PR, OESCH NW, REN G, AKILESWARAN L AND TAYLOR WR. 2005. Photoreceptor calcium channels: insight from night blindness. Visual neuroscience 22: 561-568.

MOUROT A, KIENZLER MA, BANGHART MR, FEHRENTZ T, HUBER FM, STEIN M, KRAMER RH AND TRAUNER D. 2011. Tuning photochromic ion channel blockers. ACS chemical neuroscience 2: 536-543.

MULLER F, SCHOLTEN A, IVANOVA E, HAVERKAMP S, KREMMER E AND KAUPP UB. 2003. HCN channels are expressed differentially in retinal bipolar cells and concentrated at synaptic terminals. The European journal of neuroscience 17: 2084-2096.

MULLER JM, LELIEVRE V, BECQ-GIRAUDON L AND MEUNIER AC. 1995. VIP as a cell-growth and differentiation neuromodulator role in neurodevelopment. Molecular neurobiology 10: 115-134.

MURESAN Z AND BESHARSE JC. 1993. D2-like dopamine receptors in amphibian retina: localization with fluorescent ligands. The Journal of comparative neurology 331: 149-160.

NAKAMURA T AND GOLD GH. 1987. A cyclic nucleotide-gated conductance in olfactory receptor cilia. Nature 325: 442-444.

NATHANS J, THOMAS D AND HOGNESS DS. 1986. Molecular genetics of human color vision: the genes encoding blue, green, and red pigments. Science 232: 193-202.

NAUR P ET AL. 2007. Ionotropic glutamate-like receptor delta2 binds D-serine and glycine. Proceedings of the National Academy of Sciences of the United States of America 104: 14116-14121.

NELSON R, VON LITZOW A, KOLB H AND GOURAS P. 1975. Horizontal cells in cat retina with independent dendritic systems. Science 189: 137-139.

NEUROPEPTIDES. Available: http://www.neuropeptides.nl/ [Accessed 05.01.2015.

NEVIAN T AND SAKMANN B. 2004. Single spine Ca2+ signals evoked by coincident EPSPs and backpropagating action potentials in spiny stellate cells of layer 4 in the juvenile rat somatosensory barrel cortex. The Journal of neuroscience : the official journal of the Society for Neuroscience 24: 1689-1699.

NGUYEN-LEGROS J, SIMON A, CAILLE I AND BLOCH B. 1997. Immunocytochemical localization of dopamine D1 receptors in the retina of mammals. Visual neuroscience 14: 545-551.

NISWENDER CM AND CONN PJ. 2010. Metabotropic glutamate receptors: physiology, pharmacology, and disease. Annual review of pharmacology and toxicology 50: 295-322.

NIZNIK HB AND VAN TOL HH. 1992. Dopamine receptor genes: new tools for molecular psychiatry. Journal of psychiatry & neuroscience : JPN 17: 158-180.

NOMURA A, SHIGEMOTO R, NAKAMURA Y, OKAMOTO N, MIZUNO N AND NAKANISHI S. 1994. Developmentally regulated postsynaptic localization of a metabotropic glutamate receptor in rat rod bipolar cells. Cell 77: 361-369.

NOWAK L, BREGESTOVSKI P, ASCHER P, HERBET A AND PROCHIANTZ A. 1984. Magnesium gates glutamate-activated channels in mouse central neurones. Nature 307: 462-465.

O'MALLEY DM, SANDELL JH AND MASLAND RH. 1992. Co-release of acetylcholine and GABA by the starburst amacrine cells. The Journal of neuroscience : the official journal of the Society for Neuroscience 12: 1394-1408.

OHKUMA M, KAWAI F, HORIGUCHI M AND MIYACHI E. 2007. Patch-clamp recording of human retinal photoreceptors and bipolar cells. Photochemistry and photobiology 83: 317-322.

OWSIANIK G, TALAVERA K, VOETS T AND NILIUS B. 2006. Permeation and selectivity of TRP channels. Annual review of physiology 68: 685-717.

OZAITA A, PETIT-JACQUES J, VOLGYI B, HO CS, JOHO RH, BLOOMFIELD SA AND RUDY B. 2004. A unique role for Kv3 voltage-gated potassium channels in starburst amacrine cell signaling in mouse retina. The Journal of neuroscience : the official journal of the Society for Neuroscience 24: 7335-7343.

PALCZEWSKI K. 2006. G protein-coupled receptor rhodopsin. Annual review of biochemistry 75: 743-767.

PAN ZH, GANJAWALA TH, LU Q, IVANOVA E AND ZHANG Z. 2014. ChR2 mutants at L132 and T159 with improved operational light sensitivity for vision restoration. PLoS One 9: e98924.

PAN ZH AND HU HJ. 2000. Voltage-dependent Na(+) currents in mammalian retinal cone bipolar cells. Journal of neurophysiology 84: 2564-2571.

PANDA S ET AL. 2003. Melanopsin is required for non-image-forming photic responses in blind mice. Science 301: 525-527.

PANDA S, SATO TK, CASTRUCCI AM, ROLLAG MD, DEGRIP WJ, HOGENESCH JB, PROVENCIO I AND KAY SA. 2002. Melanopsin (Opn4) requirement for normal light-induced circadian phase shifting. Science 298: 2213-2216.

PAOLETTI P, BELLONE C AND ZHOU Q. 2013. NMDA receptor subunit diversity: impact on receptor properties, synaptic plasticity and disease. Nature reviews Neuroscience 14: 383-400.

PAPE HC. 1996. Queer current and pacemaker: the hyperpolarization-activated cation current in neurons. Annual review of physiology 58: 299-327.

PENNESI ME, NEURINGER M AND COURTNEY RJ. 2012. Animal models of age related macular degeneration. Molecular aspects of medicine 33: 487-509.

PERKEL DJ, HESTRIN S, SAH P AND NICOLL RA. 1990. Excitatory synaptic currents in Purkinje cells. Proceedings Biological sciences / The Royal Society 241: 116-121.

PINTO LH AND KLUMPP DJ. 1998. Localization of potassium channels in the retina. Progress in retinal and eye research 17: 207-230.

PIOCHON C, IRINOPOULOU T, BRUSCIANO D, BAILLY Y, MARIANI J AND LEVENES C. 2007. NMDA receptor contribution to the climbing fiber response in the adult mouse Purkinje cell. The Journal of neuroscience : the official journal of the Society for Neuroscience 27: 10797-10809.

POLLOCK NS, FERGUSON SC AND MCFARLANE S. 2002. Expression of voltage-dependent potassium channels in the developing visual system of Xenopus laevis. The Journal of comparative neurology 452: 381-391.

POLOSUKHINA A ET AL. 2012. Photochemical restoration of visual responses in blind mice. Neuron 75: 271-282.

PULAGAM LP AND PALCZEWSKI K 2011. The Retina and its Disorders Phototransduction: Rhodopsin: Academic Pr Inc.

RAGOZZINO D, WOODWARD RM, MURATA Y, EUSEBI F, OVERMAN LE AND MILEDI R. 1996. Design and in vitro pharmacology of a selective gamma-aminobutyric acidC receptor antagonist. Molecular pharmacology 50: 1024-1030.

RAMSDEN CM, POWNER MB, CARR AJ, SMART MJ, DA CRUZ L AND COFFEY PJ. 2013. Stem cells in retinal regeneration: past, present and future. Development 140: 2576-2585.

RANDALL A AND TSIEN RW. 1995. Pharmacological dissection of multiple types of Ca2+ channel currents in rat cerebellar granule neurons. The Journal of neuroscience : the official journal of the Society for Neuroscience 15: 2995-3012.

REMTULLA S AND HALLETT PE. 1985. A schematic eye for the mouse, and comparisons with the rat. Vision research 25: 21-31.

REN L, LIANG H, DIAO L AND HE S. 2010. Changing dendritic field size of mouse retinal ganglion cells in early postnatal development. Dev Neurobiol 70: 397-407.

REUTSKY-GEFEN I, GOLAN L, FARAH N, SCHEJTER A, TSUR L, BROSH I AND SHOHAM S. 2013. Holographic optogenetic stimulation of patterned neuronal activity for vision restoration. Nature communications 4: 1509.

RODRIGUEZ-MORENO A, KOHL MM, REEVE JE, EATON TR, COLLINS HA, ANDERSON HL AND PAULSEN O. 2011. Presynaptic Induction and Expression of Timing-Dependent Long-Term Depression Demonstrated by Compartment-Specific Photorelease of a Use-Dependent NMDA Receptor Antagonist. Journal of Neuroscience 31: 8564-8569.

ROWE-RENDLEMAN CL ET AL. 2014. Drug and gene delivery to the back of the eye: from bench to bedside. Investigative ophthalmology & visual science 55: 2714-2730.

RYSKAMP DA ET AL. 2011. The polymodal ion channel transient receptor potential vanilloid 4 modulates calcium flux, spiking rate, and apoptosis of mouse retinal ganglion cells. The Journal of neuroscience : the official journal of the Society for Neuroscience 31: 7089-7101.

SADOVSKI O, BEHARRY AA, ZHANG F AND WOOLLEY GA. 2009. Spectral tuning of azobenzene photoswitches for biological applications. Angewandte Chemie 48: 1484-1486.

SAMARDZIJA M, NEUHAUSS S, JOLY S, KURZ-LEVIN M AND GRIMM C 2010. Animal Models for Retinal Degeneration. Animal Models for Retinal Degeneration: Springer Science+Business Media, p. 51-79.

SAPPINGTON RM, SIDOROVA T, LONG DJ AND CALKINS DJ. 2009. TRPV1: contribution to retinal ganglion cell apoptosis and increased intracellular Ca2+ with exposure to hydrostatic pressure. Investigative ophthalmology & visual science 50: 717-728.

SCHMID SM AND HOLLMANN M. 2008. To gate or not to gate: are the delta subunits in the glutamate receptor family functional ion channels? Molecular neurobiology 37: 126-141.

SCHMID SM, KOTT S, SAGER C, HUELSKEN T AND HOLLMANN M. 2009. The glutamate receptor subunit delta2 is capable of gating its intrinsic ion channel as revealed by ligand binding domain transplantation. Proceedings of the National Academy of Sciences of the United States of America 106: 10320-10325.

SCHONBERGER M AND TRAUNER D. 2014. A photochromic agonist for mu-opioid receptors. Angewandte Chemie 53: 3264-3267.

SCHWARTZ SD, HUBSCHMAN JP, HEILWELL G, FRANCO-CARDENAS V, PAN CK, OSTRICK RM, MICKUNAS E, GAY R, KLIMANSKAYA I AND LANZA R. 2012. Embryonic stem cell trials for macular degeneration: a preliminary report. Lancet 379: 713-720.

SEIFERT R, SCHOLTEN A, GAUSS R, MINCHEVA A, LICHTER P AND KAUPP UB. 1999. Molecular characterization of a slowly gating human hyperpolarization-activated channel predominantly expressed in thalamus, heart, and testis. Proceedings of the National Academy of Sciences of the United States of America 96: 9391-9396.

SHEN Y, RAMPINO MA, CARROLL RC AND NAWY S. 2012. G-protein-mediated inhibition of the Trp channel TRPM1 requires the Gbetagamma dimer. Proceedings of the National Academy of Sciences of the United States of America 109: 8752-8757.

SIMMS BA AND ZAMPONI GW. 2014. Neuronal voltage-gated calcium channels: structure, function, and dysfunction. Neuron 82: 24-45.

SLAUGHTER MM AND MILLER RF. 1981. 2-amino-4-phosphonobutyric acid: a new pharmacological tool for retina research. Science 211: 182-185.

SMITH BJ, TREMBLAY F AND COTE PD. 2013. Voltage-gated sodium channels contribute to the b-wave of the rodent electroretinogram by mediating input to rod bipolar cell GABA(c) receptors. Experimental eye research 116: 279-290.

SOLYOM S AND TARNAWA I. 2002. Non-competitive AMPA antagonists of 2,3-benzodiazepine type. Current pharmaceutical design 8: 913-939.

SONG MY AND YUAN JX. 2010. Introduction to TRP channels: structure, function, and regulation. Advances in experimental medicine and biology 661: 99-108.

SPANO PF, GOVONI S AND TRABUCCHI M. 1978. Studies on the pharmacological properties of dopamine receptors in various areas of the central nervous system. Advances in biochemical psychopharmacology 19: 155-165.

SQUIRE LR, BERG D, BLOOM FE, DU LAC S, GHOSH A AND SPITZER NC. 2008. Fundamental Neuroscience, The Eye and the Retina. Elsevier Third Edition.

STASHEFF SF. 2008. Emergence of sustained spontaneous hyperactivity and temporary preservation of OFF responses in ganglion cells of the retinal degeneration (rd1) mouse. Journal of neurophysiology 99: 1408-1421.

STAWSKI P, SUMSER M AND TRAUNER D. 2012. A photochromic agonist of AMPA receptors. Angewandte Chemie 51: 5748-5751.

STEIN M. 2014. Dissertation.

STINGL K ET AL. 2013. Artificial vision with wirelessly powered subretinal electronic implant alpha-IMS. Proceedings Biological sciences / The Royal Society 280: 20130077.

STRADLEIGH TW, OGATA G, PARTIDA GJ, OI H, GREENBERG KP, KREMPELY KS AND ISHIDA AT. 2011. Colocalization of hyperpolarization-activated, cyclic nucleotide-gated channel subunits in rat retinal ganglion cells. The Journal of comparative neurology 519: 2546-2573.

STRONKS HC AND DAGNELIE G. 2014. The functional performance of the Argus II retinal prosthesis. Expert review of medical devices 11: 23-30.

SUN M ET AL. 2000. Mucolipidosis type IV is caused by mutations in a gene encoding a novel transient receptor potential channel. Human molecular genetics 9: 2471-2478.

SZABO I, ZORATTI M AND GULBINS E. 2010. Contribution of voltage-gated potassium channels to the regulation of apoptosis. FEBS letters 584: 2049-2056.

TANAKA JC, ECCLESTON JF AND FURMAN RE. 1989. Photoreceptor channel activation by nucleotide derivatives. Biochemistry 28: 2776-2784.

TAUCHI M, MADIGAN NK AND MASLAND RH. 1990. Shapes and distributions of the catecholamine-accumulating neurons in the rabbit retina. The Journal of comparative neurology 293: 178-189.

TAUCHI M AND MASLAND RH. 1984. The shape and arrangement of the cholinergic neurons in the rabbit retina. Proceedings of the Royal Society of London Series B, Containing papers of a Biological character Royal Society 223: 101-119.

THOMPSON SM. 2005. Flashy Science: Controlling Neural Function with Light. Journal of Neuroscience 25: 10358-10365.

THORESON WB AND MANGEL SC. 2012. Lateral interactions in the outer retina. Progress in retinal and eye research 31: 407-441.

THYAGARAJAN S, VAN WYK M, LEHMANN K, LOWEL S, FENG G AND WASSLE H. 2010. Visual function in mice with photoreceptor degeneration and transgenic expression of channelrhodopsin 2 in ganglion cells. The Journal of neuroscience : the official journal of the Society for Neuroscience 30: 8745-8758.

TIAN M, ZHAO JW, YANG XL AND XIE JX. 2003. Voltage-gated K(+) channel subunits on cholinergic and dopaminergic amacrine cells. Neuroreport 14: 1763-1766.

TIBERI M, JARVIE KR, SILVIA C, FALARDEAU P, GINGRICH JA, GODINOT N, BERTRAND L, YANG-FENG TL, FREMEAU RT, JR. AND CARON MG. 1991. Cloning, molecular characterization, and chromosomal assignment of a gene encoding a second D1 dopamine receptor subtype:

differential expression pattern in rat brain compared with the D1A receptor. Proceedings of the National Academy of Sciences of the United States of America 88: 7491-7495.

TOCHITSKY I AND KRAMER RH. 2015. Optopharmacological tools for restoring visual function in degenerative retinal diseases. Current opinion in neurobiology 34C: 74-78.

TOCHITSKY I, POLOSUKHINA A, DEGTYAR VE, GALLERANI N, SMITH CM, FRIEDMAN A, VAN GELDER RN, TRAUNER D, KAUFER D AND KRAMER RH. 2014. Restoring visual function to blind mice with a photoswitch that exploits electrophysiological remodeling of retinal ganglion cells. Neuron 81: 800-813.

TRIFONOV IU. 1968. [Study of synaptic transmission between photoreceptor and horizontal cell by electric stimulations of the retina]. Biofizika 13: 809-817.

VAJNA R, SCHRAMM M, PEREVERZEV A, ARNHOLD S, GRABSCH H, KLOCKNER U, PEREZ-REYES E, HESCHELER J AND SCHNEIDER T. 1998. New isoform of the neuronal Ca2+ channel alpha1E subunit in islets of Langerhans and kidney--distribution of voltage-gated Ca2+ channel alpha1 subunits in cell lines and tissues. European journal of biochemistry / FEBS 257: 274-285.

VAN PETEGEM F AND MINOR DL, JR. 2006. The structural biology of voltage-gated calcium channel function and regulation. Biochemical Society transactions 34: 887-893.

VAN WYK M, PIELECKA-FORTUNA J, LOWEL S AND KLEINLOGEL S. 2015. Restoring the ON Switch in Blind Retinas: Opto-mGluR6, a Next-Generation, Cell-Tailored Optogenetic Tool. PLoS biology 13: e1002143.

VANEY DI. 1994. Territorial organization of direction-selective ganglion cells in rabbit retina. The Journal of neuroscience : the official journal of the Society for Neuroscience 14: 6301-6316.

VANEY DI AND YOUNG HM. 1988. GABA-like immunoreactivity in cholinergic amacrine cells of the rabbit retina. Brain research 438: 369-373.

VERUKI ML AND WASSLE H. 1996. Immunohistochemical localization of dopamine D1 receptors in rat retina. The European journal of neuroscience 8: 2286-2297.

VOGEL MW, CASTON J, YUZAKI M AND MARIANI J. 2007. The Lurcher mouse: fresh insights from an old mutant. Brain research 1140: 4-18.

VOLGRAF M. 2008. I. Photocontrol of Ionotropic Glutamate Receptors and II. Total Synthesis of Exiguamine A and B. Dissertation.

VOLGRAF M, GOROSTIZA P, SZOBOTA S, HELIX MR, ISACOFF EY AND TRAUNER D. 2007. Reversibly caged glutamate: a photochromic agonist of ionotropic glutamate receptors. Journal of the American Chemical Society 129: 260-261.

WADEL K, NEHER E AND SAKABA T. 2007. The coupling between synaptic vesicles and Ca2+ channels determines fast neurotransmitter release. Neuron 53: 563-575.

WALD G. 1968. Molecular basis of visual excitation. Science 162: 230-239.

WANG TL, HACKAM AS, GUGGINO WB AND CUTTING GR. 1995. A single amino acid in gamma-aminobutyric acid rho 1 receptors affects competitive and noncompetitive components of picrotoxin inhibition. Proceedings of the National Academy of Sciences of the United States of America 92: 11751-11755.

WASSLE H, KOULEN P, BRANDSTATTER JH, FLETCHER EL AND BECKER CM. 1998. Glycine and GABA receptors in the mammalian retina. Vision research 38: 1411-1430.

WEBB TI AND LYNCH JW. 2007. Molecular pharmacology of the glycine receptor chloride channel. Current pharmaceutical design 13: 2350-2367.

WEILAND JD, CHO AK AND HUMAYUN MS. 2011. Retinal prostheses: current clinical results and future needs. Ophthalmology 118: 2227-2237.

WERBLIN FS. 2011. The retinal hypercircuit: a repeating synaptic interactive motif underlying visual function. The Journal of physiology 589: 3691-3702.

WHITTEN DG, WILDES PD, PACIFICI JG AND IRICK GJ. 1971. Solvent and substituent on the thermal isomerization of substituted azobenzenes. Flash spectroscopic study. Journal of the American Chemical Society 93: 2004-2008.

WHO. 2014. World Health Organization. Available: http://www.who.int/mediacentre/factsheets/fs282/en/ [Accessed 09.01. 2015].

WIKLER KC AND RAKIC P. 1990. Distribution of photoreceptor subtypes in the retina of diurnal and nocturnal primates. The Journal of neuroscience : the official journal of the Society for Neuroscience 10: 3390-3401.

WIKLER KC, WILLIAMS RW AND RAKIC P. 1990. Photoreceptor mosaic: number and distribution of rods and cones in the rhesus monkey retina. The Journal of comparative neurology 297: 499-508.

WILLIAMS K, DATTILO M, SABADO TN, KASHIWAGI K AND IGARASHI K. 2003. Pharmacology of delta2 glutamate receptors: effects of pentamidine and protons. The Journal of pharmacology and experimental therapeutics 305: 740-748.

WITKOVSKY P. 2004. Dopamine and retinal function. Documenta ophthalmologica Advances in ophthalmology 108: 17-40.

WITKOVSKY P AND SCHUTTE M. 1991. The organization of dopaminergic neurons in vertebrate retinas. Visual neuroscience 7: 113-124.

WOLF M, EBERHART A, GLOSSMANN H, STRIESSNIG J AND GRIGORIEFF N. 2003. Visualization of the domain structure of an L-type Ca2+ channel using electron cryo-microscopy. Journal of molecular biology 332: 171-182.

WONG RO. 1999. Retinal waves and visual system development. Annual review of neuroscience 22: 29-47.

WU S, MOORE TM, BROUGH GH, WHITT SR, CHINKERS M, LI M AND STEVENS T. 2000. Cyclic nucleotide-gated channels mediate membrane depolarization following activation of store-operated calcium entry in endothelial cells. The Journal of biological chemistry 275: 18887-18896.

XU W, LEUNG S, WRIGHT J AND GUGGINO SE. 1999. Expression of cyclic nucleotide-gated cation channels in airway epithelial cells. The Journal of membrane biology 171: 117-126.

XU Y, DHINGRA A, FINA ME, KOIKE C, FURUKAWA T AND VARDI N. 2012. mGluR6 deletion renders the TRPM1 channel in retina inactive. Journal of neurophysiology 107: 948-957.

YANG XL. 2004. Characterization of receptors for glutamate and GABA in retinal neurons. Progress in neurobiology 73: 127-150.

YOOL AJ AND SCHWARZ TL. 1991. Alteration of ionic selectivity of a K+ channel by mutation of the H5 region. Nature 349: 700-704.

YU FH AND CATTERALL WA. 2003. Overview of the voltage-gated sodium channel family. Genome biology 4: 207.

YU W AND MILLER RF. 1995. NBQX, an improved non-NMDA antagonist studied in retinal ganglion cells. Brain research 692: 190-194.

ZALUTSKY RA AND MILLER RF. 1990a. The physiology of somatostatin in the rabbit retina. The Journal of neuroscience : the official journal of the Society for Neuroscience 10: 383-393.

ZALUTSKY RA AND MILLER RF. 1990b. The physiology of substance P in the rabbit retina. The Journal of neuroscience : the official journal of the Society for Neuroscience 10: 394-402.

ZARBIN MA. 2004. Current concepts in the pathogenesis of age-related macular degeneration. Archives of ophthalmology 122: 598-614.

ZARBIN MA, CASAROLI-MARANO RP AND ROSENFELD PJ. 2014. Age-related macular degeneration: clinical findings, histopathology and imaging techniques. Developments in ophthalmology 53: 1-32.

ZEISS CJ. 2010. Animals as models of age-related macular degeneration: an imperfect measure of the truth. Veterinary pathology 47: 396-413.

ZENISEK D, HENRY D, STUDHOLME K, YAZULLA S AND MATTHEWS G. 2001. Voltage-dependent sodium channels are expressed in nonspiking retinal bipolar neurons. The Journal of neuroscience : the official journal of the Society for Neuroscience 21: 4543-4550.

ZHANG AJ AND WU SM. 2009. Receptive fields of retinal bipolar cells are mediated by heterogeneous synaptic circuitry. The Journal of neuroscience : the official journal of the Society for Neuroscience 29: 789-797.

ZHANG D, PAN ZH, ZHANG X, BRIDEAU AD AND LIPTON SA. 1995. Cloning of a gamma-aminobutyric acid type C receptor subunit in rat retina with a methionine residue critical for picrotoxinin channel block. Proceedings of the National Academy of Sciences of the United States of America 92: 11756-11760.

ZHONG YS, WANG J, LIU WM AND ZHU YH. 2013. Potassium ion channels in retinal ganglion cells (review). Molecular medicine reports 8: 311-319.

ZHOU ZJ, FAIN GL AND DOWLING JE. 1993. The excitatory and inhibitory amino acid receptors on horizontal cells isolated from the white perch retina. Journal of neurophysiology 70: 8-19.

ZIMMER T AND BENNDORF K. 2002. The human heart and rat brain IIA Na+ channels interact with different molecular regions of the beta1 subunit. The Journal of general physiology 120: 887-895.

ZIMMERMAN DM, SMITS SE, HYNES MD, CANTRELL BE, LEANDER JD, MENDELSOHN LG AND NICKANDER R. 1985. Picenadol. Drug and alcohol dependence 14: 381-401.

ZRENNER E ET AL. 1997. The development of subretinal microphotodiodes for replacement of degenerated photoreceptors. Ophthalmic research 29: 269-280.

ZRENNER E, STETT A, WEISS S, ARAMANT RB, GUENTHER E, KOHLER K, MILICZEK KD, SEILER MJ AND HAEMMERLE H. 1999. Can subretinal microphotodiodes successfully replace degenerated photoreceptors? Vision research 39: 2555-2567.

ZUO J, DE JAGER PL, TAKAHASHI KA, JIANG W, LINDEN DJ AND HEINTZ N. 1997. Neurodegeneration in Lurcher mice caused by mutation in delta2 glutamate receptor gene. Nature 388: 769-773.

7 Appendix

7.1 Matlab scripts

7.1.1 Raster plot and photoswitch index

```
source_directory = uigetdir('C:\ ');
%source_directory='WTF2';

%get the filenames of all files in the directory
d=dir(source_directory);


names=strvcat(d.name);
%strvcat=string vertical catination
%the first two filenames are not informative (Matlab stuff)
num_files=size(names,1)-2; %how many files do I have

file_counter=1:num_files;

for file_counter=1;
    %substract 2 to get rid of Matlab/Windows-based two first file names;
    %names,1 takes only the first dimension of the names (get nur, wenn alle
filenames wirklich exakt gleich lang sind!)

    %build the filename including path as a sting
    filename=[source_directory '\' deblank(names(file_counter+2,:))];
    %try to open the file
    %file identifier (fid)
    fid=fopen(filename); %looks, if file exists; positive/negative file identifier
    %read the first line
    header=fgetl(fid);
    %read in the spike times
    [spt, count]=fscanf(fid,'%f');
    fclose(fid);
    %plot the spike times as rasterplot using spt as x-values and always the
    %same y-value depending on the counter
    max_data=spt;
    [maxdur, ind] = max(max_data);

end

%maxdur=input('for how many seconds did you record? ');
%define matrix for photoswitch values calculated in each loop
PI=[];

%define start and end point for PI calculation here

PI1_100ms = input ('Start calculation before light at [sec] ');
PI2_100ms = input ('End calculation before light at [sec] ');
%PI3=PI2 = input ('Start calculation with light at ');
%PI3_100ms=PI2_100ms;
PI3_100ms = input ('Start calculation with light at [sec] ');
PI4_100ms = input ('End calculation with light at [sec] ');

%we have 10 zeros before the histogram starts to make it fit better to the
%graph. we therefore need to add 10 for the calculation of the PI.

PI1=PI1_100ms*10+10;
PI2=PI2_100ms*10+10;
PI3=PI2;
PI4=PI4_100ms*10+10;

%how do I tell my computer that I mean the time axis?

%predefine a figure for the rasterplot
fh=figure;
```

```
%define the axis
ah=axes;
axis ij;
set(ah,'fontsize', 14,'xlim',[-1 maxdur+1],'ylim' ,[0 num_files+1])
xlabel ('Time [sec]');
ylabel ('cell #');

hold on

%define empty matrix for the summary spike times
sum_spt=[];
mean_dark_end=[];
mean_light_end=[];

% in this cell array all spt are saved as indivudial rows, not concatenated
spikes=cell(file_counter,1);

%make edges for histogramm (100ms steps)
hist_edges=-1:0.1:maxdur+1;


for file_counter=1:num_files;
    %substract 2 to get rid of Matlab/Windows-based two first file names;
    %names,1 takes only the first dimension of the names (get nur, wenn alle
filenames wirklich exakt gleich lang sind!)

    %build the filename including path as a sting
    filename=[source_directory '\' deblank(names(file_counter+2,:))];
    %try to open the file
    %file identifier (fid)
    fid=fopen(filename); %looks, if file exists; positive/negative file identifier
    %read the first line
    header=fgetl(fid);
    %read in the spike times
    [spt, count]=fscanf(fid,'%f');
    fclose(fid);
    %plot the spike times as rasterplot using spt as x-values and always the
    %same y-value depending on the counter

    xdata=spt;

    %put all spike times (spt) in one matrix; concatenate matrix next to each other;
    % this does not work because of different number of spike times...
    % sum_spt=[sum_spt spt];

    %make histogram for calcuation of PI
    hist=histc(spt, hist_edges);
    %calculate PI from hist
    Mean_Dark=mean(hist(PI1:PI2));
    Mean_Light=mean(hist(PI3:PI4));
    PI_value=((Mean_Light)-(Mean_Dark))/((Mean_Light)+(Mean_Dark));
    PI=[PI;PI_value];

    sum_spt=[sum_spt;spt];

    mean_dark_end=[mean_dark_end;Mean_Dark];
    mean_light_end=[mean_light_end;Mean_Light];

    %add all spt to individual row in cell array.
    spikes{file_counter}=spt;

    %create a vector with 1 with exactly the same size as spt
   %{
    ydata=file_counter*ones(size(spt));
    ph=plot(xdata,ydata,'k.');
    set (ph, 'markersize', 4);
    %}
      ydata=file_counter*ones(size(spt));
    ph=plot(xdata,ydata,'ko');
    set (ph, 'markersize', 1.5,'linewidth',1.2);

end

%calculate the PI by averaging the PI values the individual cells.
PI=PI(~any(isnan(PI),2),:);
PI_mean=mean(PI)

%calculate the PI by taking the average spiking rates of all cells (should
```

```
%be similar.) The difference results from the deletion of single NaN in the
%PI determination using (PI=PI(~any(isnan(PI), 2), :)). This does not
%happen for mean_values!
mean_spikes_light=mean(mean_light_end);
mean_spikes_dark=mean(mean_dark_end);
PI_spikes=((mean_spikes_light)-
(mean_spikes_dark))/((mean_spikes_light)+(mean_spikes_dark))


%figure
%bar(hist_edges,spt_hist);
%bar(hist_edges,hist);
%set (gca, 'fontsize' ,14,'xlim', [-1 maxdur+1]);

%now calculate the histogram
% be careful, this is the event number over all channels. more channels
% means more events. this is not the frequency!!! frequency will be:
% #events/#cells --> therefore I introduce 'freq', which divides the
% #events/#cells.
spt_hist=histc(sum_spt,hist_edges);
%spt_hist=histc(b,hist_edges);
freq=spt_hist./num_files;
[freq_max,ind] = max(freq);


figure
%bar(hist_edges,spt_hist);
bar(hist_edges,freq, 'k');
set (gca, 'fontsize' ,14,'xlim', [-1 maxdur+1], 'ylim', [0 10]);
ax2 = gca;

%the next section is needed, if the light stimulus protocol was added to the
%workspace before. In that case, the light stimulus protocol will be
%applied to the graph

hold on;
plot (Ts, Bit0);
hold off;

%create a new figure for subplots --> this will be the final figure
h3 = figure;
s1=subplot ('position', [0.15 0.4 0.8 0.55]);
set(gca,'fontsize', 14,'xlim',[-1 maxdur+1],'ylim' ,[0 num_files+1], 'XTickLabel',
[]);
%set(gca,'fontsize', 14,'xlim',[60 80],'ylim' ,[0 num_files+1], 'XTickLabel', []);
grid on;
%ax = copyobj(gca, gcf);
%set(ax,'color','none','xgrid','off', 'xcolor','k', 'ygrid','off', 'ycolor','k');
%set(gca,'Xcolor','r');
%set(gca,'Ycolor','r');
ylabel ('cell #')
s2=subplot ('position', [0.15 0.1 0.8 0.25]);
set (gca, 'fontsize' ,14,'xlim', [-1 maxdur+1], 'ylim', [0 freq_max+1]);
%set (gca, 'fontsize' ,14,'xlim', [60 80]);
xlabel ('Time [sec]');
fig1 = get (ah, 'children');
fig2 = get (ax2, 'children');
ylabel ('#spikes/100ms');
grid on;
%set(gca,'Xcolor','r');
%set(gca,'Ycolor','r');

%Caxes = copyobj(gca, gcf);
%set(Caxes, 'color', 'none', 'xcolor', 'k', 'xgrid', 'off', 'ycolor','k',
'ygrid','off');
copyobj (fig1, s1);
copyobj (fig2, s2);

close Figure 1;
close Figure 2;

%Make population plot for PI values;

op10=PI(PI>0.8 & PI<1);
num10=numel(op10);
op9=PI(PI>0.6 & PI<0.8);
num9=numel(op9);
op8=PI(PI>0.4 & PI<0.6);
```

```
num8=numel(op8);
op7=PI(PI>0.2 & PI<0.4);
num7=numel(op7);
op6=PI(PI>0.0 & PI<0.2);
num6=numel(op6);
op5=PI(PI>-0.2 & PI<0);
num5=numel(op5);
op4=PI(PI>-0.4 & PI<-0.2);
num4=numel(op4);
op3=PI(PI>-0.6 & PI<-0.4);
num3=numel(op3);
op2=PI(PI>-0.8 & PI<-0.6);
num2=numel(op2);
op1=PI(PI>-1 & PI<-0.8);
num1=numel(op1);

%define maximum in cell distribution to use it for plotting
num_arr = [num1, num2, num3, num4, num5, num6, num7, num8, num9, num10];
[maximum,ind] = max(num_arr);
num_dist=[num1;num2;num3;num4;num5;num6;num7;num8;num8;num9;num10];

figure

bar(num_dist, 0.6, 'k', 'EdgeColor',[1,0.5,0.5], 'LineWidth', 2);
set(gca,'XTickLabel',{'-1','-0.8','-0.6','-0.4','-
0.2','0','0.2','0.4','0.6','0.8','1'});
grid on;

%use maximum here to plot cell distribution +5
ylim ([0 (maximum+5)]);

display (PI_mean);
```

7.1.2 Find peaks

```
%first determine the 4xSD and set this as 'minpeakheight', in case of unstable
baseline use larger SD. Depending on the light stimulation protocol, i.e. the
frequency define the 'minpeakdistance'. For 0.2 Hz > 4500 ms, for 0.5 Hz > 1500, for
1 Hz > 750 ms and for 2 Hz > 450 ms.

[pks,locs]=findpeaks(freq,'minpeakheight',1.3,'MinPeakDistance', 50);

plot (freq)  % freq needs to be calculated before using the raster plot script
hold on
plot(locs,pks,'ro');


% the peaks found need then to be compared to the light stimulation protocol. A time
delay between the light stimulation can be determined, depending on the light
stimulation frequency. Further analysis of peaks found and the stimulation protocol
was performed in Microsoft excel. An automatic script still need to be written.
```

7.1.3 On- versus Off-activity distribution

```
%first the PI-values need to be determined for the light-on time frame and for the
light-off time frame using the raster plot script. These need to be saved separately
named PI_on and PI_off, respectively.

index_on = find(PI_on >0.1 & PI_on <=0.99);
index_off = find(PI_off>0.1 & PI_off <=0.99);

%index_on = find(PI_on <-0.1 & PI_on >=-0.99);
%index_off = find(PI_off <-0.1 & PI_off >=-0.99);

X_on=ismember (index_on, index_off);
X_off=ismember (index_off, index_on);

X_on_sum=sum(X_on);
X_off_sum=sum(X_off);

only_on=size (index_on,1) - X_on_sum
```

```
only_off=size (index_off,1) - X_off_sum
both=X_on_sum

PI_mean_on=mean(PI_on);
PI_mean_off=mean(PI_off);
PI_compare=PI_mean_on/PI_mean_off

%vertically concatenate index_on and off
    X=vertcat(index_on, index_off);
 %find all unique values and keep the duplicates in X.
 uniqueX = unique(X);
 countOfX = hist(X,uniqueX);
 indexToRepeatedValue = (countOfX~=1);
 repeatedValues = uniqueX(indexToRepeatedValue)

%Quotient der PI/Werte von allen Zellen, die eine on und off response haben
Quotient = (PI_on(:,1)./PI_off(:,1));
extract_quotient=Quotient((repeatedValues),:)

figure

bar(extract_quotient, 0.6, 'k', 'EdgeColor',[1,0.5,0.5], 'LineWidth', 2);
ylim ([0 (5)]);
```

7.1.4 Correlation plots

```
% For the correlation plots the histograms of each channel need to be transferred to
IGOR Pro; the time frame for the correlation analysis need to be copied into Matlab
and named 'set_of_histograms'

set_of_histograms( :, all( ~any( set_of_histograms ), 1 ) ) = []; % delete all
histograms that cotain only zeros

[rho, p] = corrcoef( set_of_histograms);
%significant p-values [R,P]=corrcoef(...) also returns P, a matrix of
%p-values for testing the hypothesis of no correlation. Each p-value is the
%probability of getting a correlation as large as the observed value by
%random chance, when the true correlation is zero. If P(i,j) is small, say
%less than 0.05, then the correlation R(i,j) is significant.


%Visulisation

imagesc(rho);
colormap('jet);colorbar;
image(rho);
colormap('gray');colorbar;

imshow(rho);
colormenu;colorbar %a colormap menu is added to your figure

spy(rho)


[i,j] = find(p<0.05);  % Find significant correlations.


%calculatate percentage of statistically significant correlations

A=size(set_of_histograms,2);

max=A*A; %maximale Anzahl aller Korrelationen

xpercent=(100/max)*size(i,1)


imagesc(p);
colormap('jet);colorbar;

image(p);
colormap('gray');colorbar;

imshow(p);
colormenu;colorbar %a colormap menu is added to your figure
```

```
spy(p)
```

Acknowledgements

First, I would like to thank my supervisor and mentor, Prof. Dr. Dirk Trauner. His enthusiasm to gain knowledge not only in organic chemistry, but in general science is truly inspiring. I especially appreciated the freedom he granted to explore new ideas and the trust in my work. I would also like to thank him for the possibilities to spend time in other labs and to present my data at many international conferences.

I would also like to thank my "second" supervisor, Dr. Martin Sumser, for teaching me patience (you succeeded at least to some degree) and for teaching me how to patch, to do calcium imaging, to prepare brain slices, and so on; and furthermore, for taking so much time to listen to my experimental designs and all that retina stuff. And of course for reading this whole thing.

Many thanks to Prof. Dr. Dr. Franz Grus for being the second reviewer of this thesis and for the discussions about vision restoration approaches and my project.

And thanks to Prof. Dr. Thomas Misgeld, Prof. Dr. Konstantin Karaghiosoff, Prof. Dr. Klaus Wanner and Prof. Roland Beckmann for being part of my thesis committee.

I would also like to thank my collaborators with whom I had a great and inspiring time, Prof. Russell Van Gelder and all the lab members, as well as Prof. Richard Kramer and Dr. Ivan Tochitsky.

Special thanks go to Angela Sandt and Dr. Kathryn L. Pepple and I very much appreciated the help from Dr. Mike Manookin.

My thanks also to Prof. Dr. Botond Roska for being part of my thesis advisory committee and the fruitful discussion about my project. And thanks to Dr. Tamas Szikra and Prof. Dr. Tim Gollisch for giving me a kick-start in retina preparation.

Of course, none of this would have been possible without the permanent staff of the lab, first of all Heike Traub and Luis de la Osa de la Rosa, Aleksandra Sarman Grilc and Carrie Louis.

I am grateful for the opportunity to spend a few months in the lab of Prof. Van Gelder, which would not have been possible without the Boehringer Ingelheim Foundation. And my thanks also go to the IMPRS-LS coordination office, Dr. Hans Joerg Schaeffer, Dr. Ingrid Wolf, Maximiliane Reif and Dr. Katharina Frank, for their constant support and for all the helpful soft skill workshops.

I would also like to thank all my lab people in the lab for creating such a motivating environment. Special thanks go to Kathi Hüll ("mit ü"), for being a friend, and just because... Thanks also to Arunas Damijonaitis for sitting next to the door and being asked all the questions I don't want to be asked and for being so very emphatic. Thanks to Philipp Leippe for taking care of my "Seelenwohl" (now you actually have to..) and Matthias Schönberger for being so cool in the most stressful situations. Thanks to Nina Vrielink for

being a truly good person, and to Philipp Stawski for being part of my first vision restoration project.

Thanks to Friederike Haberstroh for being a friend and especially for marrying my brother, and to Katja Weckmann for not having a brain-to-mouth filter.

I would like to thank my wonderful girlfriend, Désirée Decker, for the great time we had and the time we will have together.

Last but not least, I would like to thank my family, which I cannot thank enough. Their endless support made this possible and I am grateful that everything went so great the past 3.5 years.